UiO : University of Oslo

Krister Stræte Karlsen

Plate Tectonic Controls on Geodynamic Processes

Earth's Deep Water Cycle, Sea Level Change and Planetary Cooling Patterns

Thesis submitted for the degree of Philosophiae Doctor

Department of Geosciences
The Centre for Earth Evolution and Dynamics
Faculty of Mathematics and Natural Sciences

2021

Series of dissertations submitted to the
Faculty of Mathematics and Natural Sciences, University of Oslo
No. 2428

ISSN 1501-7710

Cover: Hanne Baadsgaard Utigard.
Print production: Reprosentralen, University of Oslo.

A surface shattered into pieces,
moving sideways against each other,
partly, in fact mostly, covered by water.
This is our planet.
And it is our duty to understand how it works.

Preface

This thesis is submitted in partial fulfillment of the requirements for the degree of *Philosophiae Doctor* at the University of Oslo. The research presented here was conducted at the Centre for Earth Evolution and Dynamics (CEED), at the University of Oslo, under the supervision of professor **Clinton P. Conrad**, and co-supervisors professor **Reidar G. Trønnes** and Dr. **Valentina Magni**. The thesis is a collection of three papers, presented in chronological order of writing. The common theme to them is "how plate tectonics affects geodynamic processes". The papers are preceded by an introductory chapter that relates them to each other and provides background information and motivation for the work, and a conclusion chapter that summarazies the main scientific results.

Structure of the Thesis

The introduction of this thesis starts at a popular science level, with a historical review of how we got to the magnificent theory of plate tectonics. This section (1.1) serves to honor the great efforts that lead to the plate tectonic revolution, while at the same time provide some historical context for my own work. Shifting gears, from popular science to state of the art, the next section (1.2) focuses on what we know about plate tectonics today, and how we know what we know about past plate motions. The third section (1.3) is about how plate tectonics impacts geodynamic processes. A complete discussion on the interactions between plate tectonics and the dynamical Earth system is beyond the scope of this thesis, I therefore chose to only introduce its main research topics; i.e. the deep water cycle, sea level change and surface heat flow. The Introduction section is concluded with a list of "outstanding questions" (Section 1.4), which are later addressed in the three papers and the Conclusions chapter. Finally, in the Conclusions chapter I summarize the work presented in the three papers, share some lessons learned and my thoughts on the way forward.

The research output of this thesis is three published papers which are attached at the end of the thesis, in virtually identical format to how they were published in their respective journals.

Reaching a Broad Audience

Science advances through sharing of results. Research should be as transparent and accessible as possible because it should be reproducible and confirmed by others. All of the three papers associated with this thesis are published under open access, being freely available to the public, and the **software** I developed as part of Paper II is open source.

Science should not only be "open" and available to the public, but efforts should also be made to communicate it in such a manner that a broad audience can grasp its content. To make sure that my work reaches beyond the scientific community, I have been in contact with several journalists, for range of science news outlets. A selection of the popular science summaries that resulted from these interactions are referenced at the end of Chapter 2.

Acknowledgements

The original title of this thesis was supposed to be "*Things that I am interested in, by Krister S. Karlsen*". What I like about this title is that it represents the kind of freedom that my supervisor, **Clint Conrad**, has given me during my PhD. I will forever be grateful for everything you have taught me. For always making room in your schedule for me. For valuing my opinions. For being a good friend through all of this. For being the best supervisor that anybody could ask for. Ultimately I had to chose another title for the thesis, but its contents truly represent the geodynamic problems I found the most intriguing at the time.

I would like to thank the Centre for Earth Evolution and Dynamics (CEED). I am grateful for the exciting work environment you have provided over the last four years. CEED is a great place to work, where young researchers get to be part of the international forefront of science. A special thanks for moral support and laughter goes out to my closest CEED-friends: **Eivind**, **Hans Jørgen**, **Joost**, **Thea** and **Björn**. I would also like to thank **Mathew Domeier**, **Valentina Magni**, **Carmen Gaina** and **Reidar Trønnes** for fruitful scientific collaborations.

I would like to thank my parents, **Bjørn** and **Judith**, for unconditional support in everything I pursue, and **Uncle Kjell** for encouraging my interest in science form the start.

Last, but not least, I would like to express my sincere gratitude to the University of Oslo for ∼10 phenomenal years.

Krister Stræte Karlsen
Oslo, August 2021

List of Papers

Paper I

Karlsen, K. S., Conrad, C. P. and Magni, V. "Deep Water Cycling and Sea Level Change Since the Breakup of Pangea". In: *Geochemistry, Geophysics, Geosystems*. (2019), DOI: 10.1029/2019GC008232.

Paper II

Karlsen, K. S., Domeier, M., Gaina, C. and Conrad, C. P. "A Tracer-Based Algorithm for Automatic Generation of Seafloor Age Grids from Plate Tectonic Reconstructions". In: *Computers & Geosciences*. (2020), DOI: 10.1016/j.cageo.2020.104508.

Paper III

Karlsen, K. S., Conrad, C. P., Domeier, M. and Trønnes, R. G. "Spatiotemporal Variations in Surface Heat Loss Imply a Heterogeneous Mantle Cooling History". In: *Geophysical Research Letters*. (2021), DOI: 10.1029/2020GL092119.

Contents

Chapter 1

Introduction

1.1 A Historical Perspective on Plate Tectonics

The magnificent theory of plate tectonics deserves a proper introduction. This section summarizes the historical journey from the 16th century cartographers observation of the jigsaw-puzzle fit of the continental edges (Fig. 1.1), to the widespread acceptance of plate tectonics, and is based on the book *Plate tectonics: An insider's history of the modern theory of the Earth* by Oreskes, N. & Le Grand, H. E.

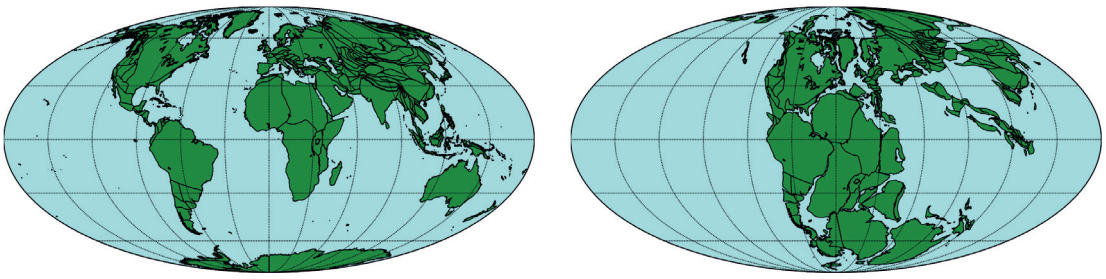

Figure 1.1: The continental jigsaw puzzle.

1.1.1 How Do Mountain Belts Form?

How could the apparently rigid surface of the Earth be squeezed and folded like putty? This was one of the most intriguing questions for 19th century geologists who had seen folded rock formation. At the time, it was widely believed that our planet had formed hot, and steadily cooled since. Because most materials shrink as they cool, it seemed plausible that Earth had been contracting over geological time as well; producing cracks, wrinkles and topography on its surface. This model of the Earth as a drying apple was popularized in Europe by Austrian geologist Edward Suess (1831-1914). Suess suggested that collapsed portions of the surface formed ocean basins, while elevated regions formed continents, and with continued cooling the original continents became unstable and collapsed to form new ocean basins, and what had formerly been ocean became dry land. This interchangeability of oceans and continents explained several puzzling geological observations, such as the discovery of marine fossils on land. An observation which long before had riddled both Leonardo Da Vinci (1452-1519), and the Greek philosopher Xenophanes (570–475 BC) who found petrified shells of clams and oysters on Mt. Olympus.

In the century that followed (the 20th), three independent lines of evidence challenged the theory of a contracting Earth. The first came from field mapping of mountain ranges. During the 19th century geologists had constructed maps and cross-sections that revealed the structure of the Swiss Alps and the North American Appalachians. These showed that the folded sequences of rock were so extensive that if one could unfold them, the rock layers would extend for several hundred kilometers. The amount of terrestrial contraction required to create such deformation of the crust seemed impossible.

The second line of evidence came from the early suggestions of the principle of isostasy. Cambridge-trained mathematician John Pratt (1807-1871) was hired by the Great Trigonometrical Survey of India to explain a discrepancy between their geodetic measurements. Pratt calculated the expected gravitational effect of the nearby mountains and discovered that the discrepancy was less than expected; it was as if parts of the mountains were missing. Pratt suggested that the observations could be explained if the surface topography of the mountains were compensated by a deficit of mass beneath them. This principle came to be known as isostasy, and it had profound implications for the interchangeability of ocean basins and continents that had earlier been suggested along with the contraction theory. To achieve isostasy the elevated landmasses (continents) must have low-density roots beneath them - and therefore they could not sink to become next generation ocean basins.

The third, and most fundamental, line of evidence came with the discovery of radiogenic heat. Our planet was no longer steadily cooling, but had a way of generating heat within its interior. With the theory of contraction shattered into pieces, geoscientists had to look elsewhere for a mechanism that could explain the massive deformations of Earth's crust.

1.1.2 Continental Drift

Alfred Wegener (1880-1930), a pioneering meteorologist, suggested that lateral migration of continents across climate zones could explain paleoclimate. Wegener's theory was widely discussed and mostly rejected, particularly by the geoscientific community in the United States, who labeled it bad science. The debate over the mechanism of continental drift was focused around the implications of isostasy: if continents "floated" in a denser substrate, then this substrate had to have fluid-like properties that allowed continents to move through them. Scandinavian geologists, and Norwegian polar explorer Fridtjof Nansen (1861–1930), had indeed documented such motions, but they were vertical. The progressive uplift of Scandinavia since the last glaciation provided indisputable evidence that when the extra ice mass on top of the continents was removed, the continents would readjust to "float" higher in the substrate. However, an essential question remained: what force would cause lateral movement?

Among the critics of Wegener's continental drift theory was Cambridge geophysicist Sir Harold Jefferys (1891-1989). He pointed out that seismic wave propagation through the Earth required a solid interior, and a solid interior would prohibit lateral migration of continents. British geologist Arthur Holmes (1890-1965) proposed that Earth's interior might act as a solid under high strain rates (seismic events), yet still be ductile and fluid-like under low strain rates applied over long time scales (continental drift). This would reconcile the observation of seismic wave travel through the Earth with "floating", migrating continents. The driving force that Holmes' suggested for the lateral motions was convection currents in the mantle fueled by radiogenic heat production (Holmes, 1931).

1.1.3 Rejection: Bad Science

Another line of resistance (mainly in North America) against Wegener's continental drift theory focused on the very principles of science. Americans were devoted to the method of multiple working hypotheses. Scientific evidence should be weighted in the light of several competing theoretical explanations. This approach to uncover the truth was believed to be slow, but rigorous; requiring years to decades. Good science was supposed to be empirical, inductive and modest, holding close to the objects of study and resisting the impulse to go beyond the scientific evidence at hand. Wegener's work was viewed as violating these principles on several counts. It put the theory first and sought evidence for it later. It arrived too quickly at single interpretation. It was too grand and too unifying.

Wegener's work also came in conflict with the framework of uniformitarianism, the idea that the best way to understand the geological record was by reference to presently observable processes. This principle was deeply embedded in the minds of 20th century geologists who routinely used fossils from the rock record to make inferences about past climate. According to Wegener, however, because of the constantly changing surface of the Earth, continents presently found on tropical latitudes did not necessarily have tropical faunas. In his view, the present was merely a snapshot in time, no more characteristic for Earth history than any other. This put a large question mark behind whether or not the present really was the key to the past, a concept American geologists were not ready to abandon. Wegener's pioneering ideas of plate tectonics were tossed aside and labeled bad science. There the matter would rest for about two decades, until new evidence reopened the discussion of horizontal crustal motions.

1.1.4 A New Age of Scientific Exploration

The applications of particularly magnetics and physical oceanography in submarine warfare during World War II propelled military funding of geophysical research. As a consequence, an enormous amount of data was collected in the years that followed. These included maps revealing the bathymetry and structure

of the seafloor, as well as the magnetic and gravity signatures of the solid rocks at the bottom of the sea. While geophysical data was being gathered from the oceans, theoretical and experimental work on Earth's magnetic field was being conducted on land. Edward Bullard (1907–1980) proposed that the Earth's magnetic field was of dynamic origin, more specifically generated by convection currents in a liquid iron core (Bullard, 1949). In light of the discovery made by Pierre Curie (1859-1906), that rocks cooled in a magnetic field take on the polarity of that field, a dynamic magnetic field suggested that the history of its variations would be recorded in the rock record. In fact, there was already evidence that this was the case: paleomagnetic data suggested that rocks had not remained stationary relative to Earth's magnetic field over the course of geological history (Creer et al., 1954). There were two possible interpretations of this: either the Earth's magnetic poles had moved relative to the rocks, or the rocks had moved relative to the poles (continental drift).

Keith Runcorn (1922-1995) at the University of Manchester realized that this ambiguity could be resolved by comparing magnetic variations in rocks from different continents. First, by comparing rocks of varying ages from the same continent, one could construct a record of how the poles had seemed to move over time with respect to the continent (apparent polar-wander). Next, if all the continents produced the same apparent polar-wander path, it would mean that the poles had moved. If they were different, it would indicate continental drift. The result? The apparent polar-wander paths differed significantly between continents. New evidence for continental drift was finally on the table.

The new paleomagnetic data reopened the discussion about the driving force of continental drift. Bullard, now working with Arthur Maxwell (1925-2019) and Roger Revelle (1909-1991), showed that heat flow through the oceanic crust was greatest at the mid-ocean ridges (Bullard et al., 1956), consistent with rising convection currents. Inspired by these developments, American geologist Harry Hess (1906–1969) suggested that mantle convection drives the crust apart at mid-ocean ridges and downward at ocean trenches, forcing the continents to move laterally with them. While Hess grew convinced of continental drift on the basis of the apparent polar-wandering paths, others doubted the paleomagnetic data.

The paleomagnetic data had shown that certain rock sequences had highly coherent patterns, while others did not. Some were in fact, "reversely magnetized". That is, the polarity of the magnetic field recorded in the rock was opposite to Earth's magnetic field. While many took this as a sign that the data were flawed, others wondered if Earth's magnetic field periodically reversed its polarity. There was indeed some evidence that suggested it did. In the 1920s, Japanese geophysicist Motonari Matuyama (1884-1958) had conducted a detailed study of magnetism in volcanic rocks in Japan (Matuyama, 1929). He demonstrated that recently erupted lavas were consistently polarized in line with the present magnetic field, while older underlying rocks were reversely magnetized. This led

Matuyama to argue that Earth's magnetic field had reversed its polarity, but his work was largely ignored in Europe and North America.

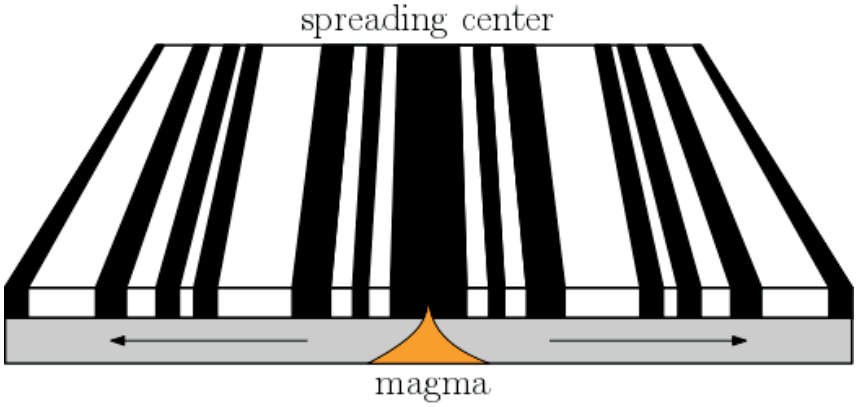

Figure 1.2: Cartoon illustrating how magnetic field reversals form "magnetic stripes" parallel to the spreading mid-ocean ridge axis.

Decades later, the question of magnetic field reversals was taken up in the United States. Thanks to the development of radiometric potassium-argon (K-Ar) dating at Berkeley, it became possible to accurately date young rocks and infer their magnetic polarity. These advances led to the establishment of a paleomagnetic timescale in the year 1963, that showed four clear reversals over the past 4 million years (Cox et al., 1963). Magnetic reversals plus Hess' suggestion of seafloor spreading at mid-ocean ridges formed a testable hypothesis. If the seafloor is spreading while Earth's magnetic field reverses, then the basalts forming the ocean floor will record parallel "stripes" of normal and reversely magnetized rocks (Fig. 1.2 and Vine and Matthews, 1963).

Researchers at Lamont Geological Observatory, at Columbia University, had throughout the 1950s collected a vast amount of magnetic data from the seafloor and found themselves in an ideal position to put Vine and Matthew's hypothesis to the test; and very quickly they did. In 1965, James Heirtzler (1925-) and Xavier Le Pichon (1937-) published the first of several articles documenting the magnetic patterns of the Atlantic Ocean (Heirtzler and Le Pichon, 1965). By 1967-1968 there was no longer any doubt, the seafloor was split down in the middle and the two sides were moving apart.

A wealth of geological data now suggested that Earth's surface was divided into rigid blocks, separated by zones of weakness. The mid-ocean ridges represented one such zone, but what were the others? Advances in seismology, accelerated by the U.S. government's funding of a world wide seismograph network, had recently made it possible to accurately determine the slip directions of faults. In 1967, seismologist Lynn Sykes (1937-) demonstrated that the mid-ocean ridges were offset by zones of crustal sliding (transform faults) (Sykes, 1967), in accordance with an earlier suggestion by J. Tuzo Wilson (1908-1993) (Wilson, 1965). Sykes,

together with co-workers, continued to analyze earthquake data, but shifted their focus from the center of the ocean basins and to the edges. They discovered that the deep-focused earthquakes there had slip directions that were consistent with the overlap of one crustal plate onto another (Oliver and Isacks, 1967). The ocean floor was being forced under the continents (subduction zones).

A global picture had now emerged. Earth's crust was divided into crustal plates (Fig. 1.3), separated by weak zones of divergence (mid-ocean ridges), convergence (subduction zones) and sliding plate motion (transform faults). The ocean crust was created at the diverging plate boundaries and moved laterally until it ultimately collided with the continents, where it was forced down into Earth's mantle. In zones of convergence, folds produced mountain belts and magmas rising to the surface formed volcanoes. In 1968 Xavier Le Pichon calculated the rates of horizontal crustal motion on the basis of paleomagnetic data, and summarized his findings on a map of the world divided into separate plates (Le Pichon, 1968). The result became known as plate tectonics, and was now the unifying theory of the earth sciences. After nearly a century, we finally had an answer to how mountain belts form.

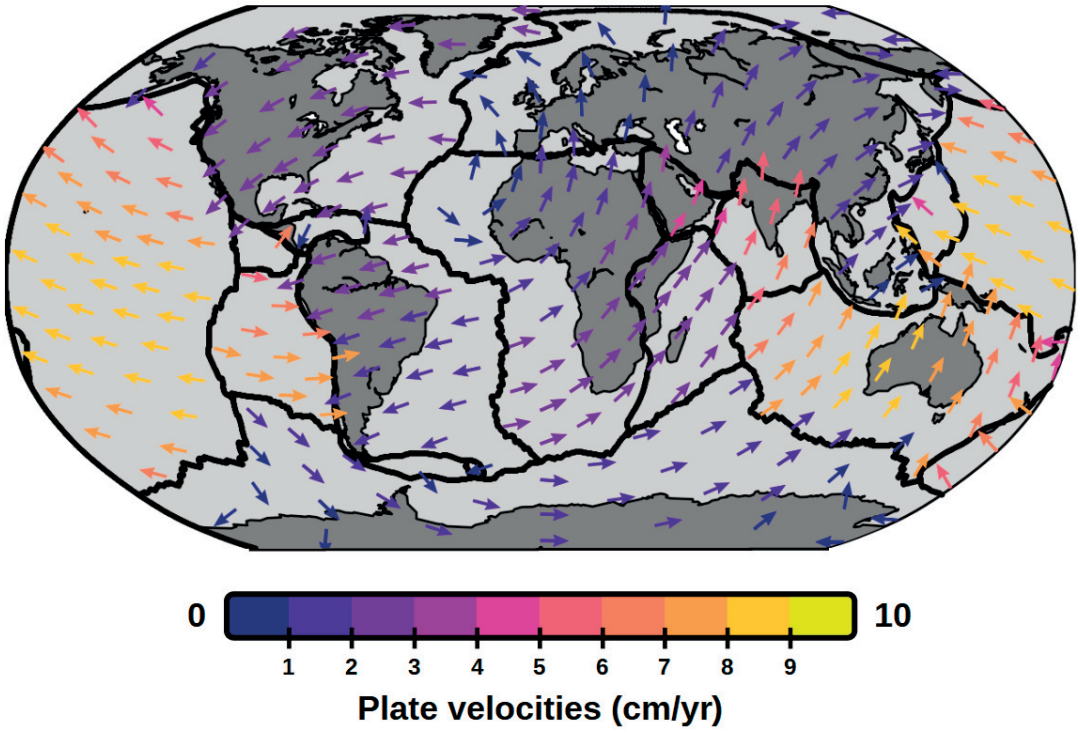

Figure 1.3: Present-day main plate boundaries (thick black lines) after Torsvik and Cocks (2016), and plate velocities (arrows) after Matthews et al. (2016).

1.2 What We Know About Plate Tectonics Today

Today, standing on the shoulders of the heroes of plate tectonics, we know a great deal more about the lateral crustal motions that uniquely characterize Earth in our Solar System. Not only do we know that the mosaic of plates that constitutes Earth's surface move, but we have a good idea about how they have moved as well. In addition to that, we are beginning to understand the geodynamical implications. Before I move on to discuss the effects of plate tectonics on geodynamic processes, I will briefly review how plate motion history can be reconstructed.

1.2.1 Constraining Past Plate Motions

The relative motion of tectonic plates can be determined with magnetic anomalies from the seafloor, just like (Vine and Matthews, 1963) predicted, but constraining their motions in an absolute sense requires the non-trivial determination of a fixed terrestrial reference frame. Here I will go through how absolute plate motions can be inferred with different methods. For a more extensive review the reader is referred to Torsvik et al. (2008a), Torsvik et al. (2012), Torsvik and Cocks (2016) and Domeier and Torsvik (2019).

1.2.1.1 The Hotspot Reference Frame

The quest to determine the absolute motion of tectonic plates with respect to the deep mantle began with Tuzo Wilson's suggestion that linear chains of seamounts and volcanoes are caused by major centers of igneous activity (Wilson, 1963). W. Jason Morgan (1935-) elaborated on this idea by suggesting that these hotspots are located over plumes of hot material rising from the deep mantle, and hence provide a fixed reference frame anchored in the lower (Morgan, 1971; Morgan, 1972). His model assumed that plumes remain fixed relative to each other over time, contradictory to our more recent understanding of mantle plumes. Therefore, fixed hotspot reference frames (at least before 40 Ma) must be replaced by a frame in which motions of plumes in a convecting mantle are assumed (Steinberger et al., 2004). A moving hotspot reference frame is constructed based on three key ingredients: (i) relative plate motions, (ii) spatiotemporal evolution of hotspot tracks and (iii) the motions of mantle plumes that they rely on (Torsvik et al., 2016). The first step is to determine relative plate motions with respect to some selected (and otherwise arbitrary) anchor plate using marine magnetic anomalies. Because we want to relate these relative surface motions to the mantle, hotspot tracks come into play. The second step is to estimate the lateral, time-dependent advection of the plumes using mantle convection modeling. The final step is to solve for time-dependent motion (or rotation) to apply to the anchor plate (which controls the positions of all the other plates) such that the plates hotspot tracks coincide with the instantaneous position of the moving plumes.

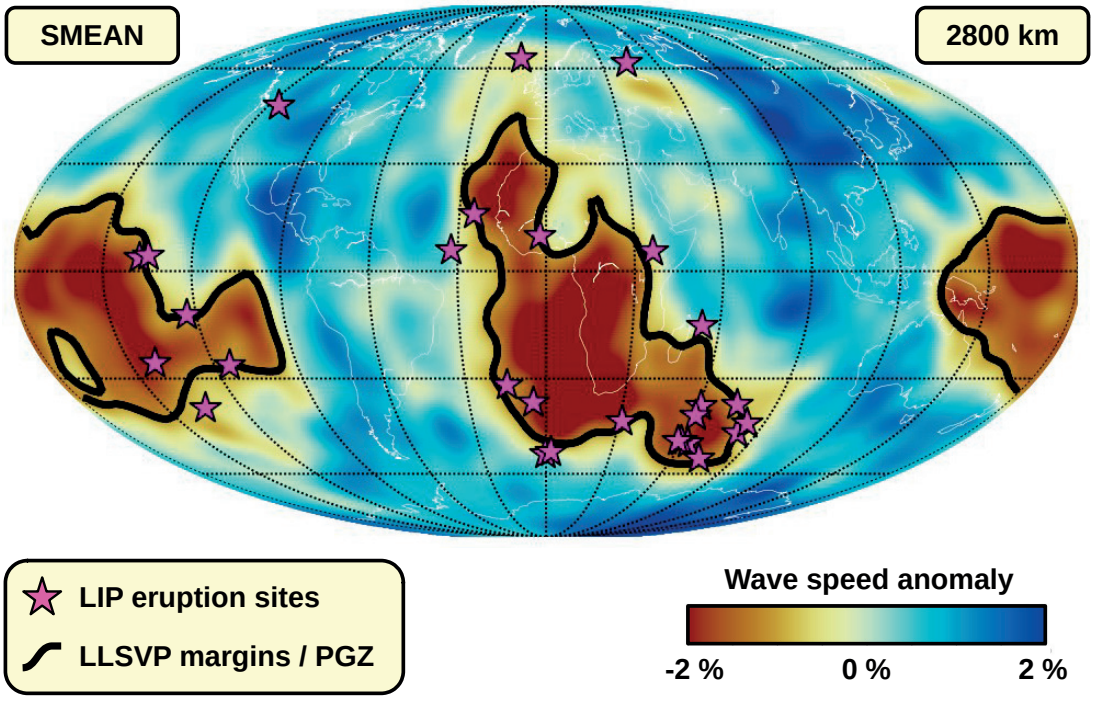

Figure 1.4: Seismic shear wave speed anomalies at 2800 km depth based on the SMEAN tomography model (Becker and Boschi, 2002). Present-day coastlines are plotted with thin white lines for geographical reference. Stars in magenta show the reconstructed eruption sites of large igneous provinces (LIPs). The thick black lines indicate the margins of the LLSVPs and the plume generation zone (PGZ), as defined by the -1 % wave speed anomaly contour.

1.2.1.2 The Paleomagnetic Reference Frame

Earth's magnetic field can be approximated by a magnetic dipole placed at the center of the Earth and aligned with its rotation axis, this is known as the geocentric axial dipole (GAD) hypothesis. Since rocks take on the magnetic field in which they formed, a rock of a certain age can be used to calculate where the magnetic pole was with respect to that rock at the time of its formation (paleomagnetic pole). Thus, a sequence of rocks of different ages can be used to construct a path of how the magnetic pole appears to have moved through time with respect to the stationary rock a sequence. This is known as an apparent polar wander (APW) path. From a paleomagnetic pole one can calculate the rotation (Euler pole + angle) required to bring that paleo-pole to the back to the "current" magnetic pole. This (finite) rotation can then be applied to a continent to reconstruct its paleo-position. However, there are two major problems for constraining the finite rotation: (i) because of the symmetry of normal and reversed magnetic fields, we cannot distinguish between north and south magnetic poles without additional information, and (ii) due to the symmetry of the GAD field with respect to the spin axis, there is no way to establish paleolongitude.

In practice, this means that we do not know on which hemisphere to place the continent, nor its longitude, from paleomagnetic data alone. The former can often be determined relatively easy from various geological constraints, while the latter can be of great challenge. Therefore, the paleomagnetic reference frame does not provide longitude.

1.2.1.3 The Longitude Problem

There are methods to constrain longitude semi-quantitatively, and one such method has been termed the **"zero-longitude" Africa approach** (Burke and Torsvik, 2004; Torsvik et al., 2008b). This approach makes use of the observation that Africa is the continent that has moved the least in longitude since the breakup of Pangea. First, all reliable paleomagnetic poles world wide are compiled and rotated to Africa-coordinates. Next, a global apparent polar wander path (GAPWaP) for Africa is constructed. Then, Euler rotations are calculated from the GAPWaP to reconstruct the positions of Africa. Finally, the remaining plates are reconstructed with respect to Africa based on relative plate motions. However, since the assumption of minimal longitudinal movement of Africa is questionable before Pangea, other techniques are applied to constrain paleo-longitude pre-Pangea.

Another method for constraining the paleo-longitude of landmasses makes use of the remarkable correlation between the eruption sites of large igneous provinces (LIPs) and margins of the deep mantle structures called the large low shear velocity provinces (LLSVPs, Fig. 1.4). These are two massive thermo-chemical heterogeneities in the lower mantle, characterized by significantly lower seismic wave speeds than the surrounding mantle. The margins of these structures are referred to as the plume generation zone (PGZ, Burke et al., 2008), and using their positions, in conjunction with LIP eruption sites, to calibrate longitude is known as the **PGZ method**. This method implicitly assumes long-term stability of the LLSVPs, which remains a controversial hypothesis.

A third method is based on mapping slabs observed in seismic tomography models to paleo-subduction zones. Van Der Meer et al. (2010) identified the depth and time of subduction for a total of 28 slabs in the mantle. By connecting these slabs to fossil arcs and orogens at the surface they derived an average slab sinking rate of 12 ± 3 mm/yr. This sinking rate provided a good global correlation between slabs at various depths with the paleo-location of subduction zones. Constraining the longitude of ancient active margins with this approach results in what is often called the **subduction reference frame**.

1.2.1.4 True Polar Wander

Motions of continents relative to Earth's spin axis, as inferred using paleomagnetic data, may not be the motions of the continents alone, but the rotation of the entire solid Earth (crust and mantle) relative to its spin axis. This phenomenon is known as true polar wander (TPW), and arises from the gradual redistribution

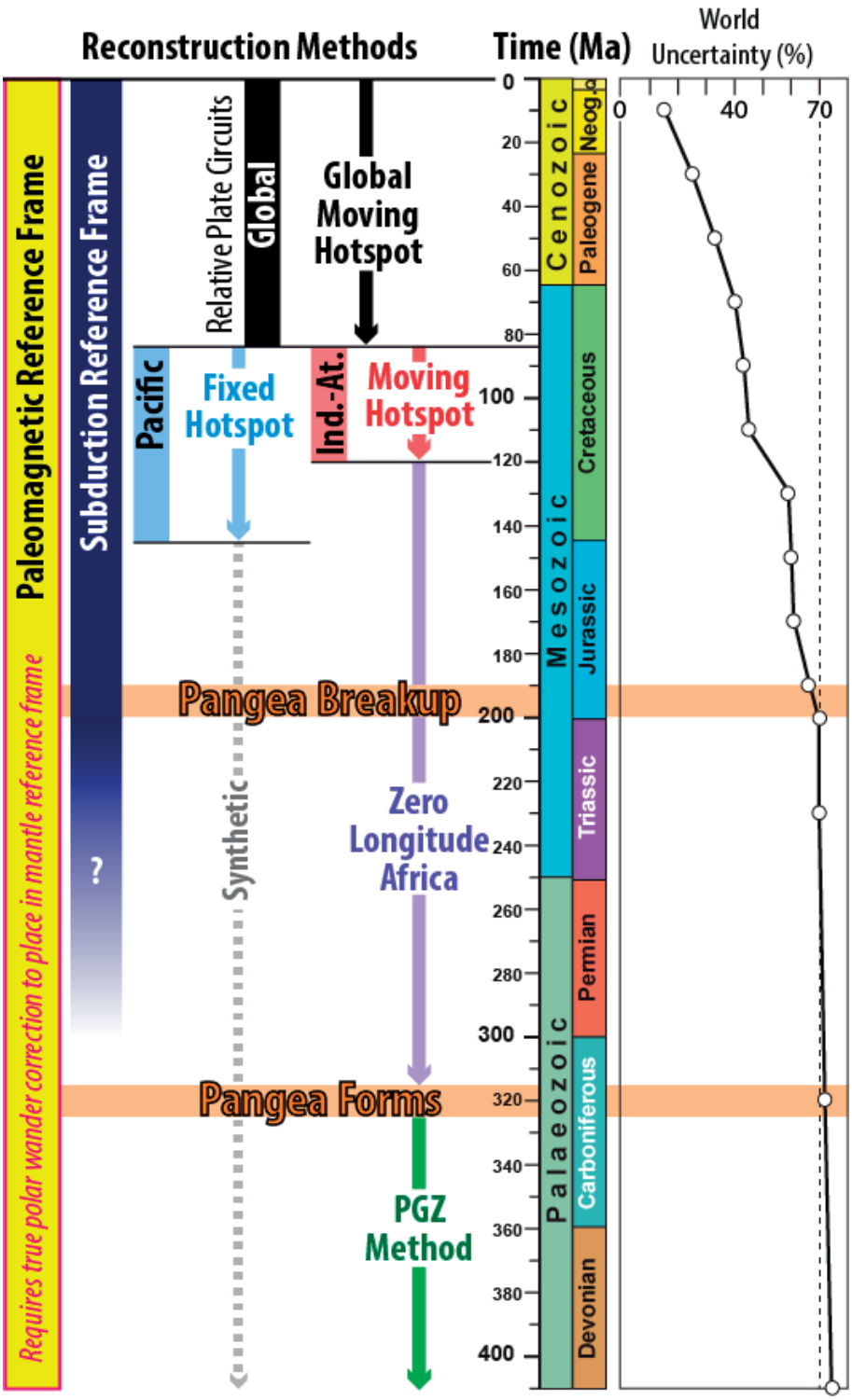

Figure 1.5: An overview of the methods discussed in Section 1.2.1 used to constrain the past motions of tectonic plates. How far into the past each of these methods can be applied are indicated by bars and arrows. The "world uncertainty" is a measure of the Earth's present-day surface area fraction that is missing (e.g. lost to subduction) at a given point in time and serves as a proxy for the uncertainty in any plate motion history model (Domeier and Torsvik, 2019).

of density heterogeneities working to realign the largest moment of inertia axis with the spin axis (Goldreich and Toomre, 1969). In order to compare surface reconstructions based on paleomagnetic data to present-day mantle structures, TPW must be accounted for.

To establish the magnitude of TPW with confidence, the absolute plate velocity field and plate geometry for both continental and oceanic lithosphere are required (Torsvik and Cocks, 2016). Then, TPW can be calculated as the difference between a global moving hotspot reference frame and the paleomagnetic reference frame. This is challenging for pre-Cretaceous time lacking preserved seafloor (and hotspot tracks), and thus estimates of TPW must rely on paleomagnetic data from the continents. To overcome these difficulties Steinberger and Torsvik (2008) proposed that the magnitude of TPW can be estimated by extracting the mean rotation of all the continents around their common center of mass using a paleomagnetic reference frame.

In Figure 1.5 we summarize the various methods that can be used (and combined) to constrain plate motions in the past, and indicate approximately how far back in time they can be applied.

1.2.2 Modern Plate Tectonic Reconstructions

By combining the methods discussed in the previous section, together with geological constraints such as alignment of orogenic features, matching of conjugate margins, oceanic lithosphere emplaced onto continents (ophiolites), etc., global "full-plate tectonic reconstructions" can be created. These modern, state-of-the-art plate tectonic reconstructions provide models for how plates and plate boundaries have moved through a certain time-interval, necessarily with increasing uncertainty going further back in time (Fig. 1.5).

Two different plate tectonic reconstructions have been used in the research presented in this thesis. Müller et al. (2016) was used for Paper I, and Matthews et al. (2016) was used for Paper II and Paper III. The plate model of Matthews et al. (2016) extends from 410 Ma to the present, and is a merger of two published models, namely Domeier and Torsvik (2014) (410-250 Ma) and Müller et al. (2016) (230-0 Ma). The Matthews et al. (2016) is based on the paleomagnetic reference frame and has been corrected for TPW, while the PGZ-method has been applied to constrain longitude. Müller et al. (2016) adopt a global moving hotspot reference frame from 0 to 70 Ma (Torsvik et al., 2008a; Torsvik et al., 2008b), and for the period from 100 to 230 Ma they adopt a TPW-corrected paleomagnetic reference frame (Steinberger and Torsvik, 2008), to which a 10° longitudinal shift is applied to produce a smooth transition between the two reference frames. The plate tectonic reconstruction of Müller et al. (2016) was published with an accompanying set of age models for the oceanic lithosphere covering the past 230 Myr (extended back to 250 Ma in Müller et al., 2019). Matthews et al. (2016) did not include such age models, even though their plate

reconstructions implicitly include the information necessary to determine the age of ocean floor. Figure 1.6 shows the positions of continents, mid-ocean ridges and subduction zones as defined in the Matthews et al. (2016) model.

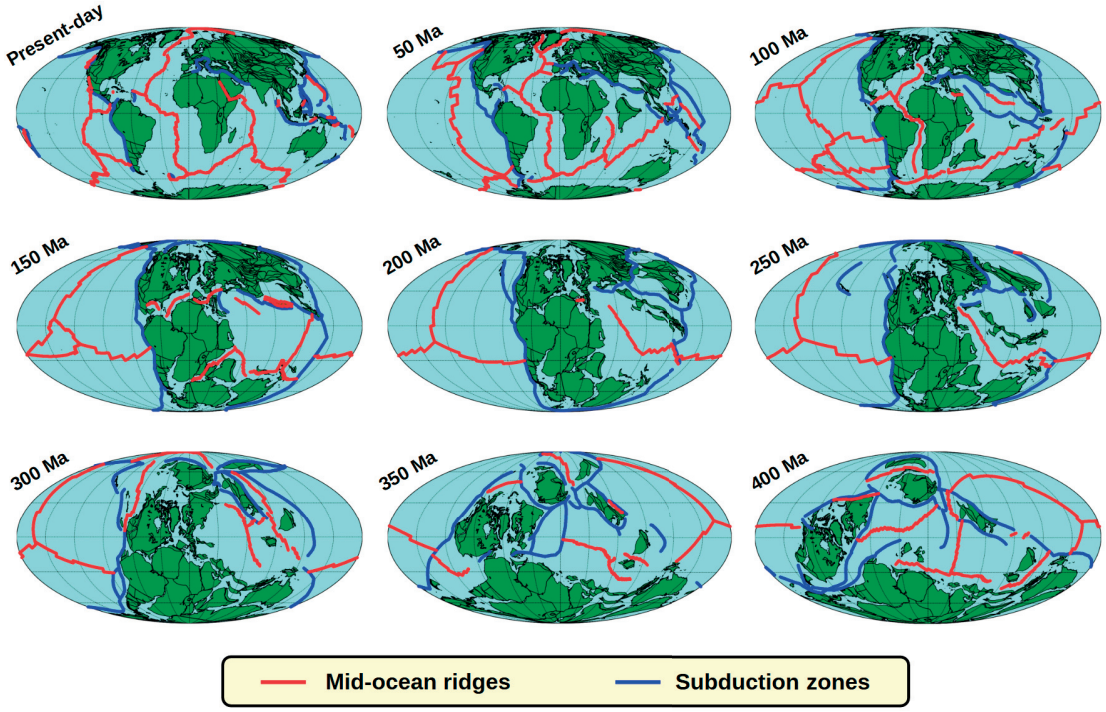

Figure 1.6: Positions of continents, mid-ocean ridges and subduction zones through time, based on the plate tectonic reconstructions of Matthews et al. (2016).

1.2.3 Supercontinents

More than 100 years has passed since Alfred Wegener (Wegener, 1912) proposed that nearly all of Earth's continental landmasses had assembled during the Late Paleozoic–Early Mesozoic into what he named Pangaea ("all lands" in Greek) – a supercontinent. However, it took more than 50 years, and the discovery of seafloor spreading (Vine and Matthews, 1963), for the existence of Pangaea to become generally accepted. The broad acceptance of Pangea paved the way for the idea that other supercontinents may have existed before it (e.g., Piper, 1974; Piper, 1975; Valentine and Moores, 1970), and later the concept of a "supercontinent cycle" (Worsley et al., 1982).

Even though paleogeographic reconstructions in Precambrian time are controversial, due to the lack of kinematic constraints (such as magnetic anomaly data from the seafloor which has been used to reconstruct Pangea; $\sim$ 180-320 Ma), most researchers now recognize at least two Precambrian supercontinents, Rodinia and Nuna (also referred to as Columbia). Rodinia lasted from approximately 1.1 Ga to 0.7 Ga, and is thought to have occupied the present-day Pacific

(Tegner et al., 2019). It has also been suggested that Rodinia may have been geologically distinct from both Nuna (∼ 1.2-1.9 Ga) and Pangea (Mitchell et al., 2021), in that Rodinia was relatively poorly endowed in mineral deposits (Leach et al., 2010) and is the only one of the three supercontinents to have experienced low-latitude Snowball Earth glaciations (e.g., Hoffman et al., 2017). Nuna on the other hand, has been noted as the most endowed supercontinent in terms of mineral deposit formation (Leach et al., 2010), and it has been proposed as Earth's first true supercontinent (Hoffman, 1989).

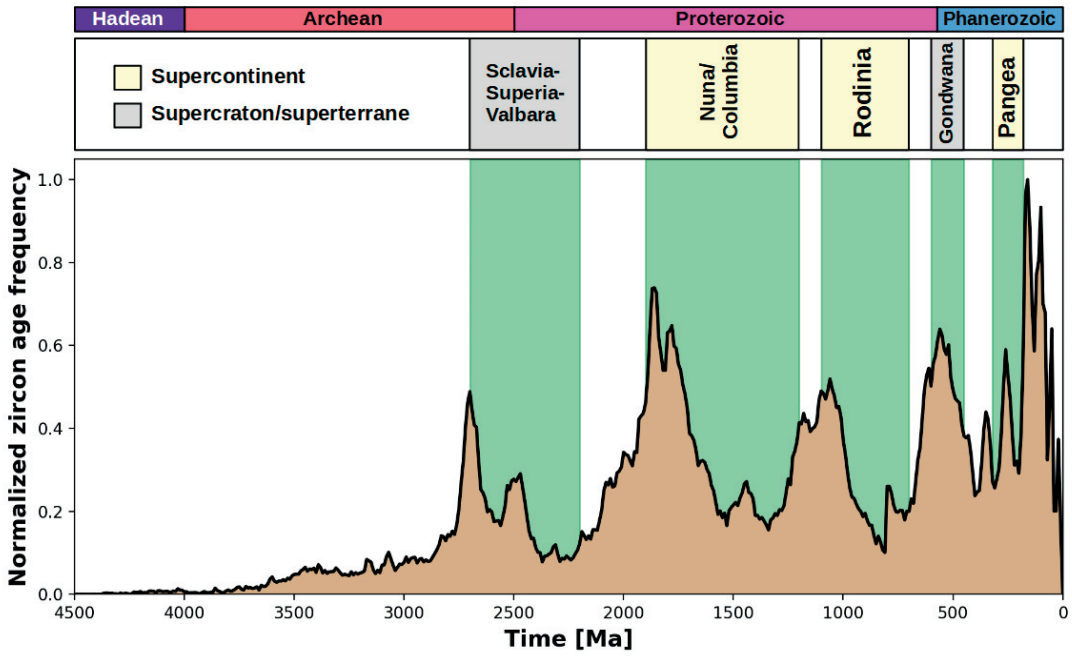

Figure 1.7: Frequency of zircon ages after Voice et al. (2011), quality-filtered after Marcilly et al. (In prep.) and normalized against the maximum value of 1928. Approximate durations of supercontinents and supercratons/superterranes are indicated for comparison.

Owing to the lack of kinematic constraints, episodes of supercontinent assembly have been established by way of peaks in the number of collisional orogenies (Pastor-Galán et al., 2019), whereas the timing of breakup has been determined from the ages of large igneous provinces (e.g. Ernst et al., 2013). The formation of supercontinents (Nuna, Rodinia and Pangea) and supercratons/superterranes (Slavia-Superia-Valbara, and Gondwana) has also been related to maxima in the frequency of detrital zircons ages (Fig. 1.7). Beyond these already-mentioned trends in geological time-series, the supercontinent cycle has been suggested to have had an effect on biotic diversification and extinctions (Ernst and Youbi, 2017), magnetic superchrons (Eide and Torsvik, 1996), true polar wander events (Evans, 2003), continental margin sedimentation (Bradley, 2008), episodes of major climate change (Hoffman et al., 1998), mantle dynamics (Zhong et al., 2007) and sea level change (Conrad, 2013). Thus the supercontinent cycle may

have affected Earth more profoundly than any other geological phenomenon.

The study of supercontinents is interdisciplinary research that connects plate tectonics with a wide range of geodynamic processes, a field with many questions that remain to be answered. In the following section I introduce how plate tectonics interact with the three specific geodynamic processes that constitute the core focus of this thesis, namely the deep water cycle, sea level change and surface heat flow.

1.3 Plate Tectonics and Geodynamic Processes

1.3.1 Earth's Deep Water Cycle

The characteristic, vast oceans on Earth's surface are just part of our planet's water story. Mantle-derived magmas containing small amounts of water made researhers realize that Earth's interior is slightly hydrated long ago. Most of the mantle consists of nominally anhydrous minerals (NAMs), such as olivine, pyroxene and garnet, and since the late 1980s it became clear that these minerals can accommodate water as trace defects (or more precisely, hydrogen ions). Experimental work has shown that even trace amounts of water affect mineral and rock properties, like viscosity, in the mantle (Hirth and Kohlstedt, 1996). The importance of water for mantle dynamics leads to critical questions about mantle water content and distribution: how much water can Earth's mantle hold? And more importantly (and not to be confused with): how much water does it hold?

Let's start with the first question. Based on experimental results (Bolfan-Casanova, 2005; Fu et al., 2019; Inoue et al., 2010; Inoue et al., 2016; Litasov et al., 2003; Peslier et al., 2017) the water-storage capacity for the different regions of the mantle has been estimated. The upper mantle has been estimated to potentially accommodate up to 0.5 ocean masses (OM = $1.4 \cdot 10^{21}$ kg), the mantle transition zone (MTZ) up to 6 OM and the lower mantle up to 1.4 OM. Particularly remarkable is the high storage capacity of the MTZ, but importantly, high water storage capacity does not imply high water content. Estimates of the actual present-day mantle water content is based on H_2O/Ce ratios in oceanic basalts, and typically range from 0.5 OM to 2 OM (Dauphas and Morbidelli, 2013; Hirschmann, 2018). The latest estimate with a rigorous error analysis suggests that the current water content is between 0.55 and 0.95 OM (Hirschmann, 2018), placing it at lower end of the 0.5–2 OM-range. However, recent studies have found localities with elevated H_2O/Ce ratios (Mazza et al., 2019), suggesting that deeper water-enriched mantle reservoirs with distinct H_2O/Ce may not have been represented in the oceanic basalts that have been previously analyzed. Therefore the estimates of Hirschmann (2018), 0.55-0.95 OM, might be relatively conservative, and the mantle heterogeneously water saturated.

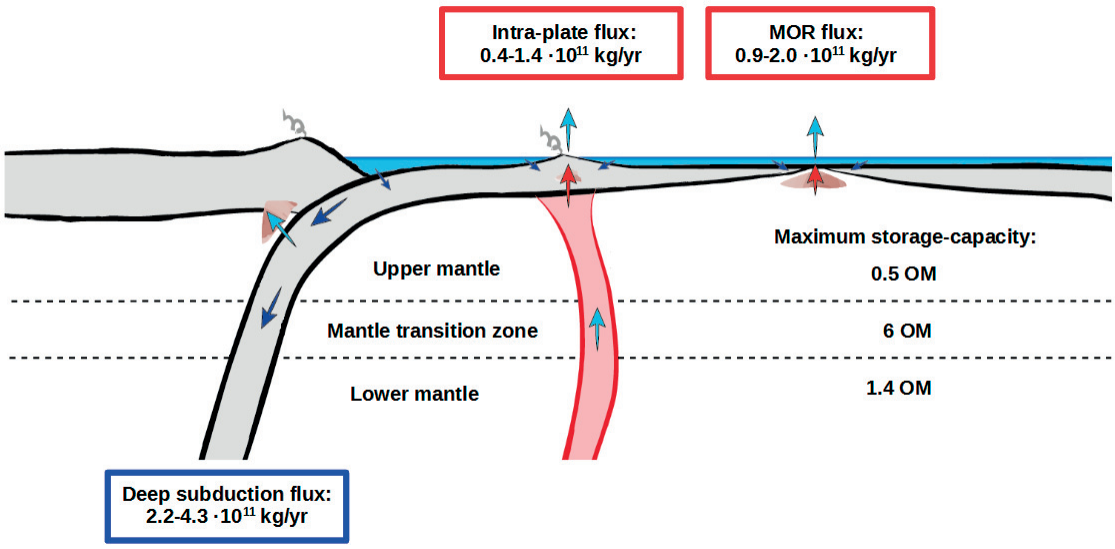

Figure 1.8: Earth's deep water cycle and mantle storage capacity. The deep subduction water flux (regassing) estimate is based on van Keken et al. (2011), the intra-plate degassing flux is based on Parai and Mukhopadhyay (2012) and the mid-ocean ridge (MOR) degassing flux is based on Hirschmann and Kohlstedt (2012), Parai and Mukhopadhyay (2012) and Hirschmann (2018).

The perhaps most remarkable part of Earth's water story is that water is cycled between Earth's interior and surface reservoirs (Fig. 1.8). The sediments, crust and lithospheric mantle parts of oceanic plates become hydrated from interactions with the oceans (Faccenda et al., 2012; Ranero and Sallarès, 2004), and when the inevitable fate that is subduction occurs, water is transported to the mantle. Of the subducting plate's initial water content, only a small fraction can be carried beyond the arc and recycled into the deeper mantle, while the rest is released to the arc via a series of metamorphic reactions. This part of the deep water cycle is often referred to as *mantle regassing*. Partial melting of the mantle extracts water from it, forming buoyant magmas that rise to the surface. Water is then outgassed into the oceans at mid-ocean ridges and intra-plate volcanos, contributing to *mantle degassing*. The estimates of the present-day magnitude of these fluxes suggest that there could be a significant net-flux of water from the oceans and to the mantle (see Fig. 1.8 or Peslier et al., 2017 for a review), but how do they change with time?

Efforts to address the time-dependence of the deep water cycle mainly stem from two types of models: i) 0D parameterized mantle convection models (e.g., Chotalia et al., 2020; Crowley et al., 2011; McGovern and Schubert, 1989; Sandu et al., 2011) and ii) 2D and 3D mantle convection models (Nakagawa et al., 2018; Nakagawa et al., 2015; Price et al., 2019). The first type of models (i) mainly investigate the feedback mechanisms between mantle temperature and water content on the planetary evolution time scales (Giga-years), but are unable to

capture changes on the $10^1 - 10^2$ Myr time scales over which drastic variations in tectonic setting can occur. The second type of models (ii) have focused on the effects of water on mantle dynamics, but have lacked realistic plate tectonics at the surface. Efforts have also been made to derive long-term averages of the deep water fluxes (without attempts to infer time-dependence) through the use of Earth's sea level and continental freeboard history (Korenaga et al., 2017; Parai and Mukhopadhyay, 2012). So far, no study has made use of Earth's plate tectonic history to constrain the deep water fluxes. Since the deep water fluxes are, at least to a large extent, controlled by the rates of plate tectonics (i.e. the rates of seafloor spreading and subduction) I think it is important that these rates are constrained as much as possible when estimates of past mantle regassing and degassing are being made. Such estimates are in turn crucial to better understand the evolution of Earth's surface ocean mass and sea level.

1.3.2 Sea Level Change

The observed global sea level is a result of a complex budget consisting of competing processes acting on very different time scales. On the shorter time scales ($10^0 - 10^2$ yr) sea level is altered due to climate-related processes like thermal expansion of the oceans, melting of landed ice and the elastic response of the lithosphere caused by loading or unloading (e.g. post-glacial rebound). On the longer time scales ($> 10^7$ yr), processes related to mantle dynamics and plate tectonics control sea level. These include dynamic topography, ocean-mantle water exchange (Fig. 1.8) and variations in seafloor depth caused by fluctuations in the mid-ocean ridge spreading rates (Fig. 1.9). For a more complete review of the drivers of sea level change and their associated time scales, see e.g. Conrad (2013).

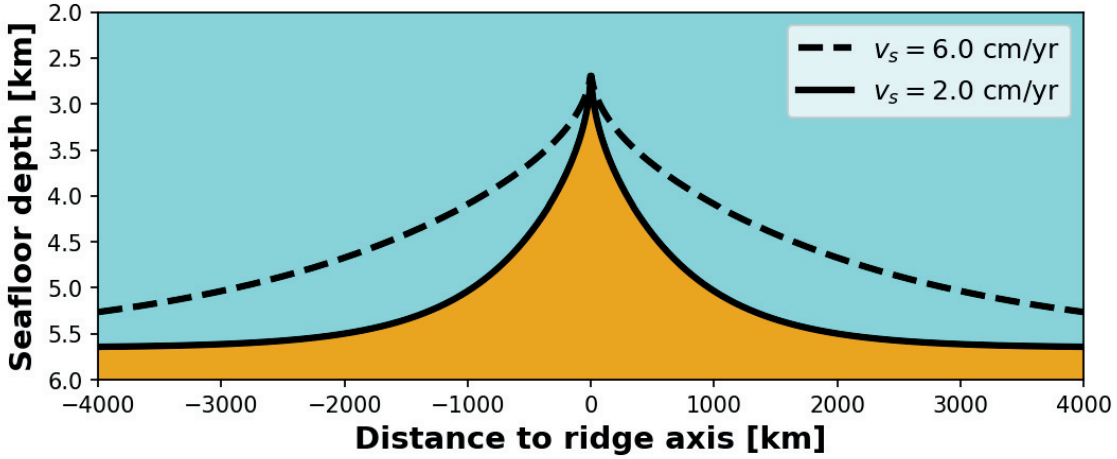

Figure 1.9: Due to thermal subsidence, fast spreading ridges generate young and shallow seafloor, while slow spreading ridges generate old and deep seafloor. Seafloor depth is computed based on age, inferred from spreading rate v_s, after Stein and Stein (1992).

The focus of this thesis is mainly on how variations in the plate tectonic rates drive sea level change through i) ocean-mantle water exchange and ii) changes in seafloor depth associated with ridge-spreading rates. These two processes change sea level in fundamentally different ways: i) modifies the water mass of the oceans, while ii) modifies the "container" volume of the ocean basins while keeping the water mass constant. Understanding both these processes are crucial to unravel sea level dynamics on geological time scales.

The Phanerozoic records of global sea level change (Fig. 1.10) show two clear peaks, one before, and one after the formation of Pangea. These two peaks, roughly spanning the Ceno-Mesozoic (0–251 Ma) and the Paleozoic (251–542 Ma), have been referred to as "megacycles" (e.g. Boulila et al., 2018). It has long been suggested these are of tectonic origin (Nance et al., 1986; Worsley et al., 1986; Worsley et al., 1985), because their massive amplitudes (several hundred meters) by far exceeds those associated with climate change (e.g. melting all presently landed ice amounts to $\sim$ 45 m of sea level rise, Conrad, 2013). Over the last few decades, the development of paleo-seafloor age grids have made it possible to put this hypothesis to the test. Indeed, Conrad (2013) and Müller et al. (2008) showed that variations in seafloor depth caused by fluctuations in mid-ocean ridge spreading rates exhibit first-order control on sea level back to 140 Ma, explaining the post-Pangea sea level peak through the widespread development of new ridge systems during the Cretaceous, which formed young and shallow ocean basins.

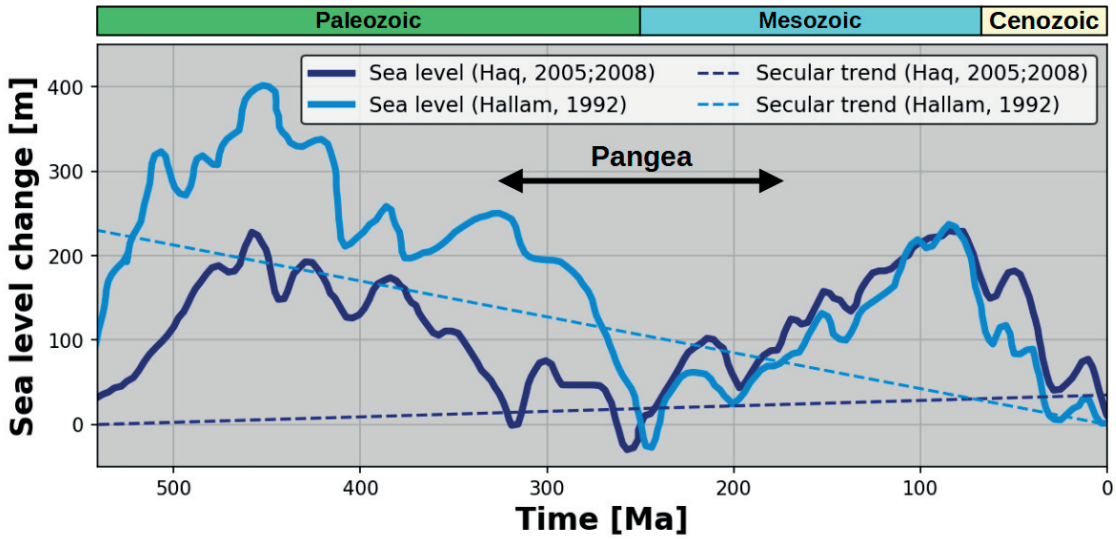

Figure 1.10: Phanerozoic sea level (Hallam, 1992; Haq and Al-Qahtani, 2005; Haq and Schutter, 2008) and estimates of secular trends after Parai and Mukhopadhyay (2012).

Attempts to link the deep water cycle to sea level change (Parai and Mukhopadhyay, 2012; Wallmann, 2001) has mainly focused on arguments that these "observed" megacycles could be superimposed on a long-term trend of

decreasing ocean mass (Fig. 1.10). As an example, Parai and Mukhopadhyay (2012) noted a secular decrease in sea level of 230 m (over 542 Myr) in the sea level record of Hallam (1992) and used this to put bounds on the magnitude of the deep water flux. In contrast, the sea level record of Haq and Al-Qahtani (2005) and Haq and Schutter (2008) does not show a secular decrease, but rather a small increase of about 35 m. Further efforts to relate sea level and deep water cycling should explore possibility of a strong time-dependence of the deep water fluxes and compare these directly with the sea level record (Hallam, 1992; Haq and Al-Qahtani, 2005; Haq and Schutter, 2008), instead of trying to derive long-term averages and secular trends that may or may not exist. Additionally, to make the direct comparison with sea level history as accurate as possible, other major sea level changing mechanisms should be estimated and accounted for, like for instance those that modify the ocean basin "container" volume.

1.3.3 Surface Heat Flow and Mantle Cooling

The realization that surface heat flow is greatest along the mid-ocean ridges (Fig. 1.11), and declining away from the ridge axis, was an important step towards the plate tectonic theory, more than fifty years ago. This phenomenon closely relates to that of seafloor depth (Section 1.3.2 and Fig. 1.9); as the seafloor spreads away from the ridges it becomes cooler, denser and thicker, making it gravitationally stable at larger depths while conducting less heat into the oceans.

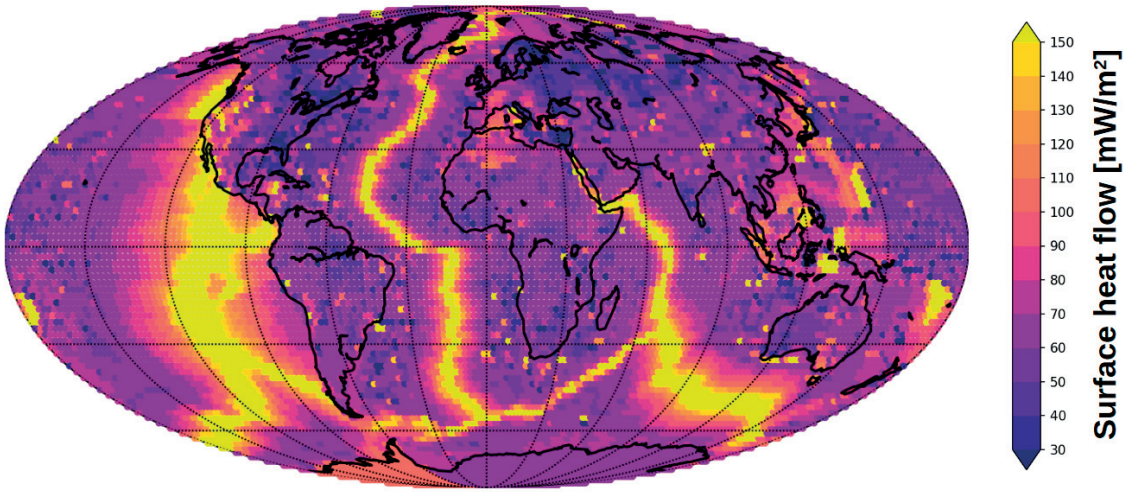

Figure 1.11: Earth's present-day surface heat flow, as constrained by over 38,000 measurements, presented on a $2^\circ \times 2^\circ$ equal area grid after Davies (2013).

Earth's present-day surface heat flow is constrained by global measurements of heat conduction based on thermal gradients in boreholes. These raw measurements indicate a total surface heat flow about 30-32 TW, which increases to about 46 TW when corrected for the underestimation due to hydrothermal circulation in the oceanic regions (Pollack et al., 1993) and heat flow associated

with plumes (Davies, 2013). More specifically, of these 46 TW; 29 TW is attributed to the cooling of oceanic crust, 3 TW is delivered to the surface via plumes and 14 TW represents heat loss from the continents (Fig. 1.12 and Jaupart et al., 2015).

Note that Earth's surface heat flow is different from mantle heat loss (which is the topic of Paper III), because a significant (8 of 14 TW) contribution to continental heat flow is radiogenic heat production within the continents (i.e. outside the mantle). Thus, a map of Earth's mantle heat loss must be corrected for the radiogenic heat production component of the continental heat flow, which is on average approximately 57 % (Jaupart et al., 2015; Turcotte and Schubert, 2002). This correction would make the continental regions in Fig. 1.11 appear darker compared to the oceans (like seen in Karlsen et al., 2021, Fig. III.1).

The oceanic regions dominate Earth's surface heat flow, and provide not only large spatial variations, but significant temporal fluctuations as well. Variations in the rates of seafloor generation and consumption affect the age distributions of the oceans, directly impacting heat loss from Earth's interior. By combining models that relate heat flow to the age of the oceanic lithosphere (e.g., Hasterok, 2013; Korenaga and Korenaga, 2008; Parsons and Sclater, 1977; Stein and Stein, 1992) and paleo-seafloor age grids, several groups (Crameri et al., 2019; Loyd et al., 2007) have reconstructed the oceanic component of surface heat flow back in time. They both noted that the present-day represents a time of unusually low oceanic heat flow, caused by the presently old ocean basins.

By combining estimates of surface heat flow with those of the internal heat sources (Fig. 1.12), mantle cooling can be inferred. Presently, mantle heat sources are estimated to be approximately 22 TW, while the heat sinks amount to 38 TW (3+29+(14-8) TW), leading to a net heat loss of 16 TW. Assuming a specific heat capacity for the mantle of 1250 J/(K kg), these numbers suggest a cooling rate of $\sim$ 100 K/Gyr. Based on the petrological mantle temperature estimates of Herzberg et al. (2010), Jaupart et al. (2015) suggested that a reasonable long-term cooling rate of the mantle should be 50–100 K/Gyr. The notion that Earth's present-day heat flow is at a low-point suggests a long-term mantle cooling rate >100 K/Gyr, exceeding the preferred range of Jaupart et al. (2015). Unless mantle heat sources have been underestimated, of course. Future studies should aim to derive representative, long-term heat flow values based on a more "average" plate tectonic setting, instead of one dominated by very old ocean basins (i.e. present-day). These should in turn be compared to, and discussed in conjunction with, petrological mantle temperature estimates.

Another promising avenue for future research is how uneven surface insulation caused by supercontinent assembly affect lateral mantle temperature variations. Results from both numerical simulations and laboratory experiments have shown that large mantle temperature variations can arise from such events (Lenardic et al., 2011). The further development of paleo-seafloor age grids that extend

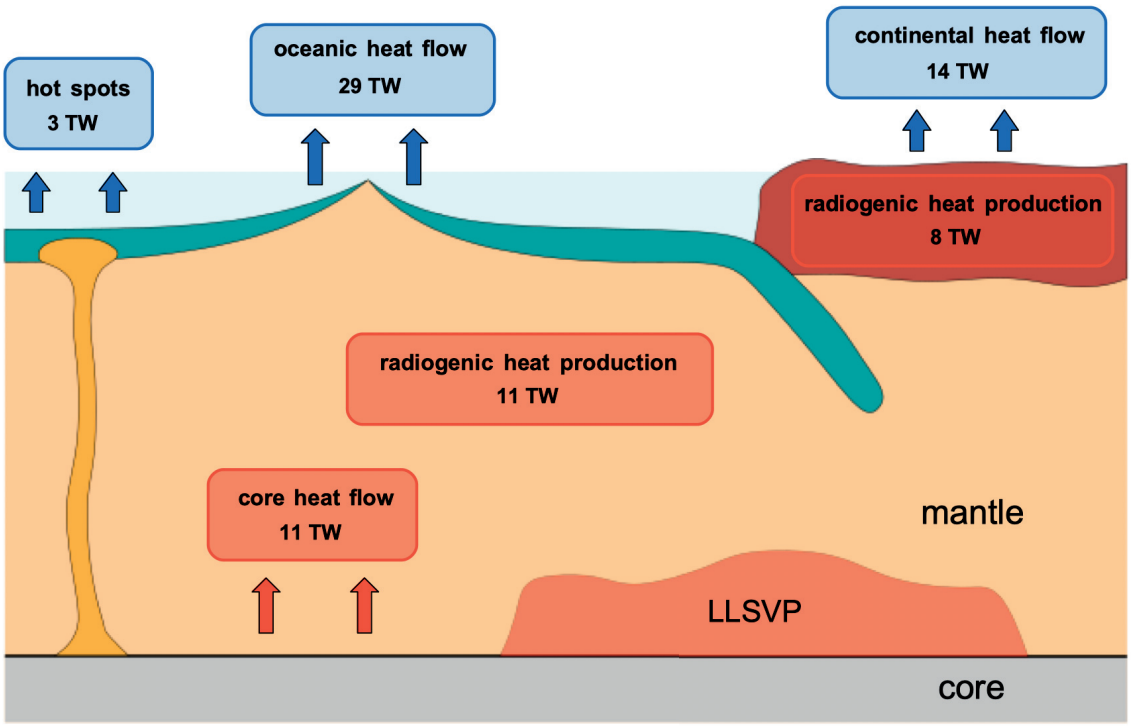

Figure 1.12: Earth's present-day surface heat flow and heat sources after Jaupart et al. (2015).

back in time, beyond Pangea, will serve as another way of studying the coupling between supercontinent formation, surface heat flow and mantle temperature variations.

1.4 Outstanding Questions

The review of relevant literature in this chapter has led to some outstanding questions. These questions serve as some of the primary motivation, and core focus, of this thesis' work:

- The deep water cycle is driven by plate tectonics, so how does fluctuations in the tectonic rates (i.e. the rates of seafloor spreading and consumption) affect the magnitude of the deep water fluxes? How are they affected by major plate tectonic events like the breakup of a supercontinent?
- Modern full-plate tectonic reconstructions provide models for how every piece of Earth's surface has moved, from its creation at a mid-ocean ridge, until its destruction and a subduction zone for the past 410 Myr. These constraints uniquely determine the age of the oceanic lithosphere. So why does paleo-seafloor age grids only extend back to 250 Ma?

- The most recent of the two peaks observed in the Phanerozoic sea level record (Fig. 1.10) has been explained by variations in mid-ocean ridge spreading rates producing young and shallow seafloor. Is the pre-Pangea peak caused by similar processes?
- Mantle cooling rates are often inferred based on present-day values of heat sinks and sources which might not be representative for Earth's long-term behavior. Of these heat budget terms, the oceanic heat flow is the most likely to exhibit large fluctuations on the time scales of plate tectonics. What is the typical (time-averaged) value of oceanic heat flow?
- The distribution of continental landmasses, and their assembly into supercontinents, provide very uneven insulation of Earth's interior. How did the last supercontinent cycle affect mantle cooling patterns?

Brief answers to these questions are provided in the next chapter (Section 2.2), while more elaborate answers can be found in the three research papers that are part of this thesis.

References

Becker, T. W. and Boschi, L. (2002). "A comparison of tomographic and geodynamic mantle models". In: *Geochemistry, Geophysics, Geosystems* vol. 3, no. 1.

Bolfan-Casanova, N. (2005). "Water in the Earth's mantle". In: *Mineralogical Magazine* vol. 69, no. 3, pp. 229–257.

Boulila, S., Laskar, J., Haq, B. U., Galbrun, B., and Hara, N. (2018). "Long-term cyclicities in Phanerozoic sea-level sedimentary record and their potential drivers". In: *Global and Planetary Change* vol. 165, pp. 128–136.

Bradley, D. C. (2008). "Passive margins through earth history". In: *Earth-Science Reviews* vol. 91, no. 1-4, pp. 1–26.

Bullard, E., Maxwell, A., and Revelle, R. (1956). "Heat flow through the deep sea floor". In: *Advances in geophysics*. Vol. 3. Elsevier, pp. 153–181.

Bullard, E. C. (1949). "The magnetic field within the Earth". In: *Proceedings of the Royal Society of London. Series A. Mathematical and Physical Sciences* vol. 197, no. 1051, pp. 433–453.

Burke, K., Steinberger, B., Torsvik, T. H., and Smethurst, M. A. (2008). "Plume generation zones at the margins of large low shear velocity provinces on the core–mantle boundary". In: *Earth and Planetary Science Letters* vol. 265, no. 1-2, pp. 49–60.

Burke, K. and Torsvik, T. H. (2004). "Derivation of large igneous provinces of the past 200 million years from long-term heterogeneities in the deep mantle". In: *Earth and Planetary Science Letters* vol. 227, no. 3-4, pp. 531–538.

Chotalia, K., Cagney, N., Lithgow-Bertelloni, C., and Brodholt, J. (2020). "The coupled effects of mantle mixing and a water-dependent viscosity on the surface ocean". In: *Earth and Planetary Science Letters* vol. 530, p. 115881.

Conrad, C. P. (2013). “The solid Earth’s influence on sea level”. In: *Geological Society of America Bulletin* vol. 125, no. 7-8, pp. 1027–1052.

Cox, A., Doell, R. R., and Dalrymple, G. B. (1963). “Geomagnetic polarity epochs and Pleistocene geochronometry”. In: *Nature* vol. 198, no. 4885, pp. 1049–1051.

Crameri, F., Conrad, C. P., Montési, L., and Lithgow-Bertelloni, C. R. (2019). “The dynamic life of an oceanic plate”. In: *Tectonophysics* vol. 760, pp. 107–135.

Creer, K., Irving, E., and Runcorn, S. (1954). “The direction of the geomagnetic field in remote epochs in Great Britain”. In: *Journal of geomagnetism and geoelectricity* vol. 6, no. 4, pp. 163–168.

Crowley, J. W., Gérault, M., and O’Connell, R. J. (2011). “On the relative influence of heat and water transport on planetary dynamics”. In: *Earth and Planetary Science Letters* vol. 310, no. 3, pp. 380–388.

Dauphas, N. and Morbidelli, A. (2013). “Geochemical and planetary dynamical views on the origin of Earth’s atmosphere and oceans”. In: *arXiv preprint arXiv:1312.1202*.

Davies, J. H. (2013). “Global map of solid Earth surface heat flow”. In: *Geochemistry, Geophysics, Geosystems* vol. 14, no. 10, pp. 4608–4622.

Domeier, M. and Torsvik, T. H. (2014). “Plate tectonics in the late Paleozoic”. In: *Geoscience Frontiers* vol. 5, no. 3, pp. 303–350.

Domeier, M. and Torsvik, T. H. (2019). “Full-plate modelling in pre-Jurassic time”. In: *Geological Magazine* vol. 156, no. 2, pp. 261–280.

Eide, E. A. and Torsvik, T. H. (1996). “Paleozoic supercontinental assembly, mantle flushing, and genesis of the Kiaman Superchron”. In: *Earth and Planetary Science Letters* vol. 144, no. 3-4, pp. 389–402.

Ernst, R. E., Bleeker, W., Söderlund, U., and Kerr, A. C. (2013). *Large Igneous Provinces and supercontinents: Toward completing the plate tectonic revolution*.

Ernst, R. E. and Youbi, N. (2017). “How Large Igneous Provinces affect global climate, sometimes cause mass extinctions, and represent natural markers in the geological record”. In: *Palaeogeography, palaeoclimatology, palaeoecology* vol. 478, pp. 30–52.

Evans, D. A. (2003). “True polar wander and supercontinents”. In: *Tectonophysics* vol. 362, no. 1-4, pp. 303–320.

Faccenda, M., Gerya, T. V., Mancktelow, N. S., and Moresi, L. (2012). “Fluid flow during slab unbending and dehydration: Implications for intermediate-depth seismicity, slab weakening and deep water recycling”. In: *Geochemistry, Geophysics, Geosystems* vol. 13, no. 1.

Fu, S., Yang, J., Karato, S.-i., Vasiliev, A., Presniakov, M. Y., Gavriliuk, A. G., Ivanova, A. G., Hauri, E. H., Okuchi, T., Purevjav, N., et al. (2019). “Water concentration in single-crystal (Al, Fe)-bearing Bridgmanite grown from the hydrous melt: Implications for dehydration melting at the topmost lower mantle”. In: *Geophysical Research Letters* vol. 46, no. 17-18, pp. 10346–10357.

Goldreich, P. and Toomre, A. (1969). “Some remarks on polar wandering”. In: *Journal of Geophysical Research* vol. 74, no. 10, pp. 2555–2567.

Hallam, A. (1992). *Phanerozoic sea-level changes*. Columbia University Press.
Haq, B. U. and Al-Qahtani, A. M. (2005). "Phanerozoic cycles of sea-level change on the Arabian Platform". In: *GeoArabia* vol. 10, no. 2, pp. 127–160.
Haq, B. U. and Schutter, S. R. (2008). "A chronology of Paleozoic sea-level changes". In: *Science* vol. 322, no. 5898, pp. 64–68.
Hasterok, D. (2013). "A heat flow based cooling model for tectonic plates". In: *Earth and Planetary Science Letters* vol. 361, pp. 34–43.
Heirtzler, J. R. and Le Pichon, X. (1965). "Crustal structure of the mid-ocean ridges: 3. Magnetic anomalies over the mid-Atlantic ridge". In: *Journal of Geophysical Research* vol. 70, no. 16, pp. 4013–4033.
Herzberg, C., Condie, K., and Korenaga, J. (2010). "Thermal history of the Earth and its petrological expression". In: *Earth and Planetary Science Letters* vol. 292, no. 1-2, pp. 79–88.
Hirschmann, M. M. (2018). "Comparative deep Earth volatile cycles: The case for C recycling from exosphere/mantle fractionation of major (H2O, C, N) volatiles and from H2O/Ce, CO2/Ba, and CO2/Nb exosphere ratios". In: *Earth and Planetary Science Letters* vol. 502, pp. 262–273.
Hirschmann, M. and Kohlstedt, D. (2012). "Water in Earth's Mantle". In: *Phys. Today* vol. 65, no. 3, p. 40.
Hirth, G. and Kohlstedt, D. L. (1996). "Water in the oceanic upper mantle: implications for rheology, melt extraction and the evolution of the lithosphere". In: *Earth and Planetary Science Letters* vol. 144, no. 1-2, pp. 93–108.
Hoffman, P. F. (1989). "Speculations on Laurentia's first gigayear (2.0 to 1.0 Ga)". In: *Geology* vol. 17, no. 2, pp. 135–138.
Hoffman, P. F., Kaufman, A. J., Halverson, G. P., and Schrag, D. P. (1998). "A Neoproterozoic snowball earth". In: *science* vol. 281, no. 5381, pp. 1342–1346.
Hoffman, P. F., Abbot, D. S., Ashkenazy, Y., Benn, D. I., Brocks, J. J., Cohen, P. A., Cox, G. M., Creveling, J. R., Donnadieu, Y., Erwin, D. H., et al. (2017). "Snowball Earth climate dynamics and Cryogenian geology-geobiology". In: *Science Advances* vol. 3, no. 11, e1600983.
Holmes, A. (1931). "XVIII. Radioactivity and earth movements". In: *Transactions of the Geological Society of Glasgow* vol. 18, no. 3, pp. 559–606.
Inoue, T., Wada, T., Sasaki, R., and Yurimoto, H. (2010). "Water partitioning in the Earth's mantle". In: *Physics of the Earth and Planetary Interiors* vol. 183, no. 1-2, pp. 245–251.
Inoue, T., Kakizawa, S., Fujino, K., Kuribayashi, T., Nagase, T., Greaux, S., Higo, Y., Sakamoto, N., Yurimoto, H., Hattori, T., et al. (2016). "Hydrous bridgmanite: water storage capacity in the lower mantle". In: *Advances in High–Pressure Research-III: Towards Geodynamic Implications-20 16. Novosibirsk, Russia*, p. 13.
Jaupart, C., Labrosse, S., Lucazeau, F., and Mareschal, J. (2015). "Temperatures, heat and energy in the mantle of the earth". In: *Treatise on geophysics* vol. 7, pp. 223–270.
Karlsen, K. S., Conrad, C. P., Domeier, M., and Trønnes, R. G. (2021). "Spatiotemporal Variations in Surface Heat Loss Imply a Heterogeneous Mantle Cooling History". In: *Geophysical Research Letters*, e2020GL092119.

Korenaga, J., Planavsky, N. J., and Evans, D. A. (2017). "Global water cycle and the coevolution of the Earth's interior and surface environment". In: *Phil. Trans. R. Soc. A* vol. 375, no. 2094, p. 20150393.

Korenaga, T. and Korenaga, J. (2008). "Subsidence of normal oceanic lithosphere, apparent thermal expansivity, and seafloor flattening". In: *Earth and Planetary Science Letters* vol. 268, no. 1-2, pp. 41–51.

Le Pichon, X. (1968). "Sea-floor spreading and continental drift". In: *Journal of Geophysical Research* vol. 73, no. 12, pp. 3661–3697.

Leach, D. L., Bradley, D. C., Huston, D., Pisarevsky, S. A., Taylor, R. D., and Gardoll, S. J. (2010). "Sediment-hosted lead-zinc deposits in Earth history". In: *Economic Geology* vol. 105, no. 3, pp. 593–625.

Lenardic, A., Moresi, L., Jellinek, A., O'neill, C., Cooper, C., and Lee, C. (2011). "Continents, supercontinents, mantle thermal mixing, and mantle thermal isolation: Theory, numerical simulations, and laboratory experiments". In: *Geochemistry, Geophysics, Geosystems* vol. 12, no. 10.

Litasov, K., Ohtani, E., Langenhorst, F., Yurimoto, H., Kubo, T., and Kondo, T. (2003). "Water solubility in Mg-perovskites and water storage capacity in the lower mantle". In: *Earth and Planetary Science Letters* vol. 211, no. 1-2, pp. 189–203.

Loyd, S., Becker, T., Conrad, C., Lithgow-Bertelloni, C., and Corsetti, F. (2007). "Time variability in Cenozoic reconstructions of mantle heat flow: plate tectonic cycles and implications for Earth's thermal evolution". In: *Proceedings of the National Academy of Sciences* vol. 104, no. 36, pp. 14266–14271.

Marcilly, C. M., Torsvik, T. H., Domeier, M., and Royer, D. L. (In prep.). "New paleogeographic and degassing parameters for long-term carbon cycle models". unpublished.

Matthews, K. J., Maloney, K. T., Zahirovic, S., Williams, S. E., Seton, M., and Mueller, R. D. (2016). "Global plate boundary evolution and kinematics since the late Paleozoic". In: *Global and Planetary Change* vol. 146, pp. 226–250.

Matuyama, M. (1929). "On the direction of magnetisation of basalt in Japan, Tyosen and Manchuria". In: *Proceedings of the Imperial Academy* vol. 5, no. 5, pp. 203–205.

Mazza, S. E., Gazel, E., Bizimis, M., Moucha, R., Béguelin, P., Johnson, E. A., McAleer, R. J., and Sobolev, A. V. (2019). "Sampling the volatile-rich transition zone beneath Bermuda". In: *Nature* vol. 569, no. 7756, pp. 398–403.

Müller, R. D., Sdrolias, M., Gaina, C., Steinberger, B., and Heine, C. (2008). "Long-term sea-level fluctuations driven by ocean basin dynamics". In: *science* vol. 319, no. 5868, pp. 1357–1362.

Müller, R. D., Seton, M., Zahirovic, S., Williams, S. E., Matthews, K. J., Wright, N. M., Shephard, G. E., Maloney, K. T., Barnett-Moore, N., Hosseinpour, M., et al. (2016). "Ocean basin evolution and global-scale plate reorganization events since Pangea breakup". In: *Annual Review of Earth and Planetary Sciences* vol. 44, pp. 107–138.

Müller, R. D., Zahirovic, S., Williams, S. E., Cannon, J., Seton, M., Bower, D. J., Tetley, M. G., Heine, C., Le Breton, E., Liu, S., et al. (2019). "A global plate

model including lithospheric deformation along major rifts and orogens since the Triassic". In: *Tectonics* vol. 38, no. 6, pp. 1884–1907.

McGovern, P. J. and Schubert, G. (1989). "Thermal evolution of the Earth: effects of volatile exchange between atmosphere and interior". In: *Earth and planetary science letters* vol. 96, no. 1-2, pp. 27–37.

Mitchell, R., Zhnag, N., Salminen, J., Liu, Y., Spencer, C., Steinberger, B., Murphy, B., and Zheng-Xian, L. (2021). "The supercontinent cycle". In: *Nature Reviews. Earth & Environments.*

Morgan, W. J. (1971). "Convection plumes in the lower mantle". In: *Nature* vol. 230, no. 5288, pp. 42–43.

Morgan, W. J. (1972). "Plate motions and deep mantle convection". In: *Geological Society of America Memoirs* vol. 132, pp. 7–22.

Nakagawa, T., Iwamori, H., Yanagi, R., and Nakao, A. (2018). "On the evolution of the water ocean in the plate-mantle system". In: *Progress in Earth and Planetary Science* vol. 5, no. 1, pp. 1–16.

Nakagawa, T., Nakakuki, T., and Iwamori, H. (2015). "Water circulation and global mantle dynamics: Insight from numerical modeling". In: *Geochemistry, Geophysics, Geosystems* vol. 16, no. 5, pp. 1449–1464.

Nance, R. D., Worsley, T. R., and Moody, J. B. (1986). "Post-Archean biogeochemical cycles and long-term episodicity in tectonic processes". In: *Geology* vol. 14, no. 6, pp. 514–518.

Oliver, J. and Isacks, B. (1967). "Deep earthquake zones, anomalous structures in the upper mantle, and the lithosphere". In: *Journal of Geophysical Research* vol. 72, no. 16, pp. 4259–4275.

Parai, R. and Mukhopadhyay, S. (2012). "How large is the subducted water flux? New constraints on mantle regassing rates". In: *Earth and Planetary Science Letters* vol. 317, pp. 396–406.

Parsons, B. and Sclater, J. G. (1977). "An analysis of the variation of ocean floor bathymetry and heat flow with age". In: *Journal of geophysical research* vol. 82, no. 5, pp. 803–827.

Pastor-Galán, D., Nance, R. D., Murphy, J. B., and Spencer, C. J. (2019). "Supercontinents: myths, mysteries, and milestones". In: *Geological Society, London, Special Publications* vol. 470, no. 1, pp. 39–64.

Peslier, A. H., Schönbächler, M., Busemann, H., and Karato, S.-I. (2017). "Water in the Earth's interior: distribution and origin". In: *Space Science Reviews* vol. 212, no. 1, pp. 743–810.

Piper, J. (1974). "Proterozoic crustal distribution, mobile belts and apparent polar movements". In: *Nature* vol. 251, no. 5474, pp. 381–384.

Piper, J. (1975). "Proterozoic supercontinent: time duration and the Grenville problem". In: *Nature* vol. 256, no. 5517, pp. 519–520.

Pollack, H. N., Hurter, S. J., and Johnson, J. R. (1993). "Heat flow from the Earth's interior: analysis of the global data set". In: *Reviews of Geophysics* vol. 31, no. 3, pp. 267–280.

Price, M. G., Davies, J., and Panton, J. (2019). "Controls on the Deep-Water Cycle Within Three-Dimensional Mantle Convection Models". In: *Geochemistry, Geophysics, Geosystems* vol. 20, no. 5, pp. 2199–2213.

Ranero, C. R. and Sallarès, V. (2004). "Geophysical evidence for hydration of the crust and mantle of the Nazca plate during bending at the north Chile trench". In: *Geology* vol. 32, no. 7, pp. 549–552.

Sandu, C., Lenardic, A., and McGovern, P. (2011). "The effects of deep water cycling on planetary thermal evolution". In: *Journal of Geophysical Research: Solid Earth* vol. 116, no. B12.

Stein, C. A. and Stein, S. (1992). "A model for the global variation in oceanic depth and heat flow with lithospheric age". In: *Nature* vol. 359, no. 6391, pp. 123–129.

Steinberger, B., Sutherland, R., and O'connell, R. J. (2004). "Prediction of Emperor-Hawaii seamount locations from a revised model of global plate motion and mantle flow". In: *Nature* vol. 430, no. 6996, pp. 167–173.

Steinberger, B. and Torsvik, T. H. (2008). "Absolute plate motions and true polar wander in the absence of hotspot tracks". In: *Nature* vol. 452, no. 7187, pp. 620–623.

Sykes, L. R. (1967). "Mechanism of earthquakes and nature of faulting on the mid-oceanic ridges". In: *Journal of Geophysical Research* vol. 72, no. 8, pp. 2131–2153.

Tegner, C., Andersen, T. B., Kjøll, H. J., Brown, E. L., Hagen-Peter, G., Corfu, F., Planke, S., and Torsvik, T. H. (2019). "A mantle plume origin for the Scandinavian dyke complex: A "piercing point" for 615 Ma plate reconstruction of Baltica?" In: *Geochemistry, Geophysics, Geosystems* vol. 20, no. 2, pp. 1075–1094.

Torsvik, T. H. and Cocks, L. R. M. (2016). *Earth History and Palaeogeography*. Cambridge University Press.

Torsvik, T. H., Müller, R. D., Van der Voo, R., Steinberger, B., and Gaina, C. (2008a). "Global plate motion frames: toward a unified model". In: *Reviews of geophysics* vol. 46, no. 3.

Torsvik, T. H., Steinberger, B., Ashwal, L. D., Doubrovine, P. V., and Trønnes, R. G. (2016). "Earth evolution and dynamics—a tribute to Kevin Burke". In: *Canadian Journal of Earth Sciences* vol. 53, no. 11, pp. 1073–1087.

Torsvik, T. H., Steinberger, B., Cocks, L. R. M., and Burke, K. (2008b). "Longitude: linking Earth's ancient surface to its deep interior". In: *Earth and Planetary Science Letters* vol. 276, no. 3-4, pp. 273–282.

Torsvik, T. H., Van der Voo, R., Preeden, U., Mac Niocaill, C., Steinberger, B., Doubrovine, P. V., Van Hinsbergen, D. J., Domeier, M., Gaina, C., Tohver, E., et al. (2012). "Phanerozoic polar wander, palaeogeography and dynamics". In: *Earth-Science Reviews* vol. 114, no. 3-4, pp. 325–368.

Turcotte, D. L. and Schubert, G. (2002). *Geodynamics*. Cambridge university press.

Valentine, J. and Moores, E. (1970). "Plate-tectonic regulation of faunal diversity and sea level: a model". In: *Nature* vol. 228, no. 5272, pp. 657–659.

Van Der Meer, D. G., Spakman, W., Van Hinsbergen, D. J., Amaru, M. L., and Torsvik, T. H. (2010). "Towards absolute plate motions constrained by lower-mantle slab remnants". In: *Nature Geoscience* vol. 3, no. 1, pp. 36–40.

van Keken, P. E., Hacker, B. R., Syracuse, E. M., and Abers, G. A. (2011). "Subduction factory: 4. Depth-dependent flux of H2O from subducting slabs worldwide". In: *Journal of Geophysical Research: Solid Earth* vol. 116, no. B1.

Vine, F. J. and Matthews, D. H. (1963). "Magnetic anomalies over oceanic ridges". In: *Nature* vol. 199, no. 4897, pp. 947–949.

Voice, P. J., Kowalewski, M., and Eriksson, K. A. (2011). "Quantifying the timing and rate of crustal evolution: global compilation of radiometrically dated detrital zircon grains". In: *The Journal of Geology* vol. 119, no. 2, pp. 109–126.

Wallmann, K. (2001). "The geological water cycle and the evolution of marine δ18O values". In: *Geochimica et Cosmochimica Acta* vol. 65, no. 15, pp. 2469–2485.

Wegener, A. (1912). "Die entstehung der kontinente". In: *Geologische Rundschau* vol. 3, no. 4, pp. 276–292.

Wilson, J. T. (1963). "Evidence from islands on the spreading of ocean floors". In: *Nature* vol. 197, no. 4867, pp. 536–538.

Wilson, J. T. (1965). "A new class of faults and their bearing on continental drift". In: *Nature* vol. 207, no. 4995, pp. 343–347.

Worsley, T. R., Nance, R. D., and Moody, J. B. (1986). "Tectonic cycles and the history of the Earth's biogeochemical and paleoceanographic record". In: *Paleoceanography* vol. 1, no. 3, pp. 233–263.

Worsley, T., Moody, J., and Nance, R. (1985). "Proterozoic to Recent tectonic tuning of biogeochemical cycles". In: *The carbon cycle and atmospheric CO2: natural variations Archean to present* vol. 32, pp. 561–572.

Worsley, T., Nance, R., and Moody, J. (1982). "Plate tectonic episodicity: a deterministic model for periodic "Pangeas"". In: *Eos, Transactions of the American Geophysical Union* vol. 65, no. 45, p. 1104.

Zhong, S., Zhang, N., Li, Z.-X., and Roberts, J. H. (2007). "Supercontinent cycles, true polar wander, and very long-wavelength mantle convection". In: *Earth and Planetary Science Letters* vol. 261, no. 3-4, pp. 551–564.

Chapter 2

Conclusions

Earth's seafloor is created and consumed at a rate that mainly varies between $6-3$ km^2/yr, implying that the ocean basins are replaced (on average) every $60-120$ Myr. These "rates of plate tectonics" manifest themselves in a range of geodynamic processes, including the efficiency of ocean-mantle water exchange, sea level change and surface heat flow and mantle cooling (Fig. 2.1). In this

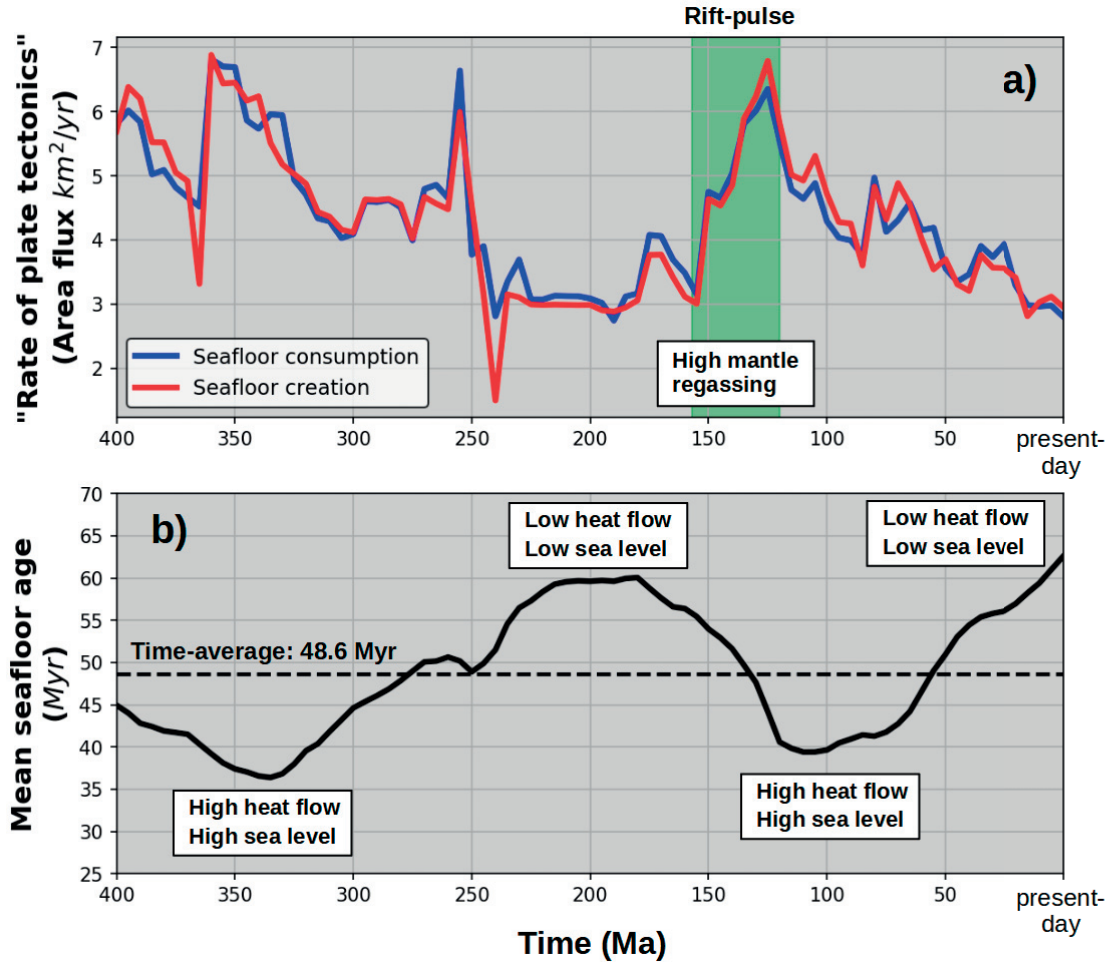

Figure 2.1: The rates of plate tectonics (i.e. seafloor generation and consumption) control the age of the seafloor, affecting a range of geodynamic processes. Here compared with highs and lows in mantle regassing, sea level and the rate of surface heat flow after Karlsen et al. (2019), Karlsen et al. (2020) and Karlsen et al. (2021).

chapter I will summarize our research into interplay between plate tectonics and geodynamic processes, revisit a provoking question and share my thoughts on future directions.

2.1 Summary of Results

2.1.1 Paper I - Deep Water Cycling and Sea Level Change

van Keken et al. (2011) combined constraints on plate boundary dynamics (i.e. length of subduction zones, subduction velocity and plate age) with finite element modeling to estimate the present-day mantle regassing rates. By analyzing their results, we found that the resulting deep subduction water fluxes could to a large extent be explained merely in terms of the key plate boundary parameters: subduction zone length and velocity, and plate age (Fig. I.3). Since these three quantities can be inferred for past subduction zones by combining plate tectonic reconstructions and paleo-seafloor age grids, we identified a way for estimating the deep subduction water fluxes back in time. Because the ultimate goal of the study was to calculate sea level change associated with deep water cycling, the mantle degassing flux had to be estimated as well. To accomplish this, we assumed that the main gateways for ocean-mantle water exchange was the subduction zones and mid-ocean ridges. This assumption was partly motivated by the fact that the amount of water outgassed due to intra-plate volcanism is very poorly constrained (Hirschmann, 2018), and partly because the rate of intra-plate volcanism cannot be inferred for the past (like mid-ocean ridge spreading rate can). To compensate for the lacking estimate of intra-plate mantle degassing, we assumed a relatively high rate of mid-ocean ridge water degassing.

By combining the parameterization we developed for the deep subduction water flux based the results of van Keken et al. (2011), with a simple paramterization for the mid-ocean ridge degassing flux (based on ridge length and spreading rate) we estimated ocean-mantle water exchange for the past 230 Myr, using tectonic reconstructions of Müller et al. (2016). In particular, we studied the sea level implications of three different cases: a case where regassing and degassing presently balance, a case which causes zero net sea level change, and a regassing-dominated present-day scenario (Fig. I.4).

The present-day balance case suggested a sea level drop of ~ 30 m over the past 230 Myr. We find that to achieve zero net sea level change over this period, degassing currently has to be about 33 % larger than regassing (in conflict with present-day estimates of the deep water fluxes). The regassing-dominated scenario predicts a sea level drop of ~ 130 m over the past 230 Myr. In the light of other work on the deep water fluxes, which suggests a regassing-dominated present-day (e.g. Peslier et al., 2017 for a review), we consider the larger sea level drop scenario possible. To further test the plausibility of this case, we assembled a sea level budget for the past 230 Myr, which included the other major sea level changing mechanisms, and found that including a sea level drop

of $\sim$ 130 m associated with deep water cycling yielded an improved agreement with the sea level record (Fig. I.7).

2.1.2 Paper II - Seafloor Age Grids and Paleozoic Sea Level

Modern, so called "full-plate tectonic reconstructions", provide models for how every piece of oceanic lithosphere has moved, from its creation at a ridge until its destruction at a subduction zone, for a given time-interval. This information can be used to uniquely determine the age of the oceanic lithosphere for a given plate model. However, due to the lack of an automated and efficient method for generating global seafloor age grids, full-plate tectonic reconstructions currently (at the time of writing this paper) extend back to the mid-Paleozoic (410 Ma, Matthews et al., 2016; Young et al., 2019), while paleo-seafloor age grids only extend back to 250 Ma (Müller et al., 2019). To fill this "age gap" we developed an algorithm, presented as a Python-package, which allows oceanic lithosphere age grids to be automatically generated from plate tectonic reconstructions.

The algorithm is based on tracers, i.e. numerical particles that follow streamlines formed by the plate velocity field at the surface. To determine the age of the oceanic lithosphere, zero-age tracers are added along the mid-ocean ridges at the beginning of each time-step, and then moved according to the plate velocities until they cross a subduction zone and are terminated. The output of the algorithm is distributions of tracers with varying age across the ocean basins, which are then interpolated on to a regular grid. To test the algorithm we had developed, we generated seafloor age grids back to 400 Ma based on the plate tectonic reconstructions of Matthews et al. (2016), providing the first set of oceanic lithosphere age grids for the Paleozoic ocean basins. We then benchmarked the age grids against a previously published paleo-seafloor age model that extends back to 230 Ma (Müller et al., 2016; Fig. II.6), and against ages inferred from magnetic anomaly data (Seton et al., 2014; Fig. II.5).

To show an application of our novel paleo-seafloor age grids, we computed changes in ocean depth and sediment thickness (which also has an age-dependence) back to 400 Ma and compared them to the sea level record as inferred from sedimentary stratigraphy (Hallam, 1992; Haq and Al-Qahtani, 2005; Haq and Schutter, 2008). The comparison showed good agreement between seafloor depth inferred from our new age grids and the sea level history estimates from proxies all the way back to 400 Ma (Fig. II.7), providing a possible explanation for the peak in sea level during the assembly phase of Pangea. This demonstrates how our automated age grid algorithm allows plate tectonic scenarios (models) to be compared almost directly to the sea level record, which extends much further back in time than the constraints from preserved seafloor. Thus, our algorithm may aid the further development of plate tectonic reconstructions by strengthening the links to geological observations of deeper time.

2.1.3 Paper III - Surface Heat Flow and Mantle Cooling

The newly developed age grid algorithm of Karlsen et al. (2020) allowed us to study spatial and temporal variations in surface heat flow back to the mid-Paleozoic. By applying the oceanic lithosphere age-heat flow relation of Hasterok (2013) to paleo-seafloor age grids generated by the method of Karlsen et al. (2020), we reconstructed patterns of oceanic mantle heat loss for the past 400 Myr. To cover heat loss through the continental regions, we assumed a mantle heat loss of 6 TW (Jaupart et al., 2015) evenly spread out over the continental area. Our reconstructed history of mantle heat loss immediately showed two things: i) the present-day mantle heat loss is unusually low and ii) the Pacific side of the world has lost heat at a much higher rate than the African side for most of the last 400 Myr.

Previous studies have also noted the present-day low mantle heat loss, although based on significantly shorter time-histories (back to 230 Ma, Crameri et al., 2019; Loyd et al., 2007). The longer record of heat flow provided by our study might be important due to variations in the seafloor's age-area distribution associated with different phases of the supercontinent cycle (Coltice et al., 2012; Nance et al., 1986; Worsley et al., 1986; Worsley et al., 1985). Thus, in order to derive a representative value of the long-term oceanic heat loss, it may be necessary to compute a time-averaged value across a wider swath of time, approximating a full supercontinent cycle. Based on our 400 Myr reconstruction of seafloor ages, we estimate the time-averaged value for oceanic heat loss to be 36.6 TW (Fig. III.1), which is ~ 25 % higher than the present-day value of ~ 29 TW. By adopting a heat budget for the mantle after Jaupart et al. (2015), we calculated the mantle cooling rate associated with this time-averaged rate of heat loss, and found it to be 149 K/Gyr. This cooling rate for the mantle is higher than some previous estimates (Jaupart et al., 2015), but still compatible with petrological estimates of mantle temperature for the past 1 Gyr (Herzberg et al., 2010).

To study the spatial distributions in surface heat loss, we divided the mantle into two domains; separated by the 60° W and 120° E meridians (Fig. III.2). These meridians approximately follow the circumpolar belt of seismically-observed slab material, which delineates a curtain of downwelling flow in the mantle that separates the two hemispheres and prevents heat transfer between them (Torsvik et al., 2016). Heat loss computed from these two domains suggests that the Pacific mantle hemisphere has lost heat at a time-averaged rate of 27.5 TW, while its African counterpart has lost heat at a rate of 18.1 TW on average. In terms of mantle cooling, the respective cooling rates are 208 K/Gyr and 90 K/Gyr, with the Pacific mantle having cooled more than twice as fast on average. This implies a differential in mantle cooling of almost 50 K since the mid-Paleozoic, caused by the long-lasting uneven distribution fast-spreading ridges and area covered by cooling oceanic crust between the Pacific and African sides of the world.

The high Pacific heat flow (compared to the African) may be the manifestation of a hotter mantle beneath (Brandl et al., 2013; Dalton et al., 2014; Van Avendonk et al., 2017), with the initial heating provided by supercontinental thermal insulation (e.g., Lenardic et al., 2011) by the long-lived Precambrian supercontinent Rodinia, which may have covered the paleo-Pacific (Panthalassic) mantle domain (e.g., Tegner et al., 2019). This "enduring hotter Pacific"-scenario could explain the consistently higher plate velocities of the Pacific hemisphere during the past 400 Myr (Fig. III.9), because a hotter mantle implies lower mantle viscosity and smaller resistance to plate motions.

2.2 Brief Answers to Outstanding Questions

The Introduction chapter was concluded with a list of outstanding questions (Section 1.4). Here I provide brief answers to these questions based on the research conducted over the course of this PhD project:

- Fluctuations in the (tectonic) rates of seafloor generation and consumption affect the mantle degassing rate and regassing rate differently. If they did not; the net-flux of water to the mantle would always be the same. This is because the tectonic rates always approximately balance to conserve the area of the Earth (Fig. 2.1a). More specifically: the regassing flux is much more sensitive to an increase in subduction velocity than the degassing flux is to an increase in spreading rate. The reason for this is that the subduction velocity affects both i) the rate of slab volume transported to the deep mantle and ii) the slab water content (through its effect on the thermal structure), while the mantle degassing rate is approximately linear in spreading rate. The difference in plate kinematic-dependence of mantle regassing and degassing causes rift-pulses, forcing rapid subduction (Fig. I.1 F,G), to be time-periods associated with a large net-flux of water to the mantle (Fig. I.4 B,F).

- Plate tectonic reconstructions are continuously updated and refined as new geological information becomes available, and since the construction of global paleo-seafloor age grids from these models presents a tedious and labor intensive task, many plate models are published an accompanying set of age models for oceanic lithosphere. The automated method of Karlsen et al. (2020) will hopefully be a great aid to the community, allowing seafloor age grids to be easily generated from plate tectonic reconstructions as they evolve.

- The development of paleo-sealoor age grids that extend back to the mid-Paleozoic (Karlsen et al., 2020) allowed us to investigate tectonically driven sea level dynamics during the assembly phase of Pangea. Our analysis showed that variations in the age of the ocean basins, causing changes

in seafloor depth, exhibit a remarkable correlation with the Phanerozoic sea level record (Fig. II.7). Thus, ocean basin volume changes have likely controlled sea level to the first order all the way back to 400 Ma, explaining the pre-Pangea sea level peak in terms of spreading rate variations.

- Over the past 400 Myr, variations in oceanic heat flow ranged from a maximum of $\sim$ 44 TW during the assembly phase of Pangea (350 Ma), to an all-time low of $\sim$ 29 TW at present-day, with a time-averaged value over the supercontinent cycle of 36.6 TW (Fig. III.1). This contributes to a total heat loss which exceeds that gained from mantle heat sources, and we estimate overall cooling of 149 K/Gyr since 400 Ma, consistent with estimates of mantle temperature during the past 1 Gyr (Herzberg et al., 2010; Fig. III.6).
- The last 400 Myr of Earth's tectonic history are dominated by the assembly of Pangea on the African hemisphere, leaving the Pacific hemisphere stripped of continental landmasses. This had profound effects on surface heat flow and mantle cooling. The uneven distribution of continents and mid-ocean ridges that resulted from this tectonic event led to a long-lasting fast cooling of the Pacific mantle, and over the last 400 Myr the Pacific mantle hemisphere may have cooled almost 50 degrees more than its African counterpart.

2.3 Is the Present Really Key to the Past?

Although there is a great deal to be learned about the past from the present state of the Earth, we should be cautious and recognize that this narrative has its limitations.

A style of mantle convection called "plate tectonics". Dispersed continents. Seafloor creation at a rate of $\sim$ 3 km^2/yr. Mean oceanic crustal age of $\sim$ 63 Myr. This is Earth's present tectonic state, but it has not always been. All of these states and parameters have changed greatly over Earth's history, and this has, without a doubt, had important implications for a range of geodynamic processes. Here we have shown that ocean-mantle water exchange has been highly variable since the breakup of Pangea, and that ocean basin volume changes has driven sea level variations with amplitudes of several hundred meters since the mid-Paleozoic. We have also shown that Earth's present-day rate of surface heat loss and associated mantle cooling is not representative for Earth's history.

What we can learn from this is that, if we were to pick any other time in history, we would likely view these geodynamic processes and their implications for the Earth system differently. An eye-witness of the 120 Ma-Earth might argue that the continents tend to stay relatively closely together, that the rates of seafloor spreading, sea level and surface heat flow is generally very high (Fig. 2.1), the ocean basins young and that the mantle is cooling at a rate of 170 K/Gyr (rather than the $\sim$ 100 K/Gyr proposed for the present-day, Fig. III.3).

This brief section is merely intended as a remainder that the present-day is just a snapshot in time, part of a complex and strongly time-dependent planetary evolution. Because this particular snapshot is by far the best resolved, it can greatly contribute to our understanding of Earth, but it must be considered in the light of our planet's ever-changing dynamics.

2.4 Future Directions

Estimates of the present-day deep subduction water flux still very much rely on the now 10 year old study of van Keken et al. (2011). Considering the continuous improvement of the quality of experimental and geophysical data, as well as advances computational power and methods, it is time to revisit the present-day mantle regassing rates. As for the time-dependence of these rates, combining models of global mantle convection with plate tectonic reconstructions remains an unexplored avenue in terms of constraining the deep water fluxes (Li et al., 2016 did this for CO_2 degassing). Another possibility is to extend the analysis of Karlsen et al. (2019) back to the mid-Paleozoic (400 Ma), using the novel paleo-seafloor age grids of Karlsen et al. (2020). Furthermore, the methodology developed by Karlsen et al. (2019) allows maps of past water fluxes to be made. These can in turn be used to predict regions in the mantle where more water may be stored, and compared to geophysical constraints on lateral variations in mantle water content (Houser, 2016) and possibly to areas of increased activity of intra-plate volcanism (Yang and Faccenda, 2020). The further development of parameterized mantle convection models that track long-term variations in the ocean water mass (along the lines of Chotalia et al., 2020) could be used to gain a better understanding of the sea level implications of deep water cycling on Earth-history time scales.

Karlsen et al. (2021) assumed that subduction history has limited thermal mixing by convection in the mantle between the Pacific and African hemisphere, through the formation of persistent downwellings between these domains. This assumption can be investigated in mantle convection models constrained by plate kinematics at the surface, and reveal if subduction history has caused the Pacific and African mantle domains to have distinct thermal histories. Analysis of the geographical distribution of non-arc lavas which provide petrological estimates of mantle temperature (like those presented in Herzberg et al., 2010), may reveal (or dismiss) hemispheric variations in mantle cooling. Better constraints on the distribution of heat producing elements and spatial variations in the core-mantle boundary heat would be important to disregard the possibility that the long-lived high Pacific heat flow could be the manifestation of an uneven distribution of mantle heat sources. Finally, improved plate kinematic constraints on pre-Pangea supercontinents will be useful to further decipher the effects of plate tectonic cycles on surface heat flow and mantle cooling patterns.

2.5 Popular Science Coverage

Our first paper was picked up by **New Scientist** who wrote a story about it. From there, several other interviews followed, including **Live Science** and **NRK Viten**. A story about the second paper was featured on **Forskning.no**, in addition to a **blog-post** on our research group's website. The third and final paper received by far the most media attention, with stories in **New Scientist**, **Popular Mechanics**, **Phys.org**, **IFL Science**, **Forskning.no** and about 20 other news outlets. References to a selection of these popular science articles are included at the very end of this chapter.

References

Brandl, P. A., Regelous, M., Beier, C., and Haase, K. M. (2013). "High mantle temperatures following rifting caused by continental insulation". In: *Nature Geoscience* vol. 6, no. 5, pp. 391–394.

Chotalia, K., Cagney, N., Lithgow-Bertelloni, C., and Brodholt, J. (2020). "The coupled effects of mantle mixing and a water-dependent viscosity on the surface ocean". In: *Earth and Planetary Science Letters* vol. 530, p. 115881.

Coltice, N., Rolf, T., Tackley, P. J., and Labrosse, S. (2012). "Dynamic causes of the relation between area and age of the ocean floor". In: *Science* vol. 336, no. 6079, pp. 335–338.

Crameri, F., Conrad, C. P., Montési, L., and Lithgow-Bertelloni, C. R. (2019). "The dynamic life of an oceanic plate". In: *Tectonophysics* vol. 760, pp. 107–135.

Dalton, C. A., Langmuir, C. H., and Gale, A. (2014). "Geophysical and geochemical evidence for deep temperature variations beneath mid-ocean ridges". In: *Science* vol. 344, no. 6179, pp. 80–83.

Hallam, A. (1992). *Phanerozoic sea-level changes*. Columbia University Press.

Haq, B. U. and Al-Qahtani, A. M. (2005). "Phanerozoic cycles of sea-level change on the Arabian Platform". In: *GeoArabia* vol. 10, no. 2, pp. 127–160.

Haq, B. U. and Schutter, S. R. (2008). "A chronology of Paleozoic sea-level changes". In: *Science* vol. 322, no. 5898, pp. 64–68.

Hasterok, D. (2013). "A heat flow based cooling model for tectonic plates". In: *Earth and Planetary Science Letters* vol. 361, pp. 34–43.

Herzberg, C., Condie, K., and Korenaga, J. (2010). "Thermal history of the Earth and its petrological expression". In: *Earth and Planetary Science Letters* vol. 292, no. 1-2, pp. 79–88.

Hirschmann, M. M. (2018). "Comparative deep Earth volatile cycles: The case for C recycling from exosphere/mantle fractionation of major (H2O, C, N) volatiles and from H2O/Ce, CO2/Ba, and CO2/Nb exosphere ratios". In: *Earth and Planetary Science Letters* vol. 502, pp. 262–273.

Houser, C. (2016). "Global seismic data reveal little water in the mantle transition zone". In: *Earth and Planetary Science Letters* vol. 448, pp. 94–101.

Jaupart, C., Labrosse, S., Lucazeau, F., and Mareschal, J. (2015). "Temperatures, heat and energy in the mantle of the earth". In: *Treatise on geophysics* vol. 7, pp. 223–270.

Karlsen, K. S., Conrad, C. P., Domeier, M., and Trønnes, R. G. (2021). "Spatiotemporal Variations in Surface Heat Loss Imply a Heterogeneous Mantle Cooling History". In: *Geophysical Research Letters*, e2020GL092119.

Karlsen, K. S., Conrad, C. P., and Magni, V. (2019). "Deep Water Cycling and Sea Level Change Since the Breakup of Pangea". In: *Geochemistry, Geophysics, Geosystems* vol. 20, no. 6, pp. 2919–2935.

Karlsen, K. S., Domeier, M., Gaina, C., and Conrad, C. P. (2020). "A tracer-based algorithm for automatic generation of seafloor age grids from plate tectonic reconstructions". In: *Computers & Geosciences* vol. 140, p. 104508.

Lenardic, A., Moresi, L., Jellinek, A., O'neill, C., Cooper, C., and Lee, C. (2011). "Continents, supercontinents, mantle thermal mixing, and mantle thermal isolation: Theory, numerical simulations, and laboratory experiments". In: *Geochemistry, Geophysics, Geosystems* vol. 12, no. 10.

Li, M., Black, B., Zhong, S., Manga, M., Rudolph, M. L., and Olson, P. (2016). "Quantifying melt production and degassing rate at mid-ocean ridges from global mantle convection models with plate motion history". In: *Geochemistry, Geophysics, Geosystems* vol. 17, no. 7, pp. 2884–2904.

Loyd, S., Becker, T., Conrad, C., Lithgow-Bertelloni, C., and Corsetti, F. (2007). "Time variability in Cenozoic reconstructions of mantle heat flow: plate tectonic cycles and implications for Earth's thermal evolution". In: *Proceedings of the National Academy of Sciences* vol. 104, no. 36, pp. 14266–14271.

Matthews, K. J., Maloney, K. T., Zahirovic, S., Williams, S. E., Seton, M., and Mueller, R. D. (2016). "Global plate boundary evolution and kinematics since the late Paleozoic". In: *Global and Planetary Change* vol. 146, pp. 226–250.

Müller, R. D., Seton, M., Zahirovic, S., Williams, S. E., Matthews, K. J., Wright, N. M., Shephard, G. E., Maloney, K. T., Barnett-Moore, N., Hosseinpour, M., et al. (2016). "Ocean basin evolution and global-scale plate reorganization events since Pangea breakup". In: *Annual Review of Earth and Planetary Sciences* vol. 44, pp. 107–138.

Müller, R. D., Zahirovic, S., Williams, S. E., Cannon, J., Seton, M., Bower, D. J., Tetley, M. G., Heine, C., Le Breton, E., Liu, S., et al. (2019). "A global plate model including lithospheric deformation along major rifts and orogens since the Triassic". In: *Tectonics* vol. 38, no. 6, pp. 1884–1907.

Nance, R. D., Worsley, T. R., and Moody, J. B. (1986). "Post-Archean biogeochemical cycles and long-term episodicity in tectonic processes". In: *Geology* vol. 14, no. 6, pp. 514–518.

Peslier, A. H., Schönbächler, M., Busemann, H., and Karato, S.-I. (2017). "Water in the Earth's interior: distribution and origin". In: *Space Science Reviews* vol. 212, no. 1, pp. 743–810.

Seton, M., Whittaker, J. M., Wessel, P., Müller, R. D., DeMets, C., Merkouriev, S., Cande, S., Gaina, C., Eagles, G., Granot, R., et al. (2014). "Community infrastructure and repository for marine magnetic identifications". In: *Geochemistry, Geophysics, Geosystems* vol. 15, no. 4, pp. 1629–1641.

Tegner, C., Andersen, T. B., Kjøll, H. J., Brown, E. L., Hagen-Peter, G., Corfu, F., Planke, S., and Torsvik, T. H. (2019). "A mantle plume origin for the Scandinavian dyke complex: A "piercing point" for 615 Ma plate reconstruction of Baltica?" In: *Geochemistry, Geophysics, Geosystems* vol. 20, no. 2, pp. 1075–1094.

Torsvik, T. H., Steinberger, B., Ashwal, L. D., Doubrovine, P. V., and Trønnes, R. G. (2016). "Earth evolution and dynamics—a tribute to Kevin Burke". In: *Canadian Journal of Earth Sciences* vol. 53, no. 11, pp. 1073–1087.

Van Avendonk, H. J., Davis, J. K., Harding, J. L., and Lawver, L. A. (2017). "Decrease in oceanic crustal thickness since the breakup of Pangaea". In: *Nature Geoscience* vol. 10, no. 1, pp. 58–61.

van Keken, P. E., Hacker, B. R., Syracuse, E. M., and Abers, G. A. (2011). "Subduction factory: 4. Depth-dependent flux of H2O from subducting slabs worldwide". In: *Journal of Geophysical Research: Solid Earth* vol. 116, no. B1.

Worsley, T. R., Nance, R. D., and Moody, J. B. (1986). "Tectonic cycles and the history of the Earth's biogeochemical and paleoceanographic record". In: *Paleoceanography* vol. 1, no. 3, pp. 233–263.

Worsley, T., Moody, J., and Nance, R. (1985). "Proterozoic to Recent tectonic tuning of biogeochemical cycles". In: *The carbon cycle and atmospheric CO2: natural variations Archean to present* vol. 32, pp. 561–572.

Yang, J. and Faccenda, M. (2020). "Intraplate volcanism originating from upwelling hydrous mantle transition zone". In: *Nature* vol. 579, no. 7797, pp. 88–91.

Young, A., Flament, N., Maloney, K., Williams, S., Matthews, K., Zahirovic, S., and Müller, R. D. (2019). "Global kinematics of tectonic plates and subduction zones since the late Paleozoic Era". In: *Geoscience Frontiers* vol. 10, no. 3, pp. 989–1013.

Popular Science Articles

New Scientist `https://www.newscientist.com/article/2204528-the-oceans-are-very-slowly-draining-into-the-rock-below-earths-crust/`

Live Science `https://www.livescience.com/65678-deep-water-cycle-sinking-ocean.html`

NRK Viten `https://www.nrk.no/viten/verdenshavene-forsvinner-sakte-inn-under-jordskorpa-1.14566200`

Forskning.no `https://forskning.no/havet/havene-vare-er-pa-sitt-dypeste-pa-250-millioner-ar/1689949`

CEED Blog `https://www.mn.uio.no/ceed/english/about/blog/2020/charting-past-ocean-basins-tractec.html`

New Scientist `https://www.newscientist.com/article/2271233-one-si`

de-of-earths-interior-is-losing-heat-much-faster-than-the-other/

Popular Mechanics https://www.popularmechanics.com/science/a35841636/why-is-one-side-of-earth-losing-heat/

Phys.org https://phys.org/news/2021-03-earth-loss-higher-side-planet.html

IFL Science https://www.iflscience.com/environment/one-side-of-the-planet-is-cooling-much-faster-than-the-other/

Forskning.no https://forskning.no/geologi/den-ene-halvdelen-av-jordens-indre-har-tapt-mer-varme-enn-den-andre-de-siste-400-millioner-arene/1827471

Papers

Paper I

Deep Water Cycling and Sea Level Change Since the Breakup of Pangea

I

Krister S. Karlsen, Clinton P. Conrad, Valentina Magni

Published in *Geochemistry, Geophysics, Geosystems*, June 2019, DOI: 10.1029/2019GC008232.

Abstract

First-order variations in sea level exhibit amplitudes of ∼200 m over periods that coincide with those of supercontinental cycles (∼300-500 Myr). Proposed mechanisms for this sea level change include processes that change the container volume of the ocean basins and the relative elevation of continents. Here we investigate how unbalanced rates of water exchange between Earth's surface and mantle interior, resulting from fluctuations in tectonic rates, can cause sea level changes. Previous modeling studies of subduction water fluxes suggest that the amount of water that reaches sub-arc depths is well correlated with the velocity and age of the subducting plate. We use these models to calibrate a parameterization of the deep subduction water flux, which we together with a parameterization of mid-ocean ridge outgassing, then apply to reconstructions of Earth's tectonic history. This allows us to estimate the global water fluxes between the oceans and mantle for the past 230 Myr, and compute the associated sea level change. Our model suggests that a sea level drop of up to 130 m is possible over this period, and that it was partly caused by the ∼150 Ma rift-pulse that opened the Atlantic and forced rapid subduction of old oceanic lithosphere. This indicates that deep water cycling may be one of the more important sea level changing mechanisms on supercontinental time scales, and provides a more complete picture of the dynamic interplay between tectonics and sea level change.

Plain Language Summary

Cycles of global sea level change through Earth history exhibit amplitudes of several hundred meters and coincide with cycles in which Earth's continents were assembled into a single large landmass (supercontinent) and later dispersed. Previously proposed mechanisms for this sea level change include processes that change the container volume of the ocean basins and the relative elevation of continents. Here we investigate the possibility of sea level change due to a net flux of water into or out of the Earth's mantle. We expect some water flux out of diverging plate boundaries (here mid-ocean ridges), where volcanic outgassing occurs as plates move apart. This divergence is compensated at convergent boundaries where plates collide and sink into the mantle, carrying some water with them as they descend. By combining estimates of these water fluxes with models that describe how Earth's tectonic plates have moved for the past 230 Myr, we predict the amount of water exchanged between Earth's surface and its interior over this period. We find that the exchange of water between Earth's surface and its interior may have caused a sea level drop of up to ∼130 m over the past 230 Myr, making this process an important sea level changing mechanism on the time-scales of supercontinent cycles.

Contents

I.1 Introduction

Liquid water on Earth's surface constitutes the blue fingerprint of our planet within the Solar System, and is a key characteristic that is considered essential for life (Kasting and Catling, 2003) and the operation of plate tectonics (Korenaga, 2013). However, surface water amounts to only a fraction of Earth's total water content, as both hydrous and nominally anhydrous minerals store water within Earth's mantle (Hirschmann, 2006; Hirschmann and Kohlstedt, 2012). Recent estimates of Earth's mantle water content range from about one present-day ocean mass (OM = $1.4 \cdot 10^{21}$ kg) (Bodnar et al., 2013) to seven OM (Nestola

and Smyth, 2016). Even more extraordinary, water is not stationary in either of these reservoirs, but is recycled between them. Through subduction of sediments and hydrated oceanic lithosphere, water is transported from the oceans into the mantle (*regassing*), and returned to the exosphere (here oceans and atmosphere) through volcanism (*degassing*). For most of Earth history (Korenaga et al., 2017) and for the present-day (Peslier et al., 2017), the regassing flux is thought to be larger than the degassing flux. Therefore the ocean water mass should be time-dependent, not only due to variations in landbound water storage (ice and groundwater), but also due to imbalanced deep water cycling.

Sedimentary stratigraphy provides evidence (fairly consistent for the last 250 Myr, less so for deeper time) for global-scale cycles of sea level change throughout the Phanerozoic that coincide well with the supercontinental cycle (see e.g. Nance et al. (2014) and Fig. I.1A). The proposed mechanisms for these sea level variations include processes that change ocean basin container volume (changes to ocean area, the volume of spreading ridges, dynamic topography, and the emplacement or removal of sedimentary and volcanic materials) and those that affect the thermal elevation of continents, for example by trapping of heat beneath them (Conrad and Husson, 2009; Worsley et al., 1984). Imbalanced exchange of water between the Earth's oceans and its mantle can also change sea level (Ito et al., 1983; Parai and Mukhopadhyay, 2012), but the time history and amplitude of this imbalance remains poorly understood (Cloetingh and Haq, 2015; Conrad, 2013).

Here we investigate deep water recycling as an additional sea level-changing mechanism operating on the time scales of supercontinent cycles. Plate reconstruction models provide evidence for significant changes to the tectonics of ocean basins (Fig. I.1B-E), and the slabs that descend from them (Fig. I.1H-I) since Pangean times. Such variations have led to global changes in plate boundary lengths and rates associated with seafloor spreading and subduction during the last supercontinental cycle (Fig. I.1F-G). As an example, during the breakup phase of Pangea and the opening of the Atlantic ocean, the global mid-ocean ridge system doubled in length. The tectonic record (e.g., Matthews et al. (2016) and Müller et al. (2016)) suggests that this rift-pulse was compensated by rapid subduction of old oceanic lithosphere (Fig. I.1 F-G) around the margins of the ancient supercontinent. These constraints are critical for understanding water exchange between the oceans and Earth's interior because ridges and subduction zones represent the main gateways for deep water fluxes (Kelemen and Manning, 2015; Keller et al., 2017).

Parameterized models of whole mantle convection have been used to study deep water recycling over the history of the Earth (Crowley et al., 2011; Korenaga, 2011; McGovern and Schubert, 1989; Sandu et al., 2011). These models provide valuable insight into the gross hydrological evolution of an Earth-like planet, but are unable to capture changes on the 10^1-10^2 Myr time scales over which drastic variations in tectonic setting can occur (Fig. I.1B-I). Here we propose a

new and improved parameterization of the subduction water flux and apply it to the tectonic reconstructions of Müller et al. (2016). This allows us to infer time-dependent rates for the exchange of water between Earth's oceans and the mantle over the last 230 Myr, and enables us to better understand the interaction between tectonics, deep water cycling and sea level change.

I.2 Methods

I.2.1 Computing Deep Water Fluxes and Sea Level Change

The deep water cycle, and the evolution of Earth's interior and surface water reservoirs, can be constrained by combining flux estimates at the main gateways (ridges and trenches). However, determining the magnitudes of these fluxes is far from trivial; the amount of water that can be transported by a slab into the deep mantle depends on factors such as mantle temperature, slab lithology, slab age, initial water content and subduction velocity. Of the slab's initial water content, only a small fraction can be carried beyond the arc and recycled into the deeper mantle, while the rest is released to the arc via a series of metamorphic reactions. The timing of dehydration, and the mass of water that can be retained at a certain depth, have been studied using thermo-petrological models (Hacker, 2008; Rüpke et al., 2004; Syracuse et al., 2010; van Keken et al., 2011). These studies find that the amount of water retained at larger depths (> 200 km) is well correlated with both the age and velocity of the subducting plate (Magni et al., 2014), which suggests that the subduction water flux can be parameterized in terms of these quantities. This is mainly because old and fast slabs maintain a colder interior for longer compared to young and slow ones and, thus, have the potential to bring water to depths at which high pressure hydrous minerals (such as phase A) are stable. Moreover, the cold geotherm of an old plate allows for deep thermal cracking (Korenaga, 2007; Korenaga, 2017) and for deep normal faults at trenches (Faccenda et al., 2012; Ranero and Sallarès, 2004) that can enhance deep hydration of the lithospheric mantle in old plates.

For a subduction zone segment (Fig. I.2) with length L_S, convergence velocity v, plate thickness d, and density ρ, the rate of mass transport of oceanic plate into the mantle is given by $\rho v d L_S$ $[\frac{kg}{yr}]$. The rate of water transport into the mantle is then given by $\alpha \rho v d L_S$, where α is the non-dimensional *regassing factor* that relates to the plate's initial bulk water content. However, of the total initial water content, only a small fraction ϵ can be carried deep into the mantle because of a significant loss to arc volcanism. We then estimate the deep mantle water flux as $\alpha \epsilon \rho v d L_S$, where we compute the plate thickness from the plate age τ using the half-space cooling model (Parsons and Sclater, 1977) while enforcing a maximum thickness of 100 km, achieved at $\tau \sim 80$ Ma (Sclater et al., 1980).

Following previous studies (Garrels, 1983; Hirschmann, 2018; Marty and Tolstikhin, 1998; McGovern and Schubert, 1989), we assume that the degassing rate at mid-ocean ridges is proportional to the sea floor production rate. This

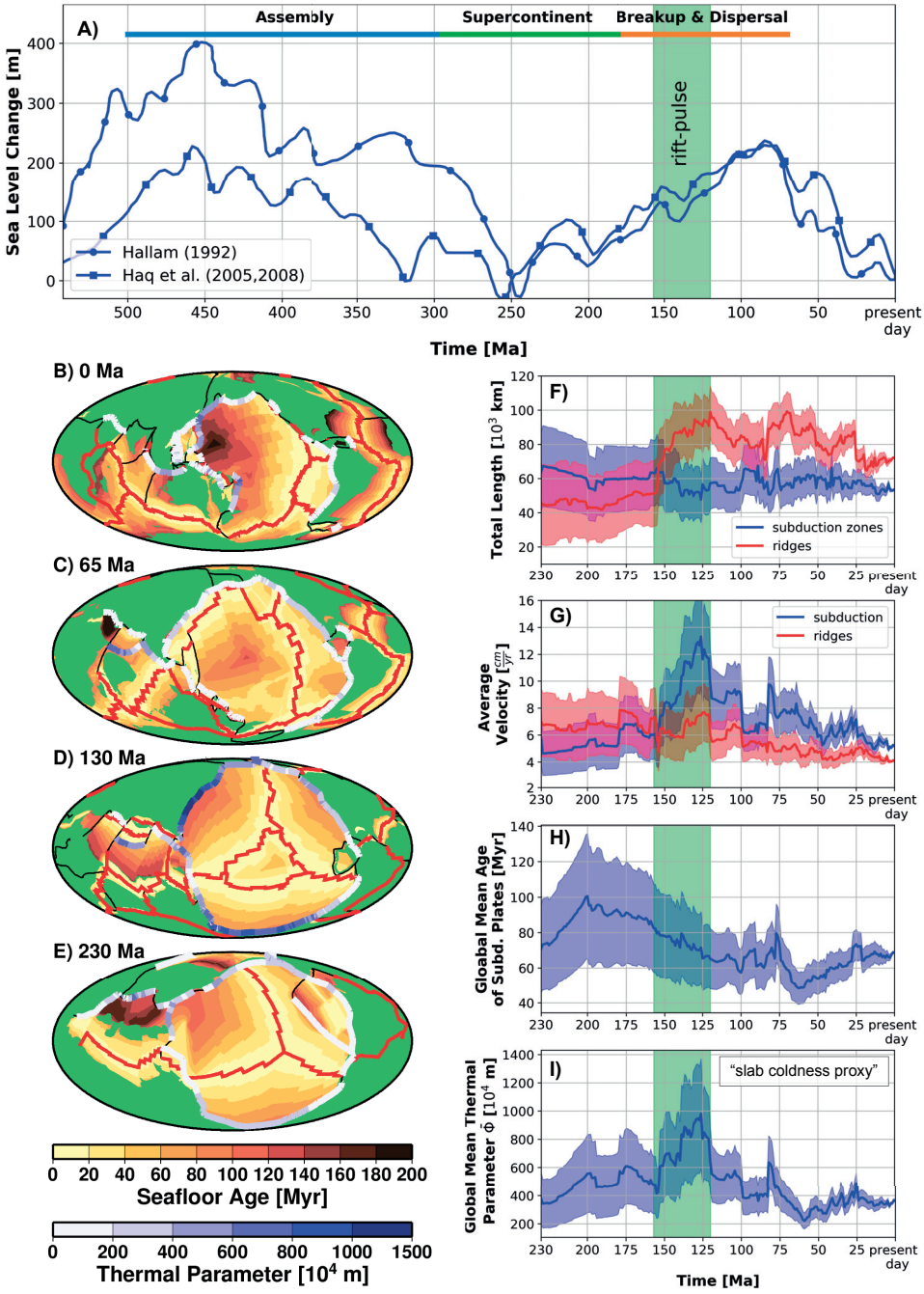

Figure I.1: Phanerozoic sea level (A) (Hallam, 1992; Haq and Al-Qahtani, 2005; Haq and Schutter, 2008) shows variations that correlate with supercontinental phases of Pangea (markers based on Cogné and Humler (2008) and Li and Zhong (2009)). Reconstructions of past seafloor configurations (B-E) back to 230 Ma (Müller et al., 2016) indicate temporal changes in length (F) and spreading rate (G) of the ridge system, and in the length (F), convergence velocity (G), age (H) and thermal parameter (I) of subduction zones. The rift pulse that led to the breakup of Pangea between 160 and 120 Ma is highlighted in green (A, F-I). Shaded envelopes (red and blue, F-I) represent one standard deviation of the considered variations in the tectonic parameters (see Appendix I.A).

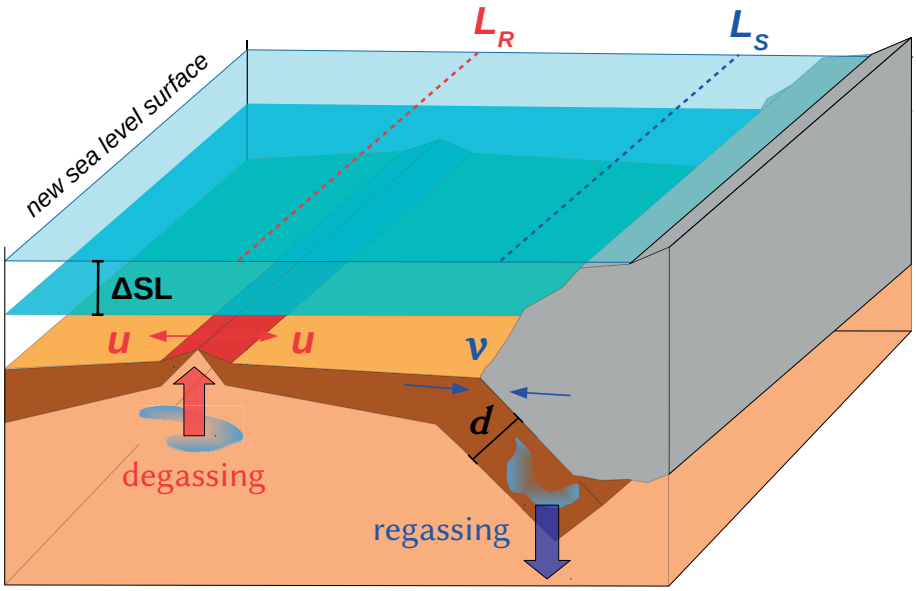

Figure I.2: A simplified illustration of the deep water cycling and sea level box-model, showing one subduction zone segment and one ridge segment, which are described by model parameters: subduction zone length L_S, ridge length L_R, full spreading velocity u, full convergence velocity v, and subducting plate thickness d. We use values for these parameters taken from the (Müller et al., 2016) tectonic reconstruction. The sea level change associated with deep water cycling is denoted ΔSL.

is a reasonable assumption if the global mean upper mantle temperature and water content does not change significantly over the period of interest (last 230 Myr). We thus compute degassing for a ridge segment of length L_R according to: $\gamma \rho u h L_R$, where u is the full spreading velocity, h is the average thickness of produced crust and γ is the *degassing factor*. Physically, the degassing factor can be interpreted as the product of the concentration of water within the melt and the fraction of that water that degasses (rather than remaining bound in the oceanic crust as it solidifies).

To estimate regassing and degassing rates back in time, we use the tectonic reconstruction model of Müller et al. (2016) which provides information about plate motions and plate boundary evolution since 230 Ma. In order to avoid including inactive plate boundaries (i.e. boundary segments classified as ridges and and subduction zones that are not diverging or converging), we apply a threshold of 0.2 cm/yr for which a plate boundary must either diverge or converge to be counted as a ridge or a subduction zone. Although this filtering affects the total length of the ridge and subduction zone systems (temporal variations are shown in Fig. I.1F), it does not significantly affect the total rate of area creation or destruction. At each point in time we obtain from plate boundary segments classified as *subduction zones*: segment length L_S, convergence velocity

v and subducting plate age τ. For *mid-ocean ridge* boundaries we collect segment length L_R and the full spreading rate u. The length-weighted average of these quantities for the past 230 Myr (Fig. I.1F-I) shows variations that should produce temporal variations in degassing and regassing rates. We compute global deep water fluxes for a given time $t \in [0, 230]$ Ma by summing over all segments:

$$Regassing: \quad R(t) = \sum_i \alpha \epsilon \rho d(\tau_i) v_i L_{Si}, \tag{I.1}$$

$$Degassing: \quad D(t) = \sum_j \gamma \rho h u_j L_{Rj}. \tag{I.2}$$

Here i sums over all subduction segments and j sums over all ridge segments. For the practical purposes of this study, α and γ serve as free parameters that are determined by assuming present-day rates of regassing $R(0)$ and degassing $D(0)$. This allows us to investigate a wide range of present-day degassing and regassing fluxes (associated with pairs of α and γ values), and their impact on sea level history.

Given time-dependent rates of regassing $R(t)$ and degassing $D(t)$, the component of sea level change associated with imbalanced deep water recycling can be computed as

$$\Delta SL(t) = -\frac{\lambda}{\rho_w \, A_o} \int_0^t R(t) - D(t) \, dt. \tag{I.3}$$

where ρ_w is the density of water, A_o is the ocean area and $\lambda = (\rho - \rho_w)/\rho \approx 0.7$ is a correction factor for isostatic adjustment of the oceanic lithosphere as sea level changes (Pitman III, 1978).

I.2.2 Uncertainty in Tectonic Reconstructions

The plate tectonic reconstructions of Müller et al. (2016) do not include measures of uncertainty. However, since the ocean floor acts as a recorder of plate motion history, uncertainty is bound to increase backwards in time as an increasingly larger fraction of Earth's present-day surface is missing. This fraction is commonly referred to as the "world uncertainty", and is a proxy for the uncertainty in any plate motion history model (Domeier and Torsvik, 2017). To account for this time-dependent uncertainty, we explore the sensitivity of our model results to variations in the tectonic parameters $(L_S, v_S, L_R, v_R, \tau)$ that scale with the world uncertainty. This is accomplished using Monte Carlo methods, where each model is run 10^4 times (after which the model output distributions have converged) with the tectonic parameters drawn from the assumed probability distribution. This enables us to infer upper and lower bounds on our model results. One standard deviation of the considered variation in the tectonic parameters is shown in Figures I.1 F-H. For a more detailed description of the Monte Carlo sampling, see Appendix.

I.2.3 Parameterization of Slab Dehydration

Parameterizations of regassing have been used in coupled thermal and water cycling models to study Earth-like planetary evolution (Crowley et al., 2011; McGovern and Schubert, 1989; Sandu et al., 2011). However, these parameterizations have been applied to global averages of plate movement, and are not well suited to predict water fluxes at individual subduction zones (Fig. I.3D). An explanation for this can be provided by the fact that slab dehydration patterns can vary greatly, depending on the thermal structure of individual subduction zones (van Keken et al., 2011), while thermal evolution models naturally assume a global average parameter ϵ that accounts for dehydration.

The thermal structure of subduction zones is controlled by the descending oceanic plate's initial temperature profile and the kinematics of subduction. This relationship is often described using the *thermal parameter* Φ, which we here define as the subduction convergence velocity times the plate age. Other definitions may include dip-angle (Kirby et al., 1996), but it has recently been suggested that the dip-angle only exhibits second-order control on the slab geotherms compared to the effects of plate age and velocity (Maunder et al., 2019). Data from tectonic reconstructions (Müller et al., 2016) show that the thermal parameter of subduction zones has varied dramatically through time (Fig. I.1I). Therefore, to better predict the mantle water flux for individual subduction zones in the past, we propose an expression for the slab's ability to retain water as function of its thermal parameter, i.e. $\epsilon(\Phi)$.

To obtain a first-order understanding of how slab water retention depends on the thermal parameter, we plot the fraction of water retained at > 200 km depth based on results from two independent studies (Fig. I.3 A-B). The overall trends are similar in the sense that the relative water retention increases with the thermal parameter until a saturation threshold is reached. They do however, differ in the magnitude of this saturation point, where results of van Keken et al. (2011) suggest that slabs can retain ~ 60 % of their initial water content, while Rüpke et al. (2004) suggest that ~ 40 % of the water that can be retained. We find that an exponential function with a negative exponent is suitable to describe a subducting plates relative water retention ϵ as a function of its thermal parameter Φ:

$$\epsilon(\Phi) = max\left(0, a + b(1 - e^{-c\,\Phi})\right). \tag{I.4}$$

The constants a, b and c used to fit the two independent data sets are given in Table I.1. Including this function in our model effectively modifies equation (I.1) by replacing ϵ with $\epsilon_{vK11}(\Phi_i)$ or $\epsilon_{r04}(\Phi_i)$, where $\Phi_i = v_i\tau_i$, and r04 and vK11 refers to the two different functional fits (defined by different values of a, b, c, Table I.1) shown in Figure I.3 A-B. Because the results reported by Rüpke et al. (2004) follow a clearer trend than those of van Keken et al. (2011), the functional fit (equation I.4) to the results of Rüpke et al. (2004) yield a higher coefficient of determination ($R^2 = 0.85$), meaning that 85 % of the variance in the relative water retention ϵ can be explained by our parameterization through the thermal

parameter Φ. On the other hand, the fit to the results of van Keken et al. (2011) can explain 71 % of the variance (Fig. I.3 A-B).

The most detailed study of water transport at individual subduction zones is van Keken et al. (2011), who estimated the H_2O flux for Earth's present-day subduction zones by combining finite element models for each subduction zone with a petrological model that tracks water retention with depth. To see if including a dependence on the thermal parameter in the water retention (I.4) improves the parameterization of subduction water flux (I.1), we apply it to the present-day subduction zones and compare it to the published estimates of van Keken et al. (2011). We see that by using both ϵ_{vK11} and ϵ_{r04} in the parameterization (I.1), we can capture differences between individual subduction zones better than we can using a constant ϵ (Fig. I.3D). Conversely, the parameterization (I.1) with constant water retention is not able to fit subduction zones with a high thermal parameter, while at the same time fit subduction zones with a low thermal parameter (Fig I.3 C-D). As an example, using a constant water retention underestimates the deep water flux at the Tonga trench, while overestimating almost all other fluxes. Therefore, applying the same constant ϵ to times during which the global mean thermal parameter was significantly higher (Fig. I.1I) would cause us to underestimate the global subduction water flux. Another improvement is that the functional form (I.4) allows for complete dehydration of slabs, which is believed to be the case for young plates subducting slowly (van Keken et al., 2011). It is also worth noting that despite having significantly different saturation points in terms of the relative water retention, the two different models (using ϵ_{vK11} and ϵ_{r04} in eq. I.1) predict very similar magnitudes for the deep water fluxes, but they require different values of the free parameter α.

I.3 Results

By applying our parameterizations for the regassing (eqs. I.1 and I.4) and degassing (eq. I.2) fluxes to the tectonic reconstructions of Müller et al. (2016), we investigate temporal changes in regassing efficiency (Fig. I.4 A and E), the magnitude of the deep water fluxes (Fig. I.4 B and F) and their related sea level change (Fig. I.4 C-D and G-H).

Because Earth's current deep water flux rates are uncertain (a recent review of Peslier et al. (2017) suggests ~ 50 % uncertainty), we explore a range of scenarios for deep water recycling associated with a range of present-day degassing and regassing rates. By tracking imbalances in these rates we can compute the change in ocean mass and estimate sea level change (Eq. I.3) over the last 230 Myr. To understand the time-dependent coupling between deep water cycling and sea level change, we study three scenarios that we find to be particularly illustrating in detail; a *present-day balance* (PB) between regassing and degassing, a *long-term balance* (LB) since 230 Ma, and a *regassing-dominated* (RD) case that assumes a significant net flux of water into the mantle for the present-day. These three cases

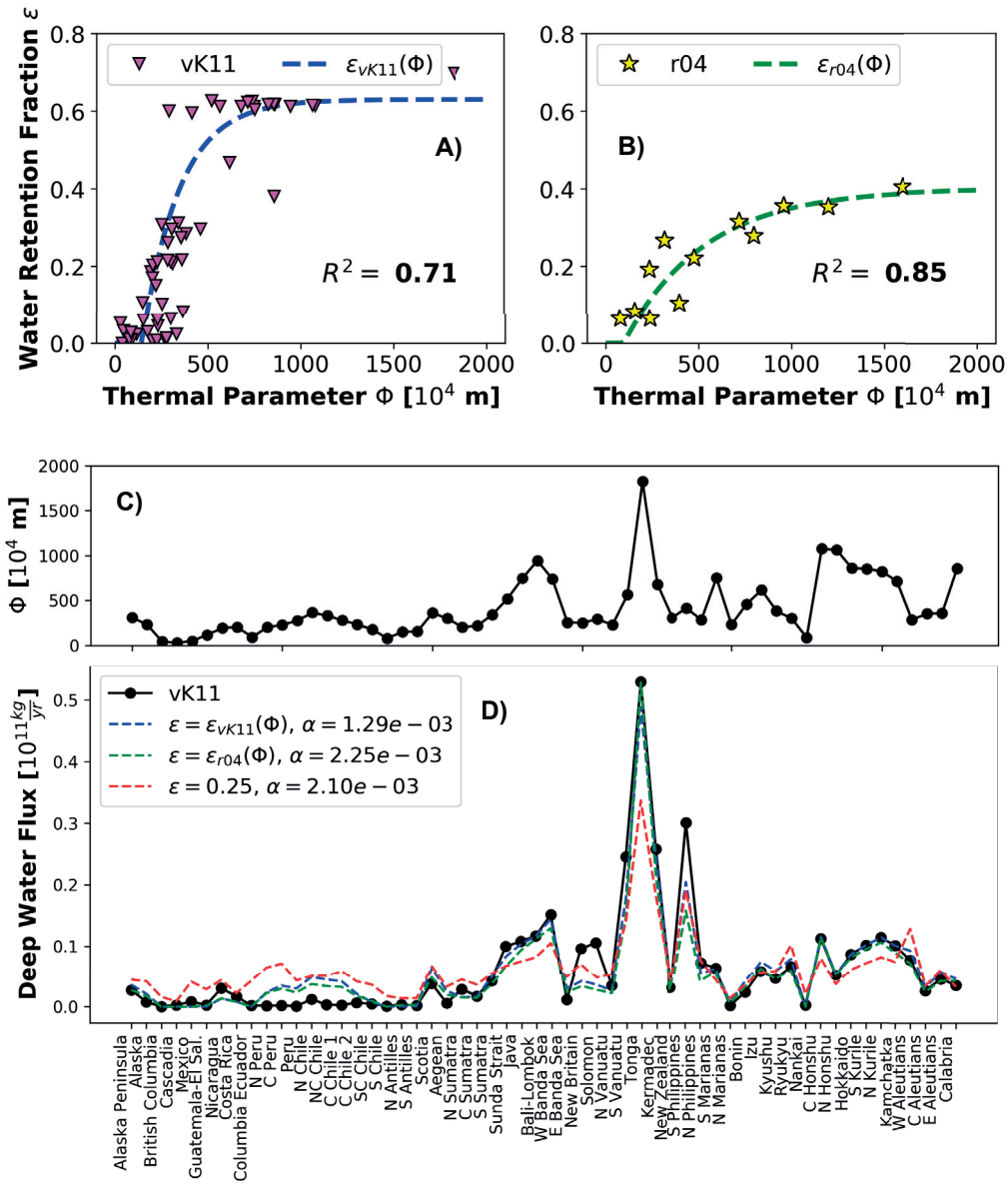

Figure I.3: Relative slab water retention ϵ as a function of the slab's thermal parameter for two independent studies, vK11 - van Keken et al. (2011) (A) and r04 - Rüpke et al. (2004) (B), and a functional (Eq. I.4, see Table I.1 for coefficients) fit to these reported values. The coefficient of determination R^2 indicates how much of the variance that can be explained by the paramterization. Present-day subduction zones' thermal parameter (C), and a comparison between their estimated deep water fluxes (D) based on the reported values (black dots) of van Keken et al. (2011) (Table 2, serpentinization 230 km) and our regassing parameterization (I.1) using a constant water retention fraction ϵ (red), the fit to vK11 (blue) and the fit to r04 (green). Values for Φ and ϵ for vK11 (A) are computed based on values from "Table 2: serpentinization", while values for r04 (B) are from "Fig. 7 A and E" in their respective publications.

Table I.1: Model parameters (constants), input parameters taken from tectonic reconstructions (Müller et al., 2016), coefficients used in the water retention paramterizations and scaling parameters used for the three deep water cycling cases considered in Figure I.4.

Model Parameters		
description	*symbol*	*value*
upper mantle density	ρ	3200 kg/m^3
water density	ρ_w	1000 kg/m^3
ocean area	A_o	$3.62 \cdot 10^{14}$ m^2
mean oceanic crust thickness	h	7.0 km
isostatic correction factor	λ	0.7

Input Parameters from Tectonic Reconstructions		
description	*symbol*	*value*
length of subduction segment i	L_{Si}	varies with time and segment
length of ridge segment j	L_{Rj}	varies with time and segment
convergence velocity for segment i	v_i	varies with time and segment
spreading velocity for segment j	u_j	varies with time and segment
age of subducting plate segment i	τ_i	varies with time and segment

Constants in Water Retention Function Fit			
paramterization	a	b	c
vK11	-0.67	1.3	0.005
r04	-0.1	0.5	0.0023

Scaling Parameters Used for Special Cases				
Regassing parameterization using: ϵ_{vK11}				
case	α	γ	R(0)	D(0)
long-term balance (LB)	5.40e-04	3.15e-03	$1.5{\cdot}10^{11}$ kg/yr	$2.0{\cdot}10^{11}$ kg/yr
present-day balance (PB)	7.00e-04	3.15e-03	$2.0{\cdot}10^{11}$ kg/yr	$2.0{\cdot}10^{11}$ kg/yr
regassing-dominated (RD)	1.18e-03	3.15e-03	$3.5{\cdot}10^{11}$ kg/yr	$2.0{\cdot}10^{11}$ kg/yr
Regassing parameterization using: ϵ_{r04}				
case	α	γ	R(0)	D(0)
long-term balance (LB)	1.07e-03	3.15e-03	$1.5{\cdot}10^{11}$ kg/yr	$2.0{\cdot}10^{11}$ kg/yr
present-day balance (PB)	1.33e-03	3.15e-03	$2.0{\cdot}10^{11}$ kg/yr	$2.0{\cdot}10^{11}$ kg/yr
regassing-dominated (RD)	2.28e-03	3.15e-03	$3.5{\cdot}10^{11}$ kg/yr	$2.0{\cdot}10^{11}$ kg/yr

are constructed by fixing the degassing parameter γ to produce a reasonable present-day degassing rate, i.e. $2.0 \cdot 10^{11}$ kg/yr (Hirschmann and Kohlstedt, 2012; Parai and Mukhopadhyay, 2012), and then finding the regassing parameter value α that satisfies the constraint for the given scenario (Eqs. I.5-I.7). For the regassing-dominated case, we chose an α-value that corresponds to the estimated subduction water flux of van Keken et al. (2011), which is $3.5 \cdot 10^{11}$ kg/yr. All these pairs of α- and γ-values can be found in Table I.1. The three cases can be

expressed mathematically as:

$$\text{PB case :} \qquad R(0) = D(0) = 2.0 \cdot 10^{11}\ kg/yr \tag{I.5}$$

$$\text{LB case :} \qquad \int_0^{230\ Ma} R(t) - D(t)\ dt = 0 \tag{I.6}$$

$$\text{RD case :} \qquad R(0) = 3.5 \cdot 10^{11}\ kg/yr,\ D(0) = 2.0 \cdot 10^{11}\ kg/yr \tag{I.7}$$

To further investigate the link between present-day deep water fluxes and past sea level change, we compute regassing, degassing and sea level history for a range of combinations of α- and γ-values, corresponding to present-day regassing and degassing rates in the interval $1.0 - 4.0\ 10^{11}$ kg/yr. These results (Fig. I.5) show the net sea level change since 230 Ma, with a black diagonal line indicating the transition between a degassing- and a regassing-dominated present-day. A green line marks the combination of present-day deep water flux rates that would cause zero net sea level change since 230 Ma. The three circle markers show where the highlighted cases (PB, LB and RD) plot in the parameter space. Finally, to link the estimated deep water fluxes to specific tectonic events we show maps of reconstructed subduction water fluxes for past times, which illustrate the regassing distribution between individual subduction zones (Fig. I.6).

Because we investigate variations in the tectonic input parameters (Fig. I.1 F-H) to our model through Monte Carlo sampling, the resulting global mean water retention histories (Fig. I.4 A and E), water fluxes (Fig. I.4 F and B), rates of sea level change (Fig. I.4 C and G) and sea level and ocean mass changes (Fig. I.4 D and G) are probability distributions (rather than single curves). These results are presented in Figure I.4 as preferred estimates (defined by the median, solid curves) with upper and lower bounds (shaded areas) defined as the median of the upper half of the distribution and the median of the lower half of the distribution. These bounds are commonly referred to as *upper quartile* and *lower quartile*.

I.3.1 Regassing Efficiency Through Time

The global regassing flux directly depends on the rate at which seafloor area is consumed at subduction zones (I.1). To preserve seafloor area, this rate is approximately equal to the rate at which seafloor is created at ridges, which directly impacts the degassing rate (I.2). Thus, we expect the net degassing and regassing fluxes to exhibit proportional variations during periods of faster or slower plate creation and destruction. However, the regassing flux also depends on subducting plate age through the thickness d and ability to retain water ϵ, both of which have varied with time differently than the seafloor area destruction rate (Fig. I.1F-H). Additionally, since the slab water retention also depends on the plate velocity (Magni et al., 2014; Rüpke et al., 2004; van Keken et al., 2011), the deep subduction water flux is nonlinear in plate velocity as well as age. Thus the rates of regassing and degassing depend on the tectonic record in

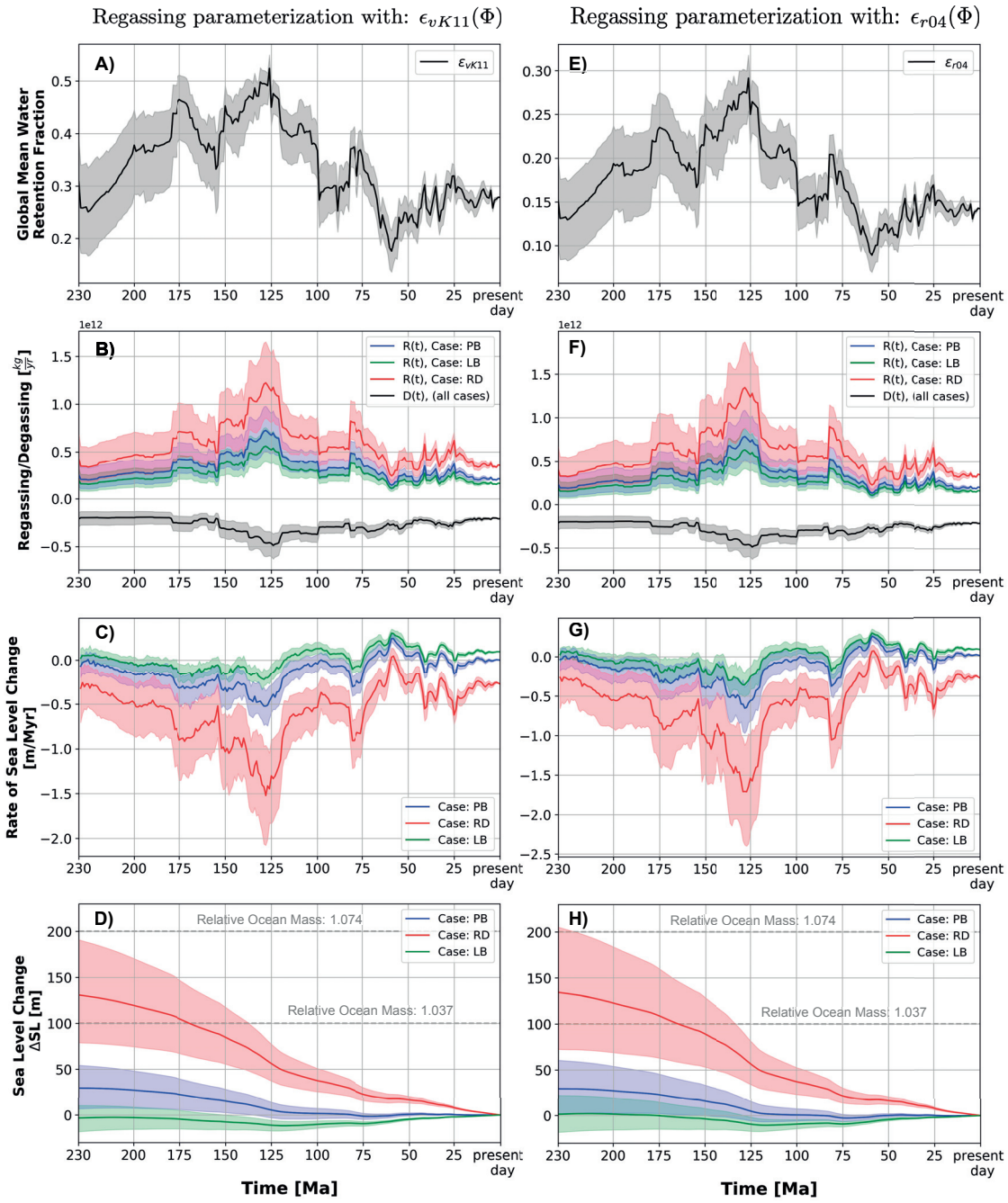

Figure I.4: Tectonically-inferred time history of deep water cycling and its associated ocean mass and sea level change for two different parameterizations of slab water retention (left and right columns correspond ϵ_{vK11} and ϵ_{r04} respectively). Global mean water retention fractions $\bar{\epsilon}$ (A and E) and deep water flux rates (B and F) for three scenarios: regassing-dominated (RD - red), present-day balance (PB - blue) and long-term balance (over the past 230 Myr) (LB - green) are presented along with corresponding sea level changes (D and H) and their rates of change (C and G). Solid curves show the median of 10^4 Monte Carlo simulations, while the enveloping shaded areas represent the upper and lower quartiles of the distributions. The α and γ values used to produce these results can be found in Table I.1 and a detailed description of the Monte Carlo methods is found in the Appendix.

different ways, which leads to time-variations in the net flux of water into or out of the mantle.

For the present-day, our two different models predict that slabs on average retain about 14-27 % of their initial water content (Fig. I.4 A and E). Here the lower estimate represents the paramterization of relative water retention based on the results of Rüpke et al. (2004), while the upper estimate corresponds to the paramterization motivated by van Keken et al. (2011). For comparison, recently published estimates include 26 % (Magni et al., 2014) and 33 % (van Keken et al., 2011). We note that despite giving significantly different values for water retention, the two models (ϵ_{vK11} and ϵ_{r04}) follow similar trends (Fig. I.4 A and E) and yield nearly identical results in terms of deep water fluxes (Fig. I.4 B and F) and associated sea level change (Fig. I.4 D and H). Although they require different values of α, see Table I.1. Our application of these models to the tectonic record suggests that today's fraction is relatively low within the last 230 Myr, and that ϵ likely have been higher in the past. The current period of strong slab dehydration is caused by the combination of slow convergence velocities at subduction zones and moderately low subducting plate ages (Fig. I.1G-H), which together diminish the global average thermal parameter (Fig. I.1I).

The most prominent peak in average plate water retention (Fig. I.4 A and E) is related to the major rift-pulse around 150 Ma, associated with the opening of the South Atlantic Ocean (Fig. I.1 and I.6). During this time, the total length of the ridge system approximately doubled, while the length of the subduction zone system actually dropped (Fig. I.1F). This caused a dramatic increase (well above a factor of 2) in the convergence velocity at the active trenches (Fig. I.1G). As old and hydrated oceanic lithosphere was rapidly forced into the mantle by the new, massive ridge system, the average age of subducting plates dropped about 20 Myr over this $\sim$ 35 Myr period (Fig. I.1H). Despite the gradual loss of old seafloor, the average thermal parameter for subduction zones also more than doubled during the rift-pulse (Fig. I.1I). This period of anomalously rapid subduction allowed for a large fractions of water (on average about 30-50 %) to be carried to sub-arc depths (Fig. I.4 A and E).

I.3.2 Time-Dependence of the Deep Water Cycling

Our estimates of regassing and degassing history (Fig. I.4 B and F) suggest that the deep water flux rates have remained fairly stable since the breakup-phase of Pangea ended about 70 Myr ago. Thus, our model indicates that any net flux to or from the mantle (including zero net flux), and the associated rate of sea level change (Fig. 4 C and G), has been approximately constant since 70 Ma. This is because the average convergence velocity at subduction zones has steadily decreased over this time period (Fig. I.1G), while the mean age of subducting plates have steadily increased (Fig. I.1H), causing the thermal parameter (Fig. I.1I) and thus the global regassing efficiency (Fig. I.4 A and E)

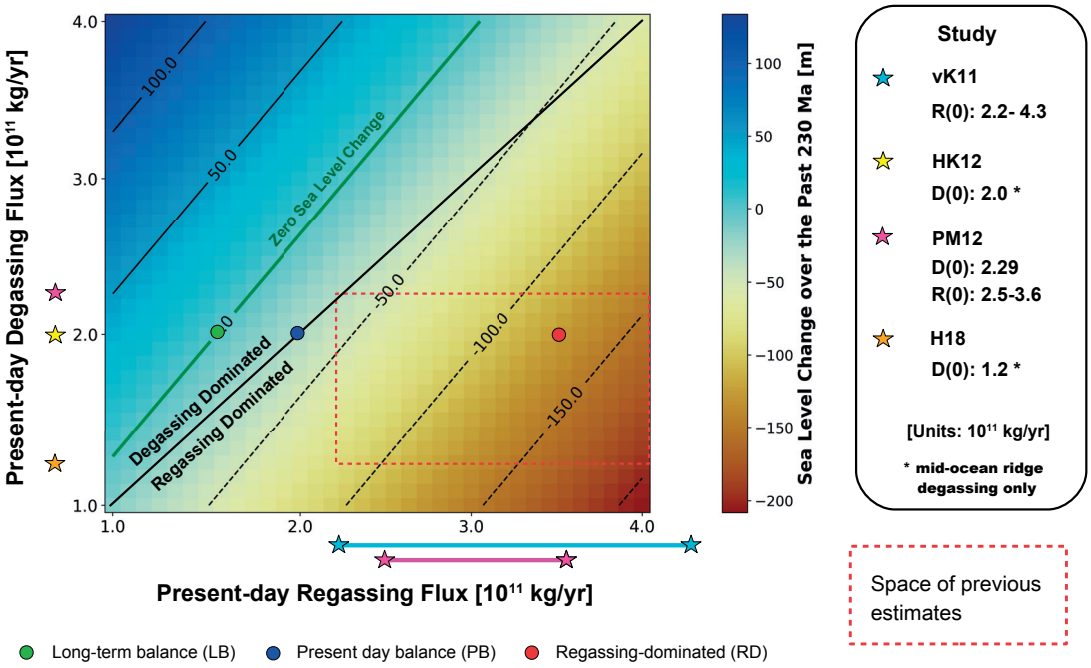

Figure I.5: Net sea level change since 230 Ma, for combinations of present-day regassing and degassing rates between 1.0-4.0 $10^{11}\frac{kg}{yr}H_2O$. The green line marks zero sea level change over this period (including case LB), and the black line shows a present-day balance between regassing and degassing (including case PB). The corresponding sea level curves (which are nearly identical for ϵ_{vK11} and ϵ_{r04}) in Fig. I.4 D and H are indicated by circle markers. Stars indicate previous estimates of present deep water fluxes (vK11 - van Keken et al. (2011), HK12 - Hirschmann and Kohlstedt (2012), PM12 - Parai and Mukhopadhyay, 2012 and H18 - Hirschmann (2018)), and define the space of previous estimates (dashed red line).

to be approximately constant. It is worth noting that also prior to the dispersal of Pangea (before 180 Ma), our calculations suggest regassing and degassing to have been relatively stable. Three prominent peaks in regassing, ($\sim$ 175, 130 and 75 Ma) coincide with those of regassing efficiency $\bar{\epsilon}$ (Fig. I.4 A-B and E-F), and can be explained through their common occurrence at times with peaks in global mean values of subducting plate age and/or velocity (Fig. I.1G-I). The maximum value of the largest regassing peak is about four times the present-day value, which is relatively low compared to last 230 Myr (Fig. I.4 B and F). For the degassing flux, the maximum value occurs at the end of the rift pulse ($\sim$ 125 Ma) and is about 2.5 times as large as the present-day value.

Too see how the subduction water flux is distributed among different subduction zones through time (following the example of van Keken et al. (2011) who did this for the present day), we show reconstructed maps with regassing flux estimates (Fig. I.6) based on our parameterization (ϵ_{vK11}). We see that presently about 30% of subduction zones carry no water beyond the arc, while the rest have

relatively low transport rates, most below 20 Tg/Myr/m (Fig. I.6E). On the other hand, right after the $\sim$ 130 Ma rift-pulse, the remnants of the ancient supercontinent was surrounded by subduction zones that transported more than 20 Tg/Myr/m water to the deep mantle (Fig. I.6G). Before the major rifting-event, in late Pangean times (230 Ma, Fig. I.6H), we interestingly see that the distribution of subduction water flux was similar to that of the present-day. These spatial and temporal variations in deep water fluxes may create a heterogeneous distribution of water in the mantle.

From the imbalanced regassing and degassing rates (Fig. I.4 B and F) we compute the change in ocean mass over time, which we translate to sea level change through equation I.3. Note that as several simplifying assumptions regarding ocean hypsometry go into this equation, our estimates in ocean mass change should be considered more robust than our sea level inferences. From the long-term balance scenario (LB, eq. I.6), we interestingly see that the degassing flux must be about 33% larger than the regassing flux at the present day in order to not change sea level (or ocean mass) over the last 230 Myr. If regassing and degassing are currently in balance (PB, eq. I.5), we expect a sea level drop of about 30 ± 25 m (~ 1 % in ocean mass change), over the last 230 Myr, with most of the drop occurring between 230 - 120 Ma. The regassing-dominated case (RD, eq. I.7) predicts an even larger sea level drop of 130 ± 50 m (~ 5 % in ocean mass change) for the same period, which translates to an average net-flux to the mantle of 2-4 $\cdot 10^{11}$ kg/yr, or an ocean mass change of about 5 %. The fastest rate of sea level change was about -1.5 ± 0.5 m/Myr at about 130 Ma (Fig. I.4 C and G).

I.4 Discussion

I.4.1 Amplitude of Sea Level Drop

Despite relatively high uncertainties tied to the present-day deep water fluxes, there seems to be consensus that there is a significant net-flux of water into the mantle at the present-day (e.g., Korenaga et al. (2017) and Peslier et al. (2017)), thus we consider the present-day balance scenario to be conservative and the long-term balance to be unlikely (Fig. I.4), but yet interesting cases to discuss. On the other hand; if there is a significant present-day net-flux of water into the mantle, as many studies suggest, the sea level drop caused by ocean-mantle water exchange may be as large as $\sim$ 130 m (Figs. I.4 and I.5). Although this scenario predicts past global subduction water fluxes that are much higher (4 times) than for the present-day, the regassing flux distribution (Fig. I.6G) shows that the vast majority of subduction zones transported water into the deep mantle at rates lower than currently estimated for the Tonga trench, i.e. 47.7 Tg/Myr/m by van Keken et al. (2011).

New constraints on the subduction water flux were recently obtained through analysis of ocean-bottom seismic data (Cai et al., 2018). They find evidence

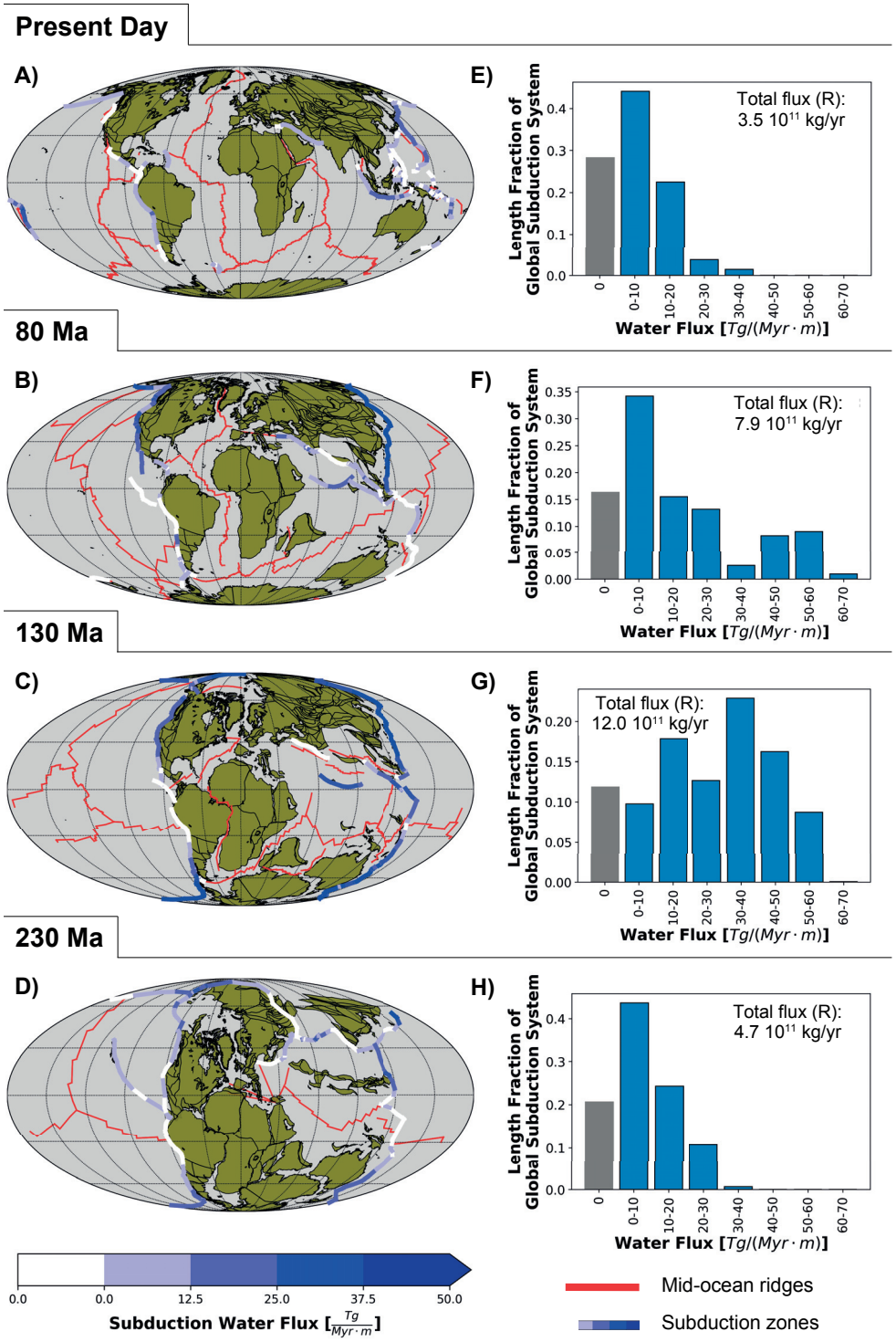

Figure I.6: Reconstructed maps (A-D) based on (Müller et al., 2016) showing ridges (red) and the subduction water flux (shades of blue) through time. Histograms (E-H) show the distribution of subduction zone segments according to how much water they transport into the deep mantle. The regassing estimates here correspond to the RD case (nearly identical for ϵ_{vK11} and ϵ_{r04}), which assumes a present-day global subduction water flux comparable to that of van Keken et al. (2011).

for a partially serpentinized (2 wt% water) slab-mantle layer at the Mariana trench that is much thicker than previously assumed, indicating a greater extent of serpentenization in old slabs. These new constraints suggest that the water input to the Maraina trench should be 4.3 times higher than estimated by van Keken et al. (2011). Assuming that other old slabs have similar amounts of partially serpentinized mantle, Cai et al. (2018) estimate the global subduction water input to be three times higher than the previous estimates. This suggests that van Keken and colleagues' computation of the subduction water flux, and our regassing-dominated scenario (case RD), might be relatively conservative.

Our regassing-dominated scenario (Fig. I.4), which assumes a subduction water flux similar to that of van Keken et al. (2011), exhibits an average net-flux of 2-4 $\cdot 10^{11}$ kg/yr into the mantle during the past 230 Myr. Constraints based on an approximately constant continental freeboard since the Early Proterozoic (Korenaga et al., 2017) suggests that the net-flux to the mantle from the oceans must have been 3-4.5 $\cdot 10^{11}$ kg/yr since $\sim$ 2.5 Ga. This indicates that the estimates from our regassing-dominated present-day scenario largely overlap and are consistent with the suggested long-term drop in ocean water mass.

The above arguments and constraints suggest that deep water cycling caused a significant drop in ocean mass and should be considered as an important sea level changing mechanism for this period. This conclusion leads to a critical question: how much sea level drop can be added to the Mesozoic-Cenozoic sea level budget without violating the sea level record inferred from sedimentary stratigraphy (Hallam, 1992; Haq and Al-Qahtani, 2005; Haq and Schutter, 2008)? Conrad (2013) added up estimated contributions for all the major sea level changing processes (changes in sediment thickness, ridge volume, dynamic topography, climate, ocean area and the volume of structures formed by intraplate seafloor volcanism) for the past 140 Myr and compared it to the sea level record. Here (Fig. I.7) we extend his analysis back to 230 Ma and include deep water cycling. We acknowledge that all these estimates, as well as the sea level observations themselves, are subject to very large uncertainties. That being said, we still consider this to be a useful exercise to place deep water cycling in the context of sea level history and other mechanisms. To highlight the effect of deep water cycling on the total sea level budget, we compare tallies with and without this effect to the observed sea level change (Fig. I.7B). We find that the deviation between observations and a sea level budget that includes deep water cycling is smaller than it is for the budget without deep water cycling over this period. This statement holds for both the sea level records we compare it to, indicating that there is room in the budget even for the largest of our sea level drop scenarios (case RD).

I.4.2 Ocean-Mantle Water Exchange over Supercontinent Cycles

Almost a century of research has taken us from the fascination of Wegener's Pangea (Wegener, 1920), Earth's ancient supercontinent, to a realization that

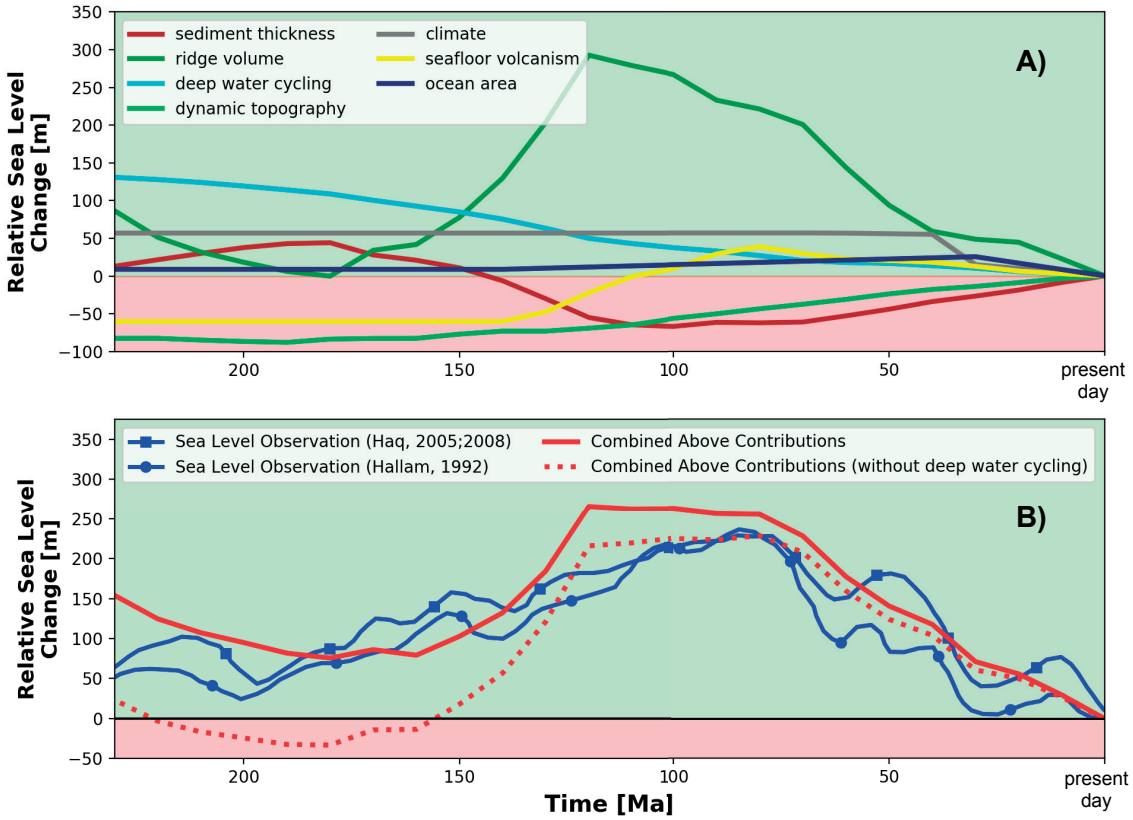

Figure I.7: Sea level budget for the past 230 Myr. Estimates of the major sea level changing mechanisms (A) and their combined effect on sea level compared to observations (B) for the past 230 Myr. We calculate changes in ridge volume and sediment thickness by applying the Crosby and McKenzie (2009) age-depth relation and the Straume et al. (2019) age-latitude-sediment relation (respectively) to the Müller et al. (2016) age grids for the past 230 Myr. We computed the contribution from dynamic topography following Conrad (2013) but using the tectonic reconstruction of Conrad et al. (2013) to extend back to 230 Ma. We use Conrad (2013) estimates for the sea level contributions from changes to climate (melting of landbound ice and thermal expansion of seawater), seafloor volcanism, and ocean area back to 140 Ma, and, for lack of better information, assume that these contributions are constant for the period 250-140 Ma. We use the regassing-dominated (RD) case from this study for the deep water cycling component, and show the combined contributions both with (solid red line) and without (dashed red line) this contribution in (B).

the formation and breakup of supercontinents is a general phenomenon of Earth history, beyond Pangea. There now seems to be acceptance that Earth has had at least five pre-Pangaen supercontinents at approximately 2.6, 2.0, 1.7, 1.1 and 0.6 Ga (Nance et al., 1986; Worsley et al., 1984; Worsley et al., 1985). These supercontinental cycles are thought to have been associated with ocean-basin volume changes that changed sea level (Worsley et al., 1984; Worsley et al., 1982). Here we have shown that such massive tectonic changes should also affect the deep water cycle, and thus induce major changes ocean water mass. Next,

we will attempt, based on the limited tectonic record available, to generalize how the deep water fluxes induce sea level variations over supercontinent cycles.

The supercontinent cycle is traditionally divided into three phases; (1) *assembly*, (2) *supercontinent* and (3) *breakup and dispersal*. It would perhaps be meaningful to add a fourth (4) *interstage*, which refers to a configuration of dispersed continents, in-between *breakup and dispersal* and a new *assembly* (corresponding to the present-day). The supercontinent and the interstage configurations represent the most stable tectonic regimes, thus we expect deep water cycling to be relatively stable as well during these phases. A similarity between these two phases is supported by our comparable predictions of the subduction water flux distributions during late Pangea and after its breakup and dispersal (Fig. I.6 E and H), as well as fairly stable regassing and degassing fluxes during both of these periods (Fig. I.4 B and F).

The breakup and dispersal of a supercontinent requires a massive rifting event that opens new oceans. The newly formed ridges must, in order to not significantly change the area of the ocean, be compensated by either (i) the creation of new subduction zones or (ii) an increase in convergence velocity at existing subduction zones. The most recent tectonic reconstructions (Matthews et al., 2016; Müller et al., 2016) suggest that the rift-pulse during the last supercontinent cycle's dispersal phase ($\sim$ 150 Myr) was indeed compensated by rapid subduction of old oceanic lithosphere (Figs. I.1 and I.6). Therefore, because of the strong velocity-dependence of regassing, we expect an increased net-flux of water from the oceans into the mantle during supercontinental breakup and dispersal (Fig. I.4).

The final stage of supercontinent assembly involves the closing of an ocean basin through massive continent-continent collision that terminates subduction zones. Taking the present-day as an example, the Atlantic Ocean has been growing at the expense of the Pacific where the major subduction zones are located. If this trend continues, the assembly of a supercontinent by closing the Pacific could potentially cause a significant drop in the subduction flux for a period of time, before new subduction zones develop (Silver and Behn, 2008). This should result in a temporary period of sea level rise. On the other hand, if the next supercontinent formed by closing the Atlantic, the majority of subduction zones located on the Pacific margins should endure, possibly without an accompanying period of sea level rise.

Generalizing rates of deep water transport over supercontinent cycles is challenging because no-two cycles are likely to be identical, and the tectonic record currently provides information about only half of the last supercontinent cycle. However, it seems reasonable to infer that the deep water fluxes are most stable during supercontinental and interstage periods. The deep water cycling-induced sea level drop we expect to be associated with supertontinent breakup and dispersal, may be balanced to some extent by sea level rise during

supercontinental assembly, although the extent of net degassing during assembly is difficult to constrain due lack of tectonic reconstructions for Pangean assembly. These expected sea level trends are generally consistent with our tectonically-inferred predictions of water fluxes and sea level change (Fig. I.4) for the last phases of the last supercontinent cycle.

Over most of Earth's history, mantle cooling is thought to be associated with net regassing (Crowley et al., 2011; Korenaga, 2011; Korenaga, 2008), leading to a substantial loss of ocean mass and an accompanying sea level drop that may be partially obscured by secular evolution of continental buoyancy (Korenaga et al., 2017). The deep water cycling-induced sea level variations that we associate with the supercontinental cycle (described in the previous paragraph) may be superimposed on top of this long-term trend of net regassing, and/or may be the manifestation of the long-term trend itself. For example, repeated application of this sea level cycle would generate a long-term net regassing that is expected form thermal history models. However, if these variations are superimposed on a long-term trend of decreasing ocean mass, as predicted by previous studies (Crowley et al., 2011; Korenaga, 2011), we would likely also see a steady drop in sea level during interstage and supercontinentality. This scenario is reflected by the regassing-dominated case (Fig. I.4), where sea level drops both before and after the breakup of Pangea ($\sim 180 - 70$ Ma), and does so even faster during the major rifting event ($\sim 150 - 120$ Ma). These pulses of water entering the mantle during supercontinent breakup may thus represent an important part of Earth's long-term thermal and hydrological evolution.

I.4.3 Uncertainty of the Degassing History

We have assumed that degassing of water from the mantle occurs mainly at mid-ocean ridges, and that the rate of this degassing is proportional to seafloor divergence rates. Two factors may complicate this assumption. First, intra-plate degassing via volcanism at hotspots and large igneous provinces may be an important degassing contributor with a time-dependence that differs from that of seafloor spreading. However, the range of degassing scenarios that we have explored (Fig. I.5) explores present-day mantle water output rates far beyond those of only mid-ocean ridges, which have been estimated for the present-day at about $1.2 \cdot 10^{11}$ kg/yr (Hirschmann, 2018; Parai and Mukhopadhyay, 2012). Second, we assume that the melting zone beneath all the mid-ocean ridges contains the same amount of water. However, if water is heterogeneously distributed throughout the mantle (Hirschmann and Dasgupta, 2009), as we would expect given the heterogeneity associated with its entry into the mantle (Fig. I.6), we expect degassing along the ridge system to reflect these variations in the mantle water distribution. This is certainly important for estimating the degassing flux along certain ridge segments, but may not be as important for the global ridge flux since it is likely to average out across the entire ridge system.

I.5 Conclusions

The transport of surface water into deep mantle by subduction zones is only partly balanced by outward water transport by seafloor volcanism, and this imbalance represents a mechanism for sea level change. Here we have shown that dramatic changes in tectonic rates since the breakup of the last supercontinent (Fig. I.1) have induced changes in the overall efficiency of mantle regassing at subduction zones (Fig. I.4 A and E). These fluctuations in regassing extend beyond fluctuations in the rate of convergence, which are always balanced by divergence at ridges. Therefore, it is unlikely that the present-day fluxes are representative for past and future fluxes, and the rate of sea level change that results from imbalanced degassing and regassing should change as the Earth's tectonic configuration changes. We find that even a present-day balance of the deep water fluxes implies a significant sea level drop over the last supercontinent cycle. A concise summary of our main findings reads:

- By parameterizing the dependence of regassing efficiency (I.4) on plate age and velocity (through the thermal parameter), we can approximately recreate estimates of present-day water fluxes for subduction zones around the world (Fig. I.3). This allows us to extend present-day predictions of the subduction water flux to past times using plate kinematic models.
- By combining our reconstructed time-history of degassing and regassing fluxes with previously published estimates for the present-day values of these fluxes, we can reconstruct the evolution of ocean water mass since 230 Ma. Our models predict a sea level drop (upper bound $\sim$ 50 m) associated with deep water cycling even if regassing and degassing are currently balanced, and we consider amplitudes as large as $\sim$ 130 m as possible if regassing currently dominates (Fig. I.4). Such amplitudes are comparable to those produced by other sea-level changing mechanisms (Fig. I.7A), and can be accommodated within the sea level budget of the past 230 Myr without violating stratigraphic observations of sea level change (Fig. I.7B).
- We expect deep water fluxes to remain more or less stable during supercontinentality and for periods between dispersal and assembly. During supercontinent dispersal we expect a significant net flux of water from the oceans into the mantle caused by the opening of a new ridge system that forces rapid subduction of old oceanic lithosphere. This period of faster sea level drop, happening repeatedly over several supercontinental cycles, may contribute significantly to the long-term regassing of the mantle that is thought to be an important part of Earth's thermal history.

Finally, looking ahead we consider better constraints on the deep water fluxes for

the present-day, combined with more information about tectonic rates further back in time, essential for improving our understanding of the deep water cycle and its associated sea level change. Such advancements would represent important steps toward linking mantle dynamics and the exosphere, and characterizing mantle water heterogeneity.

Appendix I.A Monte Carlo Methods

The world uncertainty function (Fig. I.8A) is a measure of the Earth's present-day surface area fraction that is missing at a given point in time t, and serves as a proxy for the uncertainty in any plate motion history model (Domeier and Torsvik, 2017). To capture this time-dependent uncertainty in our model results, we run a large number of simulations (10^4) for each model, and for each model run every tectonic input parameter (L_s, v_S, L_R, v_R, τ) is multiplied by a perturbation factor p (the same factor is used for all segments within one model run to avoid unphysical discontinuities in, for example, spreading velocities along a mid-ocean ridge) that scales with the world uncertainty. Each perturbation factor is defined as $p_k = 1 + r_k W_N(t)$, where $k = 1, 2, .., 5$ and r_k is a random number drawn from the uncertainty distribution defined by $N(\mu, \sigma)$ with $\mu = 0$ and $2\sigma = W_{max}$ (Fig. I.8B), $W_N(t)$ is the *normalized world uncertainty function* defined as $W_N(t) = W(t)/W_{max}$ and $W_{max} = 0.7$ is the maximum uncertainty (Fig. I.8A). We consider normal distributions around the original values because these values represent what the authors of the plate reconstructions model thought to be most plausible, and not just a random guess (which would be equivalent of assuming a uniform distribution). The equations for the perturbed tectonic parameters can then be expressed as:

$$\tilde{L_S} = p_1 L_s, \tag{I.8}$$

$$\tilde{v_S} = p_2 v_s, \tag{I.9}$$

$$\tilde{L_R} = p_3 L_R, \tag{I.10}$$

$$\tilde{v_R} = p_4 v_R, \tag{I.11}$$

$$\tilde{\tau} = p_5 \tau. \tag{I.12}$$

To see the normally distributed variation in the tectonic parameters resulting from this sampling approach, see Figure 1 F-H. Because our model outputs are also distributions (however, they are non-normal and non-symmetric), rather than singles curves, we present the results as preferred estimates defined by the median, with upper and lower bounds defined by upper and lower quartile. The *upper quartile* and the *lower quartile* are defined as the median of the lower half of the distribution, while the upper bound is defined by the median of the upper half of the distribution (where the total median divides the distribution into halves), see Figure I.4.

To ensure that the perturbations do not to violate the constant Earth surface-condition, i.e. divergence at mid-ocean ridges equals convergence at subduction

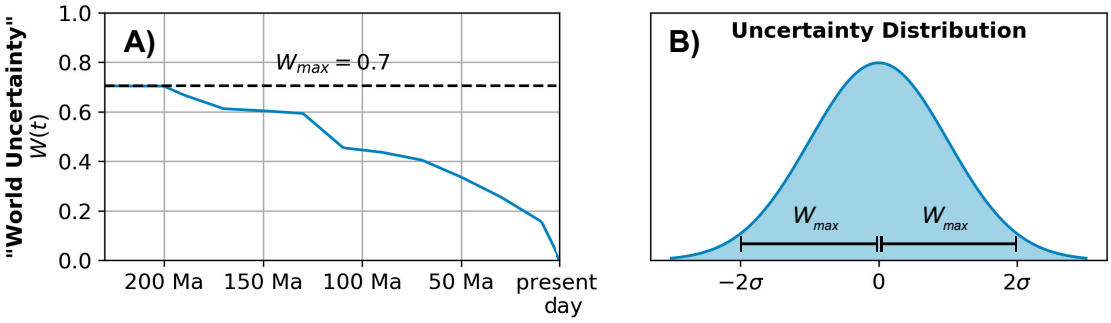

Figure I.8: The fraction of Earth's present-day surface that is missing at a given point in time (A), and the assumed uncertainty in the tectonic paramters used in our models (B).

zones $\sum \tilde{v_R} \tilde{L_R} = \sum \tilde{v_S} \tilde{L_S}$, the tectonic parameters must be sampled with care. Thus the perturbation factors $(p_1, p_2, p_3, p_4, p_5)$ can not be sampled completely independent of each other, but are subject to the constraint $p_1 p_2 = p_3 p_4$. We solve this as follows:

1. Draw three random numbers r_1, r_2, r_5.
2. Compute p_1 and p_2 according to $p_i = 1 + r_i W_N(t)$.
3. Draw a binary q number with an equal chance of 1 and 0.
4. If $q = 0 \rightarrow p_3 = p_1$ and $p_4 = p_2$
   If $q = 1 \rightarrow p_3 = p_2$ and $p_4 = p_1$

The procedure above ensures that every perturbation $(p_1, p_2, p_3, p_4, p_5)$ remains normally distributed and proportional to the world uncertainty, while satisfying $p_1 p_2 = p_3 p_4$.

Acknowledgements

This paper has benefited from discussions with, and feedback from, several people. For valuable input on the time-dependent reliability of tectonic reconstructions, we thank Trond Torsvik and Mathew Domeier. All calculations (described in the Methods and Appendix section) were preformed using Python (http://www.python.org). The input parameters from the tectonic reconstructions are available from Müller et al. (2016), and the other constants can be found in Table I.1. The published model results used to calibrate the empirical law for deep water retention (Eq. 4 and Fig. 3 A-B) are available in van Keken et al. (2011) and Rüpke et al. (2004). We thank Fabio Crameri for the development of perceptually uniform and color-vision-deficiency

friendly colormaps (Crameri, 2018b), ensuring an accurate representation of the underlying data in the figures (Crameri, 2018a). Finally, we thank Adrian Lenardic, Jun Korenaga and one anonymous reviewer for insightful suggestions that greatly improved the manuscript. This work was funded by the Research Council of Norway's *Centres of Excellence Project 223272*.

References

Bodnar, R. J., Azbej, T., Becker, S. P., Cannatelli, C., Fall, A., and Severs, M. J. (2013). "Whole Earth geohydrologic cycle, from the clouds to the core: The distribution of water in the dynamic Earth system". In: *The Geological Society of America Special Paper* vol. 500, pp. 431–61.

Cai, C., Wiens, D. A., Shen, W., and Eimer, M. (2018). "Water input into the Mariana subduction zone estimated from ocean-bottom seismic data". In: *Nature* vol. 563, pp. 389–392.

Cloetingh, S. and Haq, B. U. (2015). "Inherited landscapes and sea level change". In: *Science* vol. 347, no. 6220, p. 1258375.

Cogné, J.-P. and Humler, E. (2008). "Global scale patterns of continental fragmentation: Wilson's cycles as a constraint for long-term sea-level changes". In: *Earth and Planetary Science Letters* vol. 273, no. 3-4, pp. 251–259.

Conrad, C. P. (2013). "The solid Earth's influence on sea level". In: *Geological Society of America Bulletin* vol. 125, no. 7-8, pp. 1027–1052.

Conrad, C. P. and Husson, L. (2009). "Influence of dynamic topography on sea level and its rate of change". In: *Lithosphere* vol. 1, no. 2, pp. 110–120.

Conrad, C. P., Steinberger, B., and Torsvik, T. H. (2013). "Stability of active mantle upwelling revealed by net characteristics of plate tectonics". In: *Nature* vol. 498, no. 7455, p. 479.

Crameri, F. (2018a). "Geodynamic diagnostics, scientific visualisation and StagLab 3.0". In: *Geoscientific Model Development* vol. 11, no. 6, pp. 2541–2562.

Crameri, F. (2018b). *Scientific colour-maps*. Zenodo. http://doi.org/10.5281/zenodo.1243862.

Crosby, A. and McKenzie, D. (2009). "An analysis of young ocean depth, gravity and global residual topography". In: *Geophysical Journal International* vol. 178, no. 3, pp. 1198–1219.

Crowley, J. W., Gérault, M., and O'Connell, R. J. (2011). "On the relative influence of heat and water transport on planetary dynamics". In: *Earth and Planetary Science Letters* vol. 310, no. 3, pp. 380–388.

Domeier, M. and Torsvik, T. H. (2017). "Full-plate modelling in pre-Jurassic time". In: *Geological Magazine*, pp. 1–20.

Faccenda, M., Gerya, T. V., Mancktelow, N. S., and Moresi, L. (2012). "Fluid flow during slab unbending and dehydration: Implications for intermediate-depth seismicity, slab weakening and deep water recycling". In: *Geochemistry, Geophysics, Geosystems* vol. 13, no. 1.

Garrels, R. M. (1983). "The carbonate-silicate geochemical cycle and its effect on atmospheric carbon dioxide over the past 100 million years". In: *Am J Sci* vol. 283, pp. 641–683.

Hacker, B. R. (2008). "H2O subduction beyond arcs". In: *Geochemistry, Geophysics, Geosystems* vol. 9, no. 3.

Hallam, A. (1992). *Phanerozoic sea-level changes*. Columbia University Press.

Haq, B. U. and Al-Qahtani, A. M. (2005). "Phanerozoic cycles of sea-level change on the Arabian Platform". In: *GeoArabia* vol. 10, no. 2, pp. 127–160.

Haq, B. U. and Schutter, S. R. (2008). "A chronology of Paleozoic sea-level changes". In: *Science* vol. 322, no. 5898, pp. 64–68.

Hirschmann, M. (2006). "Water, Melting, and the Deep Earth H2O cycle". In: *Annu. Rev. Earth Planet. Sci.* Vol. 34, pp. 629–653.

Hirschmann, M. M. (2018). "Comparative deep Earth volatile cycles: The case for C recycling from exosphere/mantle fractionation of major (H2O, C, N) volatiles and from H2O/Ce, CO2/Ba, and CO2/Nb exosphere ratios". In: *Earth and Planetary Science Letters* vol. 502, pp. 262–273.

Hirschmann, M. M. and Dasgupta, R. (2009). "The H/C ratios of Earth's near-surface and deep reservoirs, and consequences for deep Earth volatile cycles". In: *Chemical Geology* vol. 262, no. 1-2, pp. 4–16.

Hirschmann, M. and Kohlstedt, D. (2012). "Water in Earth's Mantle". In: *Phys. Today* vol. 65, no. 3, p. 40.

Ito, E., Harris, D. M., and Anderson Jr, A. T. (1983). "Alteration of oceanic crust and geologic cycling of chlorine and water". In: *Geochimica et Cosmochimica Acta* vol. 47, no. 9, pp. 1613–1624.

Kasting, J. F. and Catling, D. (2003). "Evolution of a habitable planet". In: *Annual Review of Astronomy and Astrophysics* vol. 41, no. 1, pp. 429–463.

Kelemen, P. B. and Manning, C. E. (2015). "Reevaluating carbon fluxes in subduction zones, what goes down, mostly comes up". In: *Proceedings of the National Academy of Sciences*, p. 201507889.

Keller, T., Katz, R. F., and Hirschmann, M. (2017). "Volatiles beneath mid-ocean ridges: Deep melting, channelised transport, focusing, and metasomatism". In: *Earth and Planetary Science Letters* vol. 464, pp. 55–68.

Kirby, S. H., Stein, S., Okal, E. A., and Rubie, D. C. (1996). "Metastable mantle phase transformations and deep earthquakes in subducting oceanic lithosphere". In: *Reviews of geophysics* vol. 34, no. 2, pp. 261–306.

Korenaga, J. (2011). "Thermal evolution with a hydrating mantle and the initiation of plate tectonics in the early Earth". In: *Journal of Geophysical Research: Solid Earth* vol. 116, no. B12.

Korenaga, J. (2007). "Thermal cracking and the deep hydration of oceanic lithosphere: a key to the generation of plate tectonics?" In: *Journal of Geophysical Research: Solid Earth* vol. 112, no. B5.

Korenaga, J. (2008). "Plate tectonics, flood basalts and the evolution of Earth's oceans". In: *Terra Nova* vol. 20, no. 6, pp. 419–439.

Korenaga, J. (2013). "Initiation and evolution of plate tectonics on Earth: theories and observations". In: *Annual Review of Earth and Planetary Sciences* vol. 41, pp. 117–151.

Korenaga, J. (2017). “On the extent of mantle hydration caused by plate bending”. In: *Earth and Planetary Science Letters* vol. 457, pp. 1–9.

Korenaga, J., Planavsky, N. J., and Evans, D. A. (2017). “Global water cycle and the coevolution of the Earth’s interior and surface environment”. In: *Phil. Trans. R. Soc. A* vol. 375, no. 2094, p. 20150393.

Li, Z.-X. and Zhong, S. (2009). “Supercontinent–superplume coupling, true polar wander and plume mobility: plate dominance in whole-mantle tectonics”. In: *Physics of the Earth and Planetary Interiors* vol. 176, no. 3-4, pp. 143–156.

Magni, V., Bouilhol, P., and Hunen, J. van (2014). “Deep water recycling through time”. In: *Geochemistry, Geophysics, Geosystems* vol. 15, no. 11, pp. 4203–4216.

Marty, B. and Tolstikhin, I. N. (1998). “CO 2 fluxes from mid-ocean ridges, arcs and plumes”. In: *Chemical Geology* vol. 145, no. 3, pp. 233–248.

Matthews, K. J., Maloney, K. T., Zahirovic, S., Williams, S. E., Seton, M., and Mueller, R. D. (2016). “Global plate boundary evolution and kinematics since the late Paleozoic”. In: *Global and Planetary Change* vol. 146, pp. 226–250.

Maunder, B., Hunen, J. van, Bouilhol, P., and Magni, V. (2019). “Modeling Slab Temperature: A Reevaluation of the Thermal Parameter”. In: *Geochemistry, Geophysics, Geosystems*.

Müller, R. D., Seton, M., Zahirovic, S., Williams, S. E., Matthews, K. J., Wright, N. M., Shephard, G. E., Maloney, K. T., Barnett-Moore, N., Hosseinpour, M., et al. (2016). “Ocean basin evolution and global-scale plate reorganization events since Pangea breakup”. In: *Annual Review of Earth and Planetary Sciences* vol. 44, pp. 107–138.

McGovern, P. J. and Schubert, G. (1989). “Thermal evolution of the Earth: effects of volatile exchange between atmosphere and interior”. In: *Earth and planetary science letters* vol. 96, no. 1-2, pp. 27–37.

Nance, R. D., Murphy, J. B., and Santosh, M. (2014). “The supercontinent cycle: a retrospective essay”. In: *Gondwana Research* vol. 25, no. 1, pp. 4–29.

Nance, R. D., Worsley, T. R., and Moody, J. B. (1986). “Post-Archean biogeochemical cycles and long-term episodicity in tectonic processes”. In: *Geology* vol. 14, no. 6, pp. 514–518.

Nestola, F. and Smyth, J. R. (2016). “Diamonds and water in the deep Earth: a new scenario”. In: *International Geology Review* vol. 58, no. 3, pp. 263–276.

Parai, R. and Mukhopadhyay, S. (2012). “How large is the subducted water flux? New constraints on mantle regassing rates”. In: *Earth and Planetary Science Letters* vol. 317, pp. 396–406.

Parsons, B. and Sclater, J. G. (1977). “An analysis of the variation of ocean floor bathymetry and heat flow with age”. In: *Journal of geophysical research* vol. 82, no. 5, pp. 803–827.

Peslier, A. H., Schönbächler, M., Busemann, H., and Karato, S.-I. (2017). “Water in the Earth’s interior: distribution and origin”. In: *Space Science Reviews* vol. 212, no. 1, pp. 743–810.

Pitman III, W. C. (1978). “Relationship between eustacy and stratigraphic sequences of passive margins”. In: *Geological Society of America Bulletin* vol. 89, no. 9, pp. 1389–1403.

Ranero, C. R. and Sallarès, V. (2004). "Geophysical evidence for hydration of the crust and mantle of the Nazca plate during bending at the north Chile trench". In: *Geology* vol. 32, no. 7, pp. 549–552.

Rüpke, L. H., Morgan, J. P., Hort, M., and Connolly, J. A. (2004). "Serpentine and the subduction zone water cycle". In: *Earth and Planetary Science Letters* vol. 223, no. 1-2, pp. 17–34.

Sandu, C., Lenardic, A., and McGovern, P. (2011). "The effects of deep water cycling on planetary thermal evolution". In: *Journal of Geophysical Research: Solid Earth* vol. 116, no. B12.

Sclater, J., Jaupart, C., and Galson, D. (1980). "The heat flow through oceanic and continental crust and the heat loss of the Earth". In: *Reviews of Geophysics* vol. 18, no. 1, pp. 269–311.

Silver, P. G. and Behn, M. D. (2008). "Intermittent Plate Tectonics?" In: *Science* vol. 319, no. 5859, pp. 85–88. eprint: http://science.sciencemag.org/content/319/5859/85.full.pdf.

Straume, E., Gaina, C., Medvedev, S., Hochmuth, K., Gohl, K., Whittaker, J. M., Abdul Fattah, R., Doornenbal, J., and Hopper, J. R. (2019). "GlobSed: Updated Total Sediment Thickness in the World's Oceans". In: *Geochemistry, Geophysics, Geosystems*.

Syracuse, E. M., Keken, P. E. van, and Abers, G. A. (2010). "The global range of subduction zone thermal models". In: *Physics of the Earth and Planetary Interiors* vol. 183, no. 1-2, pp. 73–90.

van Keken, P. E., Hacker, B. R., Syracuse, E. M., and Abers, G. A. (2011). "Subduction factory: 4. Depth-dependent flux of H2O from subducting slabs worldwide". In: *Journal of Geophysical Research: Solid Earth* vol. 116, no. B1.

Wegener, A. (1920). *Die Entstehung der Kontinente und Ozeane*. Vol. 66. F. Vieweg.

Worsley, T. R., Nance, D., and Moody, J. B. (1984). "Global tectonics and eustasy for the past 2 billion years". In: *Marine Geology* vol. 58, no. 3-4, pp. 373–400.

Worsley, T., Moody, J., and Nance, R. (1985). "Proterozoic to Recent tectonic tuning of biogeochemical cycles". In: *The carbon cycle and atmospheric CO2: natural variations Archean to present* vol. 32, pp. 561–572.

Worsley, T., Nance, R., and Moody, J. (1982). "Plate tectonic episodicity: a deterministic model for periodic "Pangeas"". In: *Eos, Transactions of the American Geophysical Union* vol. 65, no. 45, p. 1104.

Paper II

A Tracer-Based Algorithm for Automatic Generation of Seafloor Age Grids from Plate Tectonic Reconstructions

Krister S. Karlsen, Mathew Domeier, Carmen Gaina, Clinton P. Conrad

Published in *Computers & Geosciences*, July 2020, DOI: 10.1016/j.cageo.2020.104508.

II

Abstract

The age of the ocean floor and its time-dependent age distribution control fundamental features of the Earth, such as bathymetry, sea level and mantle heat loss. Recently, the development of increasingly sophisticated reconstructions of past plate motions has provided models for plate kinematics and plate boundary evolution back in geological time. These models implicitly include the information necessary to determine the age of ocean floor that has since been lost to subduction. However, due to the lack of an automated and efficient method for generating global seafloor age grids, many tectonic models, most notably those extending back into the Paleozoic, are published without an accompanying set of age models for oceanic lithosphere. Here we present an automatic, tracer-based algorithm that generates seafloor age grids from global plate tectonic reconstructions with defined plate boundaries. Our method enables us to produce novel seafloor age models for the Paleozoic's lost ocean basins. Estimated changes in sea level based on bathymetry inferred from our new age grids show good agreement with sea level record estimations from proxies, providing a possible explanation for the peak in sea level during the assembly phase of Pangea. This demonstrates how our seafloor age models can be directly compared with observables from the geologic record that extend further back in time than the constraints from preserved seafloor. Thus, our new algorithm may also aid the further development of plate tectonic reconstructions by strengthening the links between geological observations and tectonic reconstructions of deeper time.

Plain Language Summary

After the ocean floor is created, it spreads away from the mid-ocean ridge axis and becomes older, cooler, denser and thicker. These changes make older seafloor deeper and less efficient at transferring heat into the oceans. Therefore, maps of the ages of ancient ocean basins are useful to infer sea level change, interior heat loss, paleo-ocean circulation and several other geodynamic processes during the past several hundred millions of years. However, the creation of maps of seafloor age from models of how the tectonic plates have moved, has proven to be difficult and time-consuming. For this reason, seafloor age maps have only been constructed back to 250 Ma, while models for how the tectonic plates have moved extend all the way back to the mid-Paleozoic (410 Ma). Here we present a new automated method for generating grids of seafloor ages from reconstructions of past plate motions. Our method enables us to produce the first seafloor age models for the Paleozoic's lost ocean basins. From these models we compute changes in seafloor depth through time and use them to estimate sea level change, which we in turn can compare to stratigraphic constraints on sea level history. This comparison shows promising agreement between models and observations, providing a possible explanation for the peak in sea level during the assembly phase of Pangea. Since our automated method allows for easy conversion of plate motion reconstructions into seafloor ages and seafloor depth, we have strengthened the links between geological observations and tectonic reconstructions.

Contents

II.1 Introduction

The discovery of a method to determine the age of the present-day oceanic crust, using reversals of the Earth's magnetic field (Vine and Matthews, 1963), gave rise to the recognition that the seafloor is spreading, and ultimately to the development and broad acceptance of plate tectonics. In the half-century since the plate tectonic revolution, detailed age models of the present-day oceanic lithosphere have been constructed, and digital global oceanic age grids are

continuously refined (Müller et al., 1997; Müller et al., 2008a; Müller et al., 2016). A wealth of information, mainly from marine geophysical data, but also from geology of continental margins, were used to reconstruct the extent and age distribution of oceanic lithosphere of the past, including portions that have been subducted (Müller et al., 2008b). These "paleo-seafloor age grids" present rich new opportunities for scientific inquiry, as a wide range of Earth processes can be further interrogated with the use of such age grids. Example applications include the estimation of paleobathymetry (spatial and temporal changes in ocean basin depth, which in turn is important for understanding past ocean currents and their effect on paleoclimate, e.g., Straume et al. 2019), sea level change (Müller et al., 2008b), global seafloor heat flow (Crameri et al., 2019; Loyd et al., 2007), and the subduction volume flux, which impacts geomagnetic reversals (Hounslow et al., 2018), the thermal structure of paleo-subduction zones (Maunder et al., 2019), transport of water (Karlsen et al., 2019a) and carbon (Merdith et al., 2019) to the deep mantle, and the slab pull force on tectonic plates (Conrad and Lithgow-Bertelloni, 2004; Faccenna et al., 2012). Seafloor ages for past times are also important as a boundary condition for global mantle convection models (Gurnis et al., 2012).

Present day age grid models are based on a set of isochrons (lines defined by equal seafloor ages) constructed using information from magnetic and gravity data available at various resolutions in most oceanic basins. Ages for seafloor locations between isochrons are computed based on rotation parameters that describe the plate motions for various time intervals. The isochrons and rotation parameters are linked to a specific geomagnetic timescale, and the choice of timescales will influence the calculated values of spreading velocities. To ensure a smooth grid of ocean floor ages that maintains sharp age discontinuities at fracture zones, Müller et al. (1997) designed an algorithm where they first created a set of densely interpolated isochrons along plate flow lines, and then used a minimum curvature routine to obtain age values on a regular grid. This method for reconstructing seafloor age from present-day seafloor age data and a plate kinematic model is time-consuming and requires significant human input, and consequently may be subjective or introduce errors. Because of this, seafloor ages are usually only determined after a plate reconstruction model has been finalized; they have not previously been computed "on the fly" from the plate kinematic model itself.

The mid-ocean ridges constitute the locus of seafloor generation through time, while plate kinematics define the seafloor's subsequent journey until its destruction at a subduction zone. Thus, global plate tectonic reconstructions that define the motions of the plates and the locations and types of plate boundaries (see Gurnis et al. 2012 for further descriptions of such models) also implicitly define the age and structure of oceanic basins. Global plate tectonic models with dynamic plate boundaries (Gurnis et al., 2012) have been constructed back into the mid-Paleozoic (410 Ma; Domeier and Torsvik 2014; Matthews et al. 2016), but published paleo-seafloor age grids are only available globally

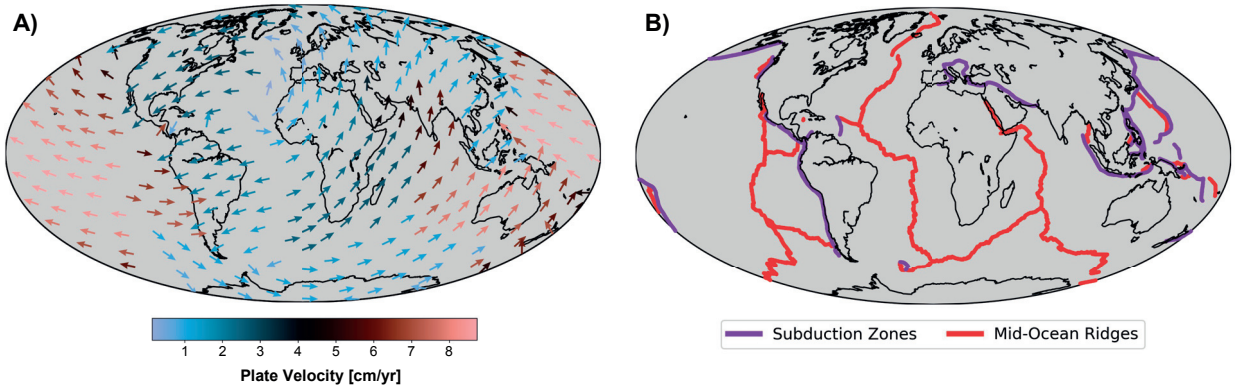

Figure II.1: Present day global surface velocity field (A) and locations of mid-ocean ridges and subduction zones (B) derived from global plate tectonic reconstructions (Matthews et al., 2016).

for the last 250 Ma (Müller et al., 2019). This timing discrepancy has, partly, occurred because the reconstruction of global paleo-seafloor age grids from a plate tectonic reconstruction presents a tedious and labor intensive task in the absence of an automatic method. Moreover, these reconstructions are subject to continuous changes as new geological information becomes available. It follows that an automatic and more efficient method for seafloor age determination is needed to allow the use of plate tectonic reconstructions to better decipher Earth's processes and dynamics through time. An automatic method also allows detecting inconsistencies in kinematic models, which would help to improve them. In this study we present such an automatic method for generating seafloor age grids, and introduce a specific implementation of it as an open-source Python code called *Tracer Tectonics* (or *TracTec*) (Karlsen et al., 2019b).

II.2 Methods

The algorithm specifically acts upon "self-closing" plate polygon models (Gurnis et al., 2012) that evolve over time from a set of dynamically evolving plate boundaries. Conventionally, such models comprise a *rotation file*, a *plate boundary file* and a *continent polygon file*. The rotation file (*.rot file) represents a series of finite rotations that describe the time-dependent motions of each plate, which are identified by their associated Plate ID. The motion of plates by rotations about Euler poles (Greiner, 1999), and the surface velocity field (Fig. II.1A), can be described at each point in time $t \in [0, T]$, where $t = 0$ defines the present-day and $t = T$ is the earliest point in time for which the plate reconstruction is defined. We prefer to refer to t as time, rather than age, to avoid confusion with the age of the seafloor.

The time-dependent motions described by the *.rot file can be used to reconstruct any framework of points, polylines (continuous lines composed of one or more line segments) and polygons that are ascribed PlateIDs defined in the *.rot file. The continent polygon file, for example, contains static polygons (tagged with metadata Plate IDs) that represent blocks of continental lithosphere that can be reconstructed and passively rotated through time by the *.rot file. The plate boundary file contains the polylines that are used (in conjunction with the *.rot file) to reconstruct the dynamic plate polygons at any time t, following the method of Gurnis et al. (2012). These polylines are associated with metadata tags that identify the type of plate boundary that they represent; in the following, we will be interested in those that are either identified as mid-ocean ridge or subduction zone (Fig. II.1B).

We divide the computational approach for generating seafloor age grids from kinematic plate models into three modules: *preprocessing*, *main algorithm* and *post-processing* (Fig. II.2). The Python scripts that we developed for each of these modules are part of the TracTec-package, and can be downloaded from: http://doi.org/10.5281/zenodo.3687548.

II.2.1 Preprocessing

As the time-dependent spatial distribution of mid-ocean ridges and subduction zones, together with plate kinematics, dictates the age of the ocean floor, we need to extract these properties from a given full-plate model and output them in a convenient format. To accomplish this, we use *pyGPlates*, which is a Python-based scripting interface to GPlates (Boyden et al., 2011) that allows for easy automation of such tasks. For each point in time t we extract plate boundaries labelled as mid-ocean ridges from the plate boundary file, and re-sample these polyline segments at user-defined intervals Δ_R (50 km by default). Subduction zone plate boundary segments are extracted and sampled in the same manner ($\Delta_S = 20$ km by default).

II.2.2 Main Algorithm

To simulate and track the journey of oceanic lithosphere through space and time, from its creation along a mid-ocean ridge until its destruction at a subduction zone, we use tracers. These are numerical particles on which quantities of interest are tracked. The essential property we want to track with the tracers is the age of the oceanic lithosphere. A secondary property we track is the Plate ID associated with each tracer, i.e. the plate to which each tracer currently belongs. We track Plate IDs to determine when a tracer crosses a plate boundary (recognized by a change in its associated Plate ID), which in turn is useful to detect subduction of tracers. At a given time t, the number of tracers is $N_T(t)$, their positions are $\mathbf{x}_n(t)$, their ages $\tau_n(t)$, and their associated Plate IDs are $p_n(t)$, for $n = 0, 1, .., N_T(t) - 1$.

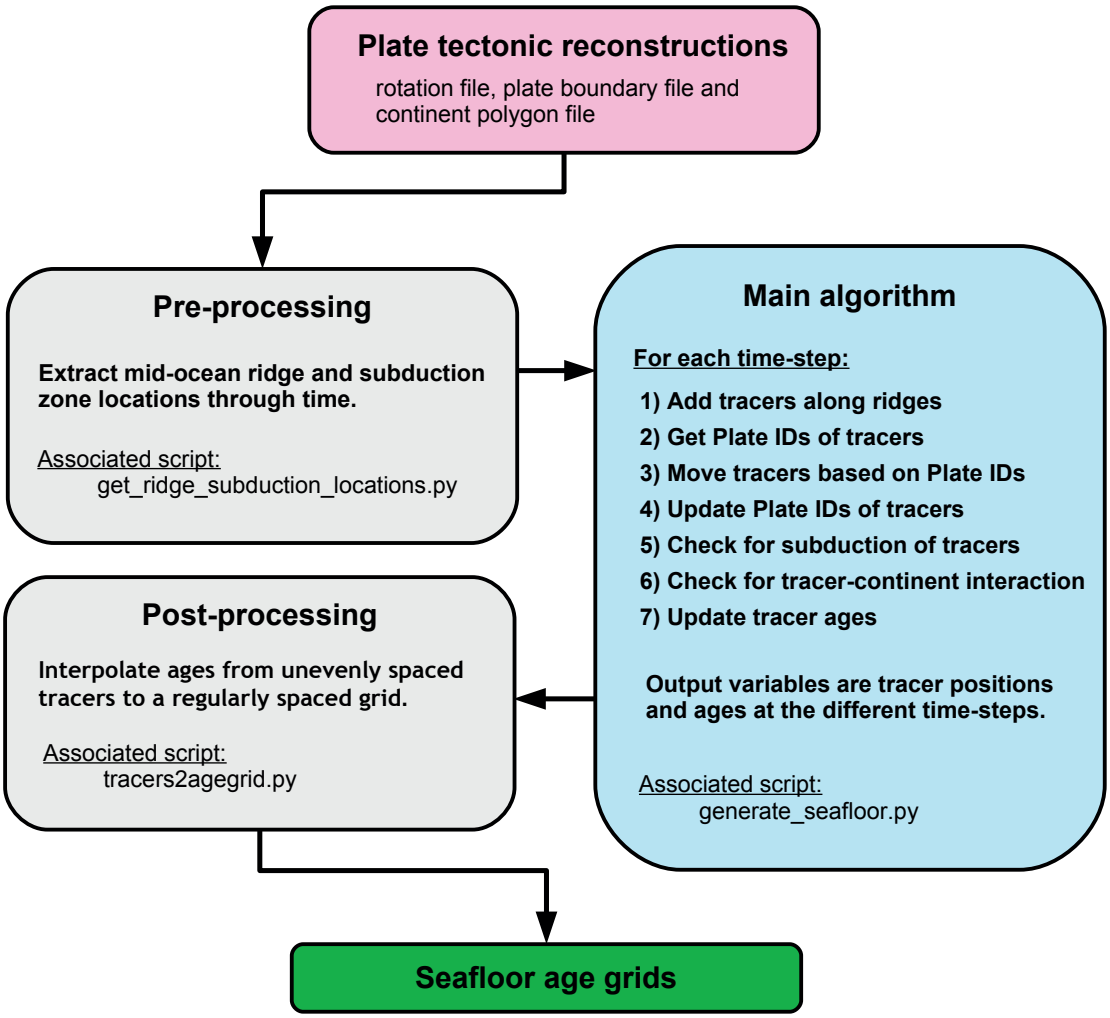

Figure II.2: Flow chart of TracTec (Karlsen et al., 2019b) showing an overview of the algorithm and the steps used to generate seafloor age grids from plate tectonic reconstructions.

We break the algorithm into individual sub-steps (see below, 1-7) that are completed at every integer time-step $t \in [0, T]$, before moving on to the next. Although our algorithm is capable of operating at any arbitrary time-step, we fix the time-step size Δt to 1 Myr in accordance with the inherent temporal resolution that modern plate tectonic reconstructions are made. The use of larger time-steps would yield sparse age-grids and omit meaningful kinematic data, whereas smaller time-steps could result in erroneous behavior owing to deficiencies in the input plate model below the standard assumed temporal resolution of 1 Myr.

1) Add tracers
At the beginning of each time-step we add tracers at intervals given by Δ_R on

each side of the mid-ocean ridges (Fig. II.3A). The tracers are added at a small offset distance ϵ_R (1 km by default) from the ridge to ensure that they are within the polygons that define the two spreading plates. Their initial ages $\tau_n(t)$ are set to zero. The uncertainty introduced by adding tracers at this offset distance is given by ϵ_R/v_s, where v_s is the half-spreading rate. For an average mid-ocean ridge ($v_s \sim 26$ mm/yr) $\epsilon_R/v_s \approx 0.04$ Myrs.

2) Get tracer Plate IDs
Based on the tracers' positions $\mathbf{x}_n(t)$, we use pyGPlates' point-in-polygon algorithm to assign them their Plate IDs $p_n(t)$.

3) Move tracers
To determine how the tracers move from t to $t + \Delta t$ (Fig. II.3 B-C), we use pyGPlates to query the *rotation file* to obtain the finite rotation associated with each tracer (which is based on their Plate IDs $p_n(t)$). Next, by applying that rotation to their current positions $\mathbf{x}_n$, we obtain their new positions $\mathbf{x}_n(t + \Delta t)$.

4) Update tracer Plate IDs
Based on the tracers' new positions $\mathbf{x}_n(t + \Delta t)$, we use pyGPlates' point-in-polygon algorithm to assign them their new Plate IDs $p_n(t + \Delta t)$.

5) Check for subduction
After having moved the tracers from $\mathbf{x}_n(t)$ to $\mathbf{x}_n(t + \Delta t)$, we check if any tracers have been subducted (Fig. II.3 H-I). This is accomplished by first determining which tracers have changed Plate ID by comparing $p_n(t)$ against $p_n(t + \Delta t)$. Given the sub-set of tracers that have changed Plate ID, we determine if any are within distance R_{min} of a subduction zone boundary. The default value of R_{min} is set to 100 km, which we have found to be appropriate. Any tracers that fulfill both of these criteria are considered subducted and are thus terminated at this time-step.

6) Check for tracer-continent interaction
To ensure that tracers don't end up on continents (which could happen in nature, e.g. ophiolites, but shouldn't happen in conventional dynamic plate polygon models, but nevertheless occurs due to inexorable flaws in such models), we delete all tracers that end up inside continent polygons (checked using pyGPlates' point-in-polygon algorithm against the continent polygon file).

7) Update tracer ages
Before moving on to the next time-step, which practically means returning to step 1) of the algorithm, we update the age of the tracers that are left after the two filtering steps 5-6), by simply by adding Δt to their current age, obtaining $\tau_n(t + \Delta t)$.

II.2.3 Post-Processing

The output from steps 1-7) is unevenly distributed tracer positions $\mathbf{x}_n(t)$ associated with ages $\tau_n(t)$. However, for most applications, it is convenient to express the seafloor ages on a regular grid, rather than at arbitrary points. This calls for a post-processing step that interpolates seafloor ages from tracer positions onto a regular grid. There are countless ways of doing this, ranging from simple nearest neighbor algorithms, to weighted means, to splines etc. Depending on the application, smoothing of resulting age grids may be preferred or required. In our online repository we provide an example of a simple post-processing script that uses GMT's linear interpolation algorithm (Wessel et al., 2013) to obtain seafloor ages on a regular grid.

The Python scripts to generate age grids based on the steps described above using Tracer Tectonics are provided in the Zenodo repository (Karlsen et al., 2019b). A summary and a general overview of the algorithm are shown in Figure II.2.

II.2.4 Initial Condition

Running the algorithm without any initial condition, as in the example of Figure II.3 D-G, we see that it takes some tens of millions of years before the ocean basins are entirely covered by tracers. Technically, this is the time it takes for the predicted seafloor ages to result solely from the plate kinematics of the input model. Alternatively, one could apply an initial condition that incorporates some educated guess of the seafloor ages for the initial time step. This is straightforward to include in the framework presented (steps 1-7 of the main algorithm), by simply initializing $\mathbf{x}_n(t = T)$ and $\tau_n(t = T)$. As with any time-dependent model, one should be aware of the assumptions implicit to the chosen initial condition, and its effects on the model output. For this algorithm, it is straightforward to track the effect of an applied initial condition. This can be achieved by simply tracking the fraction of initial tracers through time (Fig. II.8); at some point, all the initial tracers will be eliminated, from which point the output will no longer depend on the initial condition.

II.3 Discussion

II.3.1 Validation and Benchmarking

To validate our algorithm and its implementation, we compare the seafloor age grids generated by our algorithm against published present-day seafloor age models (Benchmark #1, Fig. II.4), direct point observations of present-day seafloor ages (Benchmark #2, Fig. II.5) and against the time-dependent age-area distribution of the oceanic lithosphere for the last 230 Myr (Benchmark #3, Fig. II.6) based on M16 (Müller et al., 2016).

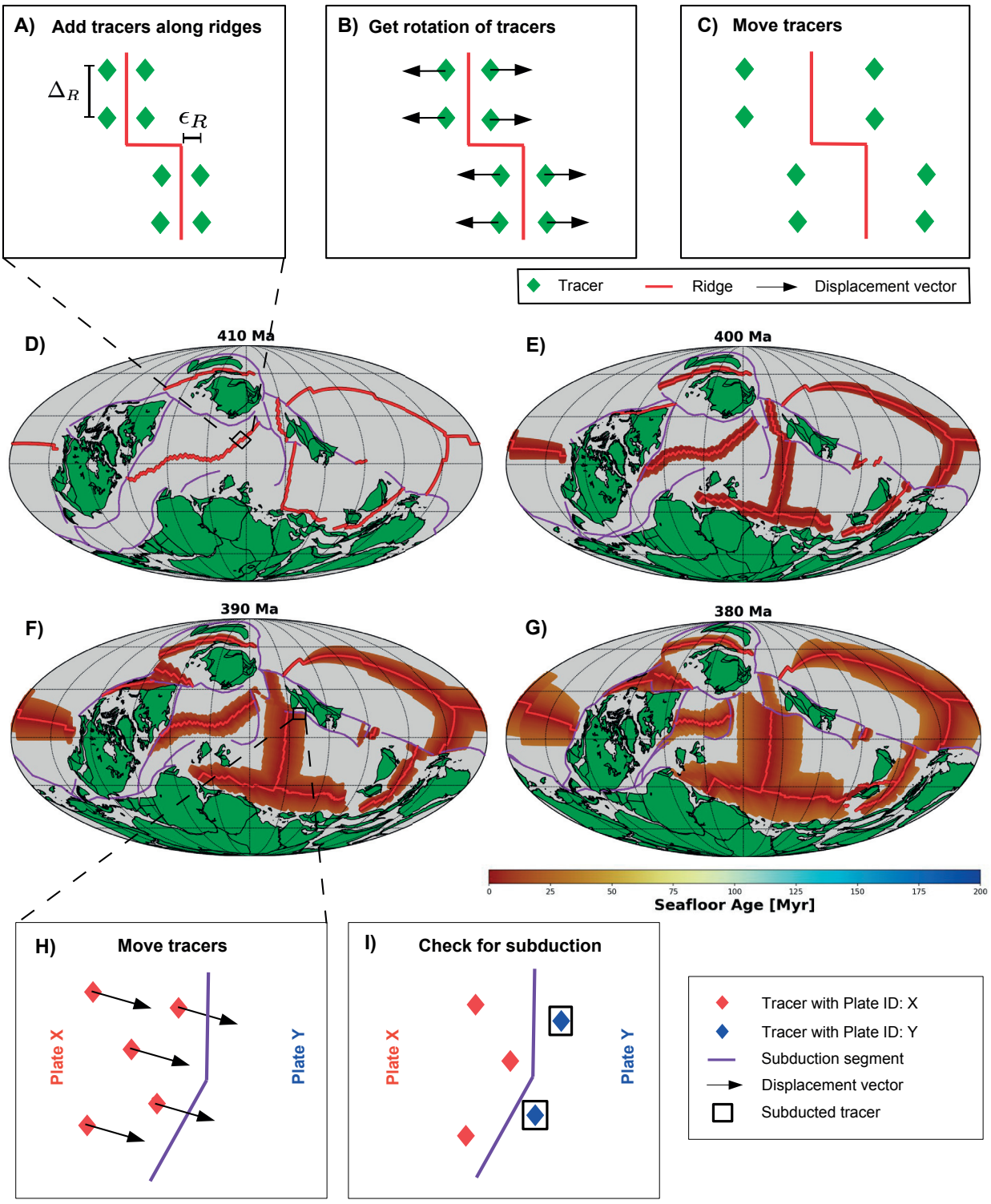

Figure II.3: Schematics illustrating how tracers are added along mid-ocean ridges (A), moved (B-C), and checked for subduction (H-I). The repeated application of these steps over time leads to an ocean basin gradually filled with tracers that track the age of the ocean floor (D-G). In this example the model of Matthews et al. (2016) is used. Note that (A-C, H-I) are not to scale.

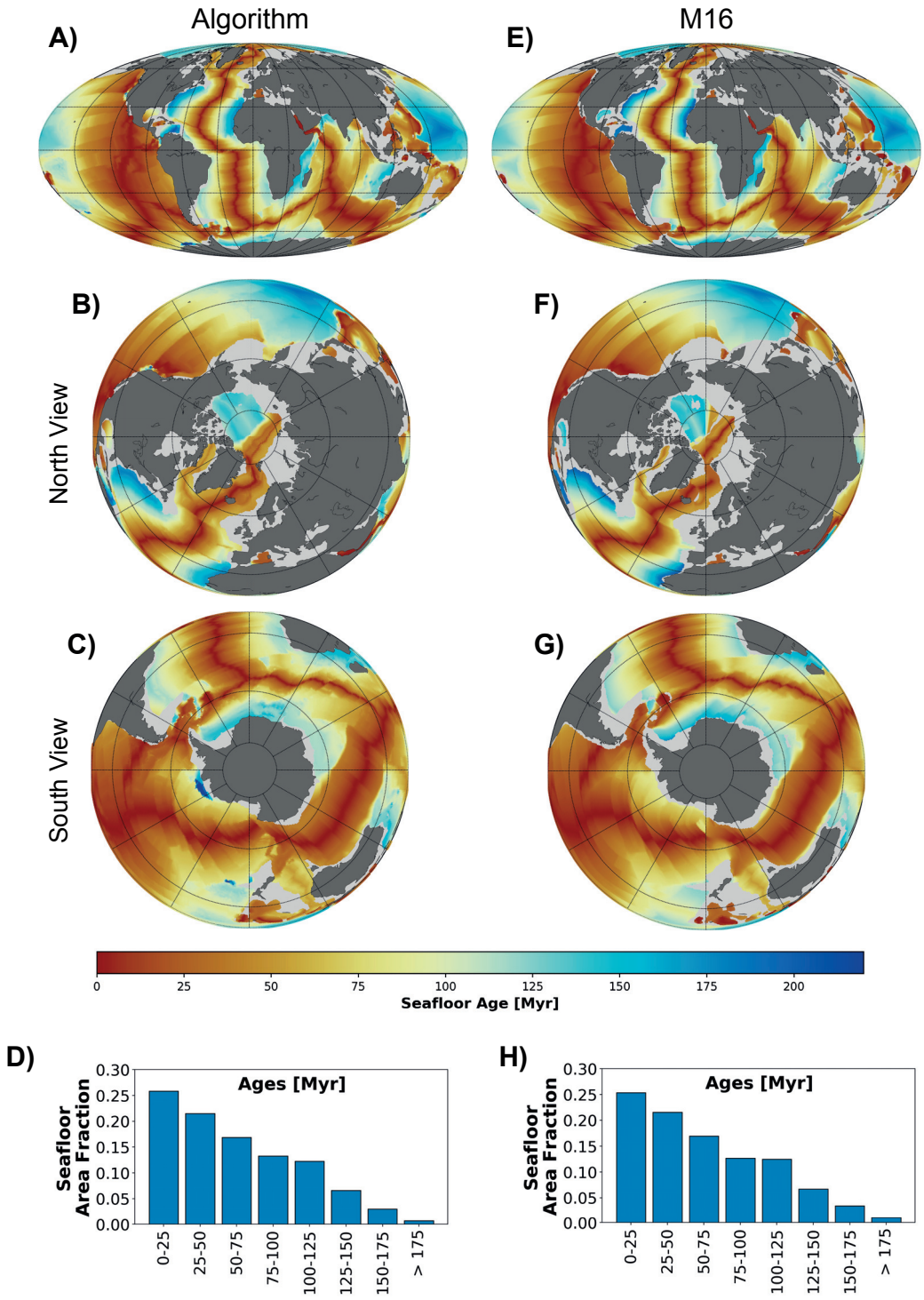

Figure II.4: Benchmark #1: Maps comparing present-day seafloor ages generated by our algorithm (A-C) to those of M16 (Müller et al., 2016) model (E-G), and their corresponding age-area distributions (D and H). The input plate model used here was Matthews et al. (2016).

To generate the seafloor age grids used to evaluate the performance of our algorithm (with its default settings), we employed Matthews et al. (2016) as the input plate model with the initial condition shown in Figure II.7A. Notably, the effect of an initial condition applied at 400 Ma is very small already by 300 Ma (only 11 % of the initial tracers remain), and zero at the present-day (Fig. II.8). The initial condition and the age grids are available from our online repository (Karlsen et al., 2019b).

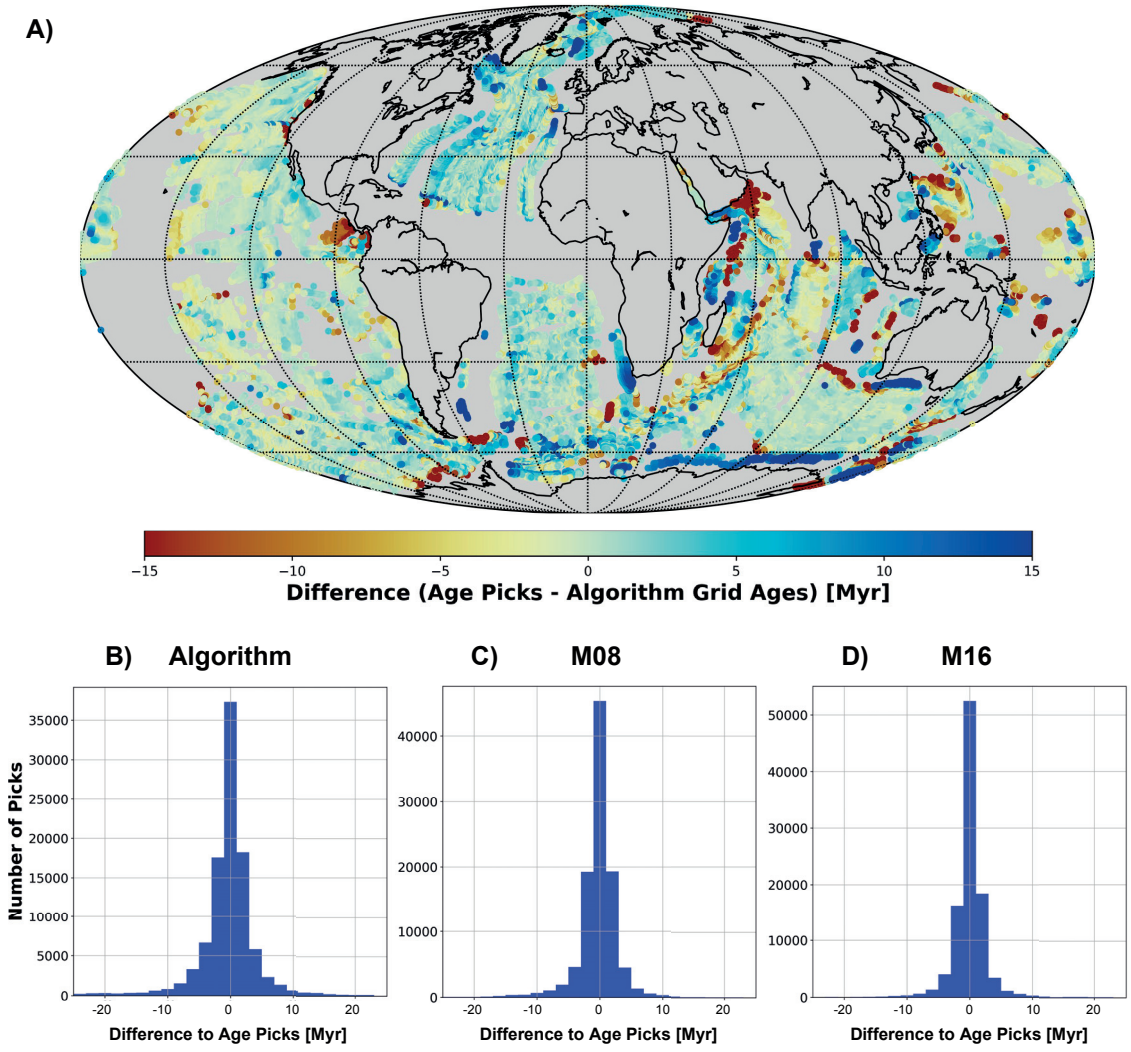

Figure II.5: Benchmark #2: Map (A) comparing the present-day age grid generated by our automatic algorithm to ages inferred from magnetic reversal picks (Seton et al., 2014). Distributions (B-D) show the number of pick ages that fall within a certain deviation from (B) our algorithm-generated age grid, (C) M08 - Müller et al. (2008a) and (D) M16 - Müller et al. (2016). The total number of pick ages is 101418.

Our algorithm reproduces the present-day seafloor well (Fig. II.4 A-C), as can be seen from the maps comparing the resulting age grids to those of M16 (Fig. II.4

E-G). The characteristic triangular present-day seafloor age-area distribution (Cogné and Humler 2004; Sclater et al. 1980), which shows the fraction of the ocean floor that falls within a certain age range, is also well reproduced. On the regional scale, some minor differences can be seen, for example there are three narrow bands of artificially young seafloor branching from the Mid-Atlantic Ridge near the Caribbean and the south-west of Iberia. These are merely consequences of the underlying plate model (Matthews et al., 2016), for which these plate boundaries are erroneously designated as mid-ocean ridges, either at present (Fig. II.1), or in the recent past. This demonstrates that a combined work-flow for developing plate tectonic reconstructions, which incorporates the generation and analysis of seafloor age grids, can reveal flaws and inconsistencies in the plate model. In the case of the aforementioned errors in the mid-Atlantic, simply re-labeling the offending boundaries as transform features and re-running the age grid algorithm addresses the issue.

To further evaluate the performance of our algorithm, we compare the generated present-day age grid against ages inferred from magnetic reversal picks (Fig. II.5). This global dataset provides by far the most comprehensive, direct sources of oceanic lithosphere ages, and is available from the Global Seafloor Fabric and Magnetic Lineation (GSFML) database (Seton et al., 2014). We see that $\sim$ 37 % of the 101418 pick ages are within $\pm$1 Myr of the ages from our age grids, and $\sim$ 84 % are within $\pm$5 Myr (Fig. II.5B). These numbers are slightly higher for models of the present-day ocean floor that are based on more labor-intensive methods (described in Section II.1) such as Muller et al. (2008b), for which they are $\sim$ 45 % and $\sim$ 92 % respectively (Fig. II.5C), and $\sim$ 52 % and $\sim$ 93 % for M16 (Fig. II.5D).

As pointed out in several studies (e.g. Becker et al. 2009; Coltice et al. 2012; Sim et al. 2016), the triangular age-area distribution of the present-day ocean floor is unlikely to be a constant feature through Earth's history. In particular, large fluctuations are predicted to have occurred in the rates of seafloor spreading and global subduction (e.g. Hays and Pitman 1973), which should preclude a constant age-area distribution of the seafloor. Moreover, the age-area distribution of the seafloor is an important feature of our planet because it exhibits a first-order control on e.g. bathymetry, sea level, and planetary cooling through regulation of surface heat flow (i.e. loss of mantle heat). Therefore, as a third benchmark, we compare the time-dependent age-area distributions of the seafloor as generated by our algorithm with those published in Müller et al. (2016).

We observe a clear time-dependence in the age-area distributions computed from our age grids, and this time-dependence is nearly identical to that predicted by M16 (Fig. II.6). Given the broad observed trend toward relatively younger seafloor ages between 140-80 Ma, we anticipate that some of these seafloor age variations are related to the widespread development of new ridge systems during the Cretaceous. The initiation of some of these new ridge systems (including the southern mid-Atlantic) was associated with late-stage Pangea

breakup, whereas other new ridges appeared in the Paleo-Pacific basin, probably related to the emplacement of large igneous provinces (Torsvik et al., 2019). The rapid development of these new ridges, producing juvenile oceanic lithosphere, must have been synchronously balanced with increased subduction that would have accelerated the destruction of relatively old seafloor. These two processes combined thus explains the tendency toward relatively younger seafloor during the Cretaceous (Fig. II.6).

In summary, our algorithm reproduces detailed reconstructions of seafloor ages like those of M16. We observe only minor regional differences between the algorithm-generated present-day seafloor age grid and the M16 model. These differences mainly occur in regions where Matthews et al. (2016) inferred plate boundary locations that deviate from the interpreted isochrons of M16. This merely demonstrates that our algorithm is an automatic and fast way to detect inconsistencies between data and models. Global features like the age-area distribution, which is important for many geodynamic applications, are robustly reproduced over time. Thus, as plate tectonic reconstructions improve, so will the reliability and regional resolution of the age-grids produced by our algorithm.

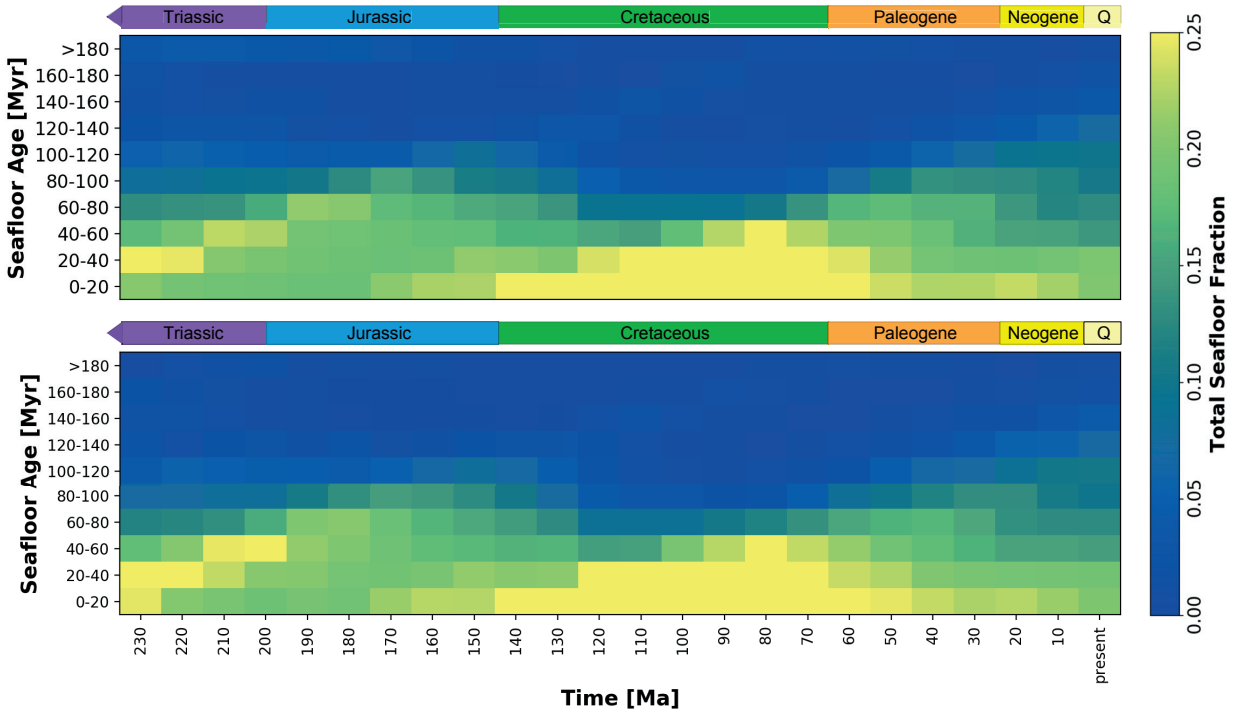

Figure II.6: Benchmark #3: Comparison of the age-area distribution of the seafloor through time for our algorithm created age grids (top) and the Müller et al. (2016) (M16) model (bottom).

II.3.2 An Example Application: Paleo Sea Level

In this section we will demonstrate how our new algorithm and paleo-age grids (computed as described in Section II.3.1) can be used to study tectonic mechanisms for sea level variations during the last 400 Myr. We would like to stress that the age-grids generated by our algorithm are bound to the input plate model, and as is the case for all plate models operating in times earlier than 200 Ma, the kinematics of all oceanic plates are necessarily synthetic (because no in situ oceanic lithosphere older than 200 Ma has survived to the present-day). This naturally implies that the construction of age-grids for earlier times is much more uncertain, and interpretation of them should be done with caution and care; here we only use these synthetic age grids to consider some global, first-order trends for the sake of demonstration.

From the generated seafloor age grids, we compute bathymetry by applying the age-depth relation of Crosby and McKenzie (2009) (alternative age-depth relations are explored in Figure II.9). Next, we use these bathymetry grids (e.g., Fig. II.7C) to compute the change in average ocean basin depth relative to the present-day. To account for temporal changes in sediment thickness (which depend directly on seafloor age as well as on latitude) we follow Straume et al. (2019). Finally, we compare how these changes in ocean depth would affect sea level, and relate them to the sea level history (Fig. II.7D) as inferred from the sedimentary record (Hallam, 1992; Haq and Al-Qahtani, 2005; Haq and Schutter, 2008). Although many other processes affect sea level fluctuations on tectonic time scales, the age-area distribution of the seafloor (through thermal subsidence of the ageing oceanic lithosphere) exhibits the first-order control, and is the only process that shows a direct correlation with the sea level record (Conrad, 2013; Karlsen et al., 2019a; Müller et al., 2008b). Therefore, an automatic method for generating seafloor age grids (from which ocean depth can be computed) enables sea level to be used as a first-order order deep-time constraint on plate tectonic reconstructions. A selection of our new seafloor age grids from the Paleozoic, with corresponding bathymetry, is shown in Figure II.10.

Our prediction of sea level fluctuations caused by ocean depth changes inferred from our 400 Myr reconstruction of age grids shows a first-order agreement with established sea level records (Hallam, 1992; Haq and Al-Qahtani, 2005; Haq and Schutter, 2008). Such a correlation has been noted previously into the Mesozoic (e.g., Conrad 2013; Müller et al. 2008b), but our algorithm applied to the plate reconstructions of Matthews et al. (2016) shows that this correlation may extend back into the late Paleozoic. Our age models predict a clear peak in sea level during the late stages of Pangea assembly ($\sim$ 340 Ma, Fig. II.7D), in agreement with the early predictions of sea-level change based on conceptual models of a supercontinental cycle (Nance et al., 1986; Worsley et al., 1986; Worsley et al., 1985). Moreover, the consistency between predicted and observed sea level indicates that the tectonic rates (seafloor spreading and its counterpart, seafloor subduction) in the underlying plate tectonic model might be reasonable

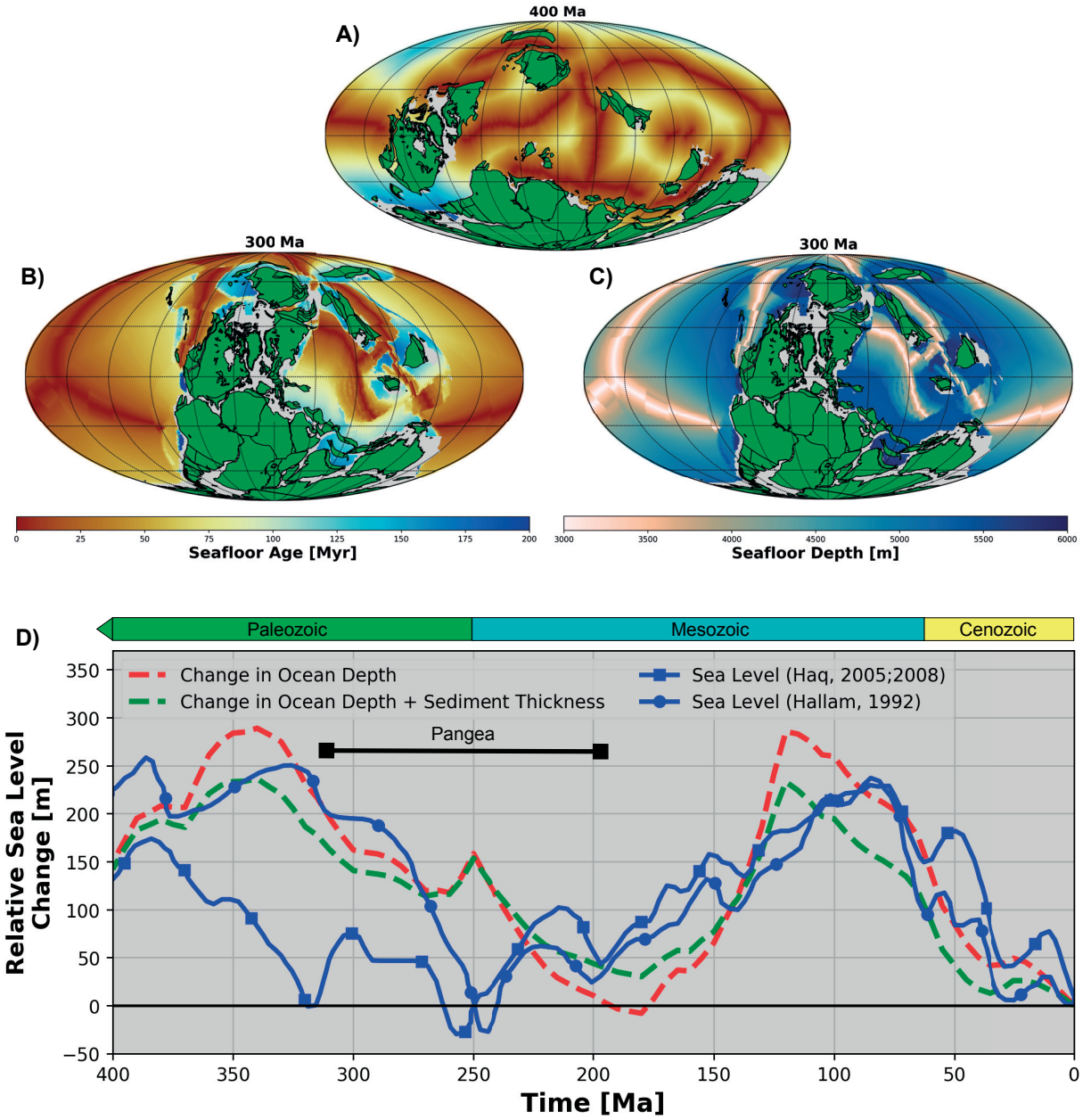

Figure II.7: Initial condition (A) used to generate seafloor age grids from the plate reconstruction of Matthews et al. (2016) from 400 Ma to the present. A snapshot at 300 Ma shows seafloor ages (B) and bathymetry (C) computed by applying the age-depth relation of Crosby and McKenzie (2009). Panels (A) and (B) use the same colorbar. From the bathymetry models we compute changes in mean ocean depth and isostatically compensate them (Pitman III, 1978) to compare sea level changes relative to the present day (C, red dashed line) to Phanerozoic sea level reconstructions (C, blue lines) inferred from the sedimentary record (Hallam, 1992; Haq and Al-Qahtani, 2005; Haq and Schutter, 2008). The effect of time-variations in sediment thickness on the sea level prediction (C, green dashed line) is computed after equation 2a in Straume et al. (2019). Thick black bar shows the approximate duration of Pangea.

for this period of time.

II.3.3 Limitations

The uncertainties in the generated seafloor age grids are directly linked to, and controlled by, the underlying plate tectonic model. Thus, the generated age-grids are dependent on global plate motions and the locations of mid-ocean ridges and subduction zones, for which the assignment of formal errors is impractical to impossible. For these reasons, we expect uncertainty in the age grids to be proportional to those of the underlying plate tectonic reconstructions, with negligible additional uncertainty introduced through the rather straightforward computational steps of our algorithm (Fig. 2). A final word of caution is that the generated age grids will never be better than the input plate model. We thus advise users to familiarize themselves with the uncertainties tied to the underlying plate tectonic reconstructions.

II.4 Conclusions

The development of plate tectonic reconstructions in the past decade has been rapid, with the introduction of powerful new tools (Boyden et al., 2011; Clark et al., 2012; Gurnis et al., 2012; Gurnis et al., 2018; Shephard et al., 2017; Wu et al., 2015) and the augmentation of global kinematic datasets (Gaina and Jakob, 2019; Seton et al., 2014) propelling a concomitant proliferation of new and emergent full-plate models, of both regional (Domeier, 2016; Domeier, 2018; Gibbons et al., 2015; Shephard et al., 2013; Torsvik et al., 2019; Zahirovic et al., 2014; Zahirovic et al., 2016) and global scope (Domeier and Torsvik, 2014; Matthews et al., 2016; Müller et al., 2016; Müller et al., 2019; Merdith et al., 2017; Seton et al., 2012). Part of the power of these latest full-plate models is that they implicitly provide information on plate kinematics across the entire global (or regional) surface (Gurnis et al., 2012), and so can be used to derive seafloor age grids to test and evaluate them, as well as to potentially explore other geophysical questions that relate to seafloor ages. Unfortunately, while the information needed to compute seafloor ages is implicitly available, the presently-established workflows to retrieve and process this information are time-consuming, laborious and not publicly available. This emphasizes the need for a method that can automatically generate seafloor age grids from full-plate tectonic reconstructions.

In this study we have presented an algorithm for generating seafloor age grids that robustly predicts the known present-day ocean floor ages, as well as a previously published model for the time-dependent age-area distribution. This new method has been applied to generate the first set of publicly available oceanic lithosphere age grids that approximate the first order age distribution of the Paleozoic oceans. Application of our generated seafloor models to estimate past sea level changes reveals a general agreement with observations from the sedimentary stratigraphy record (Hallam, 1992; Haq and Al-Qahtani, 2005; Haq

and Schutter, 2008), and provides a possible explanation for a peak in sea level during the assembly phase of Pangea. We hope that our automated algorithm will enable such comparisons between age-grid predictions and existing geological constraints to become a routine procedure of the full-plate model development process. Such an improved workflow should ultimately lead to better and more self-consistent combined reconstructions of both plate tectonics and seafloor ages.

Computer Code Availability

Name of code: Tracer Tectonics (TracTec)
Developer: Krister S. Karlsen (e-mail: k.s.karlsen@geo.uio.no; phone: +47 22 85 40 80).
Year first available: 2019.
Hardware required: No requirements.
Program language: Python 2.7.
Software dependencies: GMT (only post-processing) and the following Python libraries: pyGPlates, scipy, numpy.
Program size: 86 MB (including benchmark age grids)
Source code: http://doi.org/10.5281/zenodo.3687548

Acknowledgements

This paper has benefited from discussions with members of the CEED Earth Modelling group. Additionally, we thank Michael Gurnis and one anonymous reviewer for excellent suggestions that help improve the algorithm. Calculations in the main algorithm were preformed with Python (Van Rossum and Drake, 2011) and pyGPlates, while GMT (Wessel et al., 2013) was used for post-processing. We thank Fabio Crameri for the development of perceptually uniform and color-vision-deficiency friendly color maps (Crameri, 2018b), ensuring an accurate representation of the underlying data in the figures (Crameri, 2018a).

This research was funded by the Research Council of Norway's (RCN) Centres of Excellence Project 223272 and RCN project 250111.

Appendix II.A Supplementary Figures

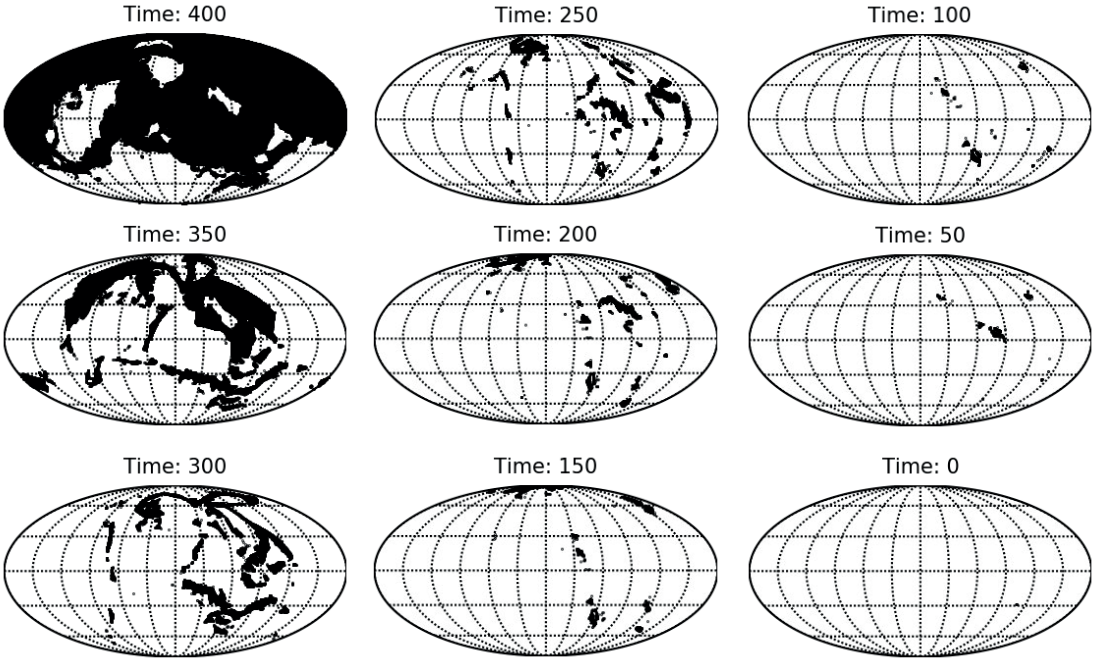

Figure II.8: Maps showing the effect of an initial condition applied at 400 Ma. Dark regions represent the area covered by the initially added tracers through time (Ma).

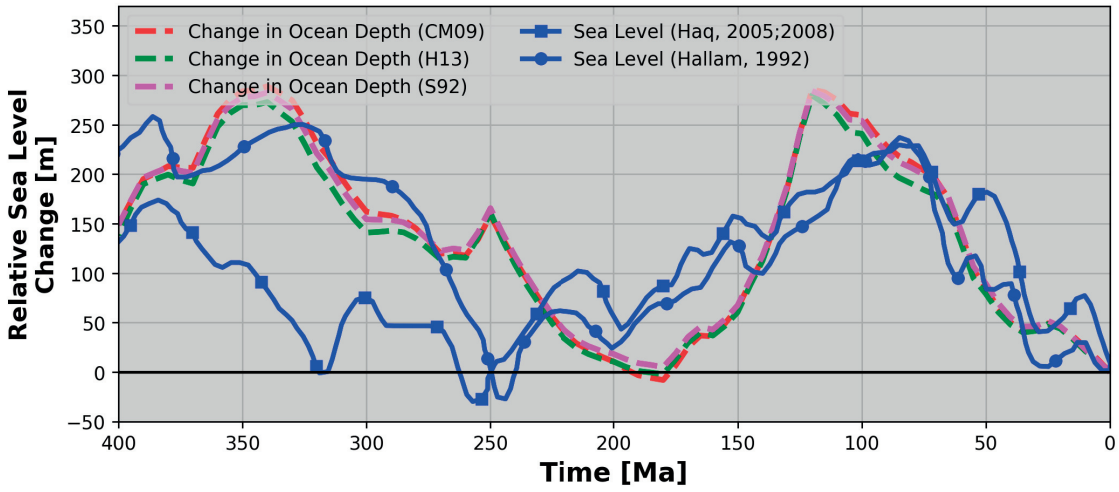

Figure II.9: Alternative sea level predictions to those in Figure II.7, based on age-depth relations CM09 - Crosby and McKenzie (2009), H13 - Hasterok (2013) and S92 - Stein and Stein (1992).

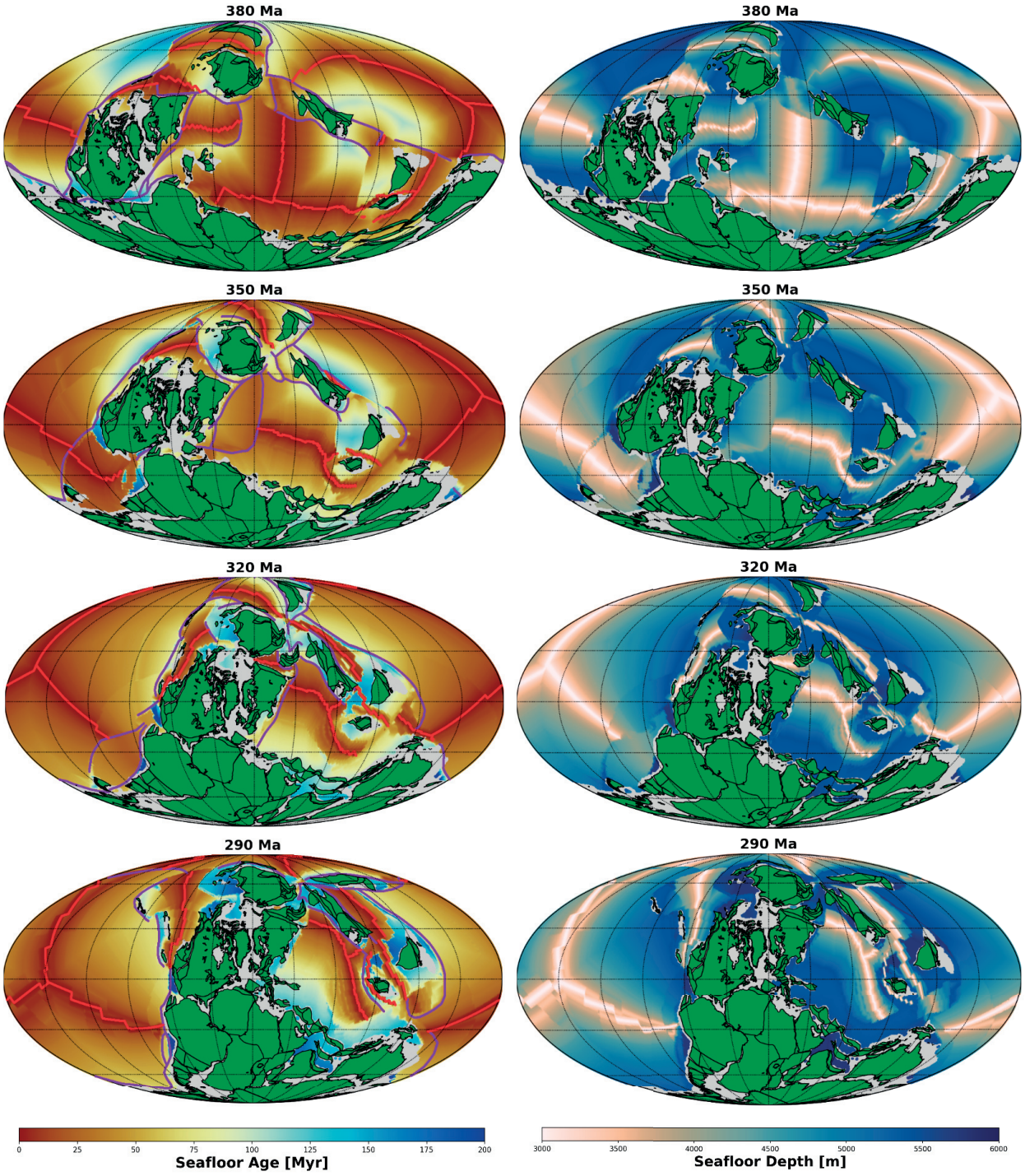

Figure II.10: Maps showing reconstructed seafloor ages (left) based on our algorithm and inferred bathymetry (right) using the age-depth relation of Crosby and McKenzie (2009).

References

Becker, T. W., Conrad, C. P., Buffett, B., and Müller, R. D. (2009). "Past and present seafloor age distributions and the temporal evolution of plate tectonic heat transport". In: *Earth and Planetary Science Letters* vol. 278, no. 3-4, pp. 233–242.

Boyden, J. A., Müller, R. D., Gurnis, M., Torsvik, T. H., Clark, J. A., Turner, M., Ivey-Law, H., Watson, R. J., and Cannon, J. S. (2011). "Next-generation plate-tectonic reconstructions using GPlates". In:

Clark, S. R., Skogseid, J., Stensby, V., Smethurst, M. A., Tarrou, C., Bruaset, A. M., and Thurmond, A. K. (2012). "4DPlates: On the fly visualization of multilayer geoscientific datasets in a plate tectonic environment". In: *Computers & geosciences* vol. 45, pp. 46–51.

Cogné, J.-P. and Humler, E. (2004). "Temporal variation of oceanic spreading and crustal production rates during the last 180 My". In: *Earth and Planetary Science Letters* vol. 227, no. 3-4, pp. 427–439.

Coltice, N., Rolf, T., Tackley, P. J., and Labrosse, S. (2012). "Dynamic causes of the relation between area and age of the ocean floor". In: *Science* vol. 336, no. 6079, pp. 335–338.

Conrad, C. P. (2013). "The solid Earth's influence on sea level". In: *Geological Society of America Bulletin* vol. 125, no. 7-8, pp. 1027–1052.

Conrad, C. P. and Lithgow-Bertelloni, C. (2004). "The temporal evolution of plate driving forces: Importance of "slab suction" versus "slab pull" during the Cenozoic". In: *Journal of Geophysical Research: Solid Earth* vol. 109, no. B10.

Crameri, F. (2018a). "Geodynamic diagnostics, scientific visualisation and StagLab 3.0". In: *Geoscientific Model Development* vol. 11, no. 6, pp. 2541–2562.

Crameri, F. (2018b). *Scientific colour-maps*. Zenodo. http://doi.org/10.5281/zenodo.1243862.

Crameri, F., Conrad, C. P., Montési, L., and Lithgow-Bertelloni, C. R. (2019). "The dynamic life of an oceanic plate". In: *Tectonophysics* vol. 760, pp. 107–135.

Crosby, A. and McKenzie, D. (2009). "An analysis of young ocean depth, gravity and global residual topography". In: *Geophysical Journal International* vol. 178, no. 3, pp. 1198–1219.

Domeier, M. (2016). "A plate tectonic scenario for the Iapetus and Rheic oceans". In: *Gondwana Research* vol. 36, pp. 275–295.

Domeier, M. (2018). "Early Paleozoic tectonics of Asia: Towards a full-plate model". In: *Geoscience Frontiers* vol. 9, no. 3, pp. 789–862.

Domeier, M. and Torsvik, T. H. (2014). "Plate tectonics in the late Paleozoic". In: *Geoscience Frontiers* vol. 5, no. 3, pp. 303–350.

Faccenna, C., Becker, T. W., Lallemand, S., and Steinberger, B. (2012). "On the role of slab pull in the Cenozoic motion of the Pacific plate". In: *Geophysical Research Letters* vol. 39, no. 3.

Gaina, C. and Jakob, J. (2019). “Global Eocene tectonic unrest: Possible causes and effects around the North American plate”. In: *Tectonophysics* vol. 760, pp. 136–151.

Gibbons, A., Zahirovic, S., Müller, R., Whittaker, J., and Yatheesh, V. (2015). “A tectonic model reconciling evidence for the collisions between India, Eurasia and intra-oceanic arcs of the central-eastern Tethys”. In: *Gondwana Research* vol. 28, no. 2, pp. 451–492.

Greiner, B. (1999). “Euler rotations in plate-tectonic reconstructions”. In: *Computers & Geosciences* vol. 25, no. 3, pp. 209–216.

Gurnis, M., Turner, M., Zahirovic, S., DiCaprio, L., Spasojevic, S., Müller, R. D., Boyden, J., Seton, M., Manea, V. C., and Bower, D. J. (2012). “Plate tectonic reconstructions with continuously closing plates”. In: *Computers & Geosciences* vol. 38, no. 1, pp. 35–42.

Gurnis, M., Yang, T., Cannon, J., Turner, M., Williams, S., Flament, N., and Müller, R. D. (2018). “Global tectonic reconstructions with continuously deforming and evolving rigid plates”. In: *Computers & geosciences* vol. 116, pp. 32–41.

Hallam, A. (1992). *Phanerozoic sea-level changes*. Columbia University Press.

Haq, B. U. and Al-Qahtani, A. M. (2005). “Phanerozoic cycles of sea-level change on the Arabian Platform”. In: *GeoArabia* vol. 10, no. 2, pp. 127–160.

Haq, B. U. and Schutter, S. R. (2008). “A chronology of Paleozoic sea-level changes”. In: *Science* vol. 322, no. 5898, pp. 64–68.

Hasterok, D. (2013). “A heat flow based cooling model for tectonic plates”. In: *Earth and Planetary Science Letters* vol. 361, pp. 34–43.

Hays, J. D. and Pitman, W. C. (1973). “Lithospheric plate motion, sea level changes and climatic and ecological consequences”. In: *Nature* vol. 246, no. 5427, pp. 18–22.

Hounslow, M. W., Domeier, M., and Biggin, A. J. (2018). “Subduction flux modulates the geomagnetic polarity reversal rate”. In: *Tectonophysics* vol. 742, pp. 34–49.

Karlsen, K. S., Conrad, C. P., and Magni, V. (2019a). “Deep Water Cycling and Sea Level Change Since the Breakup of Pangea”. In: *Geochemistry, Geophysics, Geosystems* vol. 20, no. 6, pp. 2919–2935.

Karlsen, K. S., Domeier, M., Gaina, C., and Conrad, C. P. (2019b). *TracerTectonics (Version 2.0)*. Zenodo.

Loyd, S., Becker, T., Conrad, C., Lithgow-Bertelloni, C., and Corsetti, F. (2007). “Time variability in Cenozoic reconstructions of mantle heat flow: plate tectonic cycles and implications for Earth’s thermal evolution”. In: *Proceedings of the National Academy of Sciences* vol. 104, no. 36, pp. 14266–14271.

Matthews, K. J., Maloney, K. T., Zahirovic, S., Williams, S. E., Seton, M., and Mueller, R. D. (2016). “Global plate boundary evolution and kinematics since the late Paleozoic”. In: *Global and Planetary Change* vol. 146, pp. 226–250.

Maunder, B., Hunen, J. van, Bouilhol, P., and Magni, V. (2019). “Modeling Slab Temperature: A Reevaluation of the Thermal Parameter”. In: *Geochemistry, Geophysics, Geosystems*.

Müller, R. D., Roest, W. R., Royer, J.-Y., Gahagan, L. M., and Sclater, J. G. (1997). "Digital isochrons of the world's ocean floor". In: *Journal of Geophysical Research: Solid Earth* vol. 102, no. B2, pp. 3211–3214.

Müller, R. D., Sdrolias, M., Gaina, C., and Roest, W. R. (2008a). "Age, spreading rates, and spreading asymmetry of the world's ocean crust". In: *Geochemistry, Geophysics, Geosystems* vol. 9, no. 4.

Müller, R. D., Sdrolias, M., Gaina, C., Steinberger, B., and Heine, C. (2008b). "Long-term sea-level fluctuations driven by ocean basin dynamics". In: *science* vol. 319, no. 5868, pp. 1357–1362.

Müller, R. D., Seton, M., Zahirovic, S., Williams, S. E., Matthews, K. J., Wright, N. M., Shephard, G. E., Maloney, K. T., Barnett-Moore, N., Hosseinpour, M., et al. (2016). "Ocean basin evolution and global-scale plate reorganization events since Pangea breakup". In: *Annual Review of Earth and Planetary Sciences* vol. 44, pp. 107–138.

Müller, R. D., Zahirovic, S., Williams, S. E., Cannon, J., Seton, M., Bower, D. J., Tetley, M. G., Heine, C., Le Breton, E., Liu, S., et al. (2019). "A global plate model including lithospheric deformation along major rifts and orogens since the Triassic". In: *Tectonics* vol. 38, no. 6, pp. 1884–1907.

Merdith, A. S., Atkins, S. E., and Tetley, M. G. (2019). "Tectonic controls on carbon and serpentinite storage in subducted upper oceanic lithosphere for the past 320 Ma". In: *Frontiers in Earth Science* vol. 7, p. 332.

Merdith, A. S., Collins, A. S., Williams, S. E., Pisarevsky, S., Foden, J. D., Archibald, D. B., Blades, M. L., Alessio, B. L., Armistead, S., Plavsa, D., et al. (2017). "A full-plate global reconstruction of the Neoproterozoic". In: *Gondwana Research* vol. 50, pp. 84–134.

Nance, R. D., Worsley, T. R., and Moody, J. B. (1986). "Post-Archean biogeochemical cycles and long-term episodicity in tectonic processes". In: *Geology* vol. 14, no. 6, pp. 514–518.

Pitman III, W. C. (1978). "Relationship between eustacy and stratigraphic sequences of passive margins". In: *Geological Society of America Bulletin* vol. 89, no. 9, pp. 1389–1403.

Sclater, J., Jaupart, C., and Galson, D. (1980). "The heat flow through oceanic and continental crust and the heat loss of the Earth". In: *Reviews of Geophysics* vol. 18, no. 1, pp. 269–311.

Seton, M., Whittaker, J. M., Wessel, P., Müller, R. D., DeMets, C., Merkouriev, S., Cande, S., Gaina, C., Eagles, G., Granot, R., et al. (2014). "Community infrastructure and repository for marine magnetic identifications". In: *Geochemistry, Geophysics, Geosystems* vol. 15, no. 4, pp. 1629–1641.

Seton, M., Müller, R., Zahirovic, S., Gaina, C., Torsvik, T., Shephard, G., Talsma, A., Gurnis, M., Turner, M., Maus, S., et al. (2012). "Global continental and ocean basin reconstructions since 200Ma". In: *Earth-Science Reviews* vol. 113, no. 3, pp. 212–270.

Shephard, G. E., Müller, R. D., and Seton, M. (2013). "The tectonic evolution of the Arctic since Pangea breakup: Integrating constraints from surface geology and geophysics with mantle structure". In: *Earth-Science Reviews* vol. 124, pp. 148–183.

Shephard, G. E., Matthews, K. J., Hosseini, K., and Domeier, M. (2017). "On the consistency of seismically imaged lower mantle slabs". In: *Scientific reports* vol. 7, no. 1, p. 10976.

Sim, S. J., Stegman, D. R., and Coltice, N. (2016). "Influence of continental growth on mid-ocean ridge depth". In: *Geochemistry, Geophysics, Geosystems* vol. 17, no. 11, pp. 4425–4437.

Stein, C. A. and Stein, S. (1992). "A model for the global variation in oceanic depth and heat flow with lithospheric age". In: *Nature* vol. 359, no. 6391, pp. 123–129.

Straume, E., Gaina, C., Medvedev, S., Hochmuth, K., Gohl, K., Whittaker, J. M., Abdul Fattah, R., Doornenbal, J., and Hopper, J. R. (2019). "GlobSed: Updated Total Sediment Thickness in the World's Oceans". In: *Geochemistry, Geophysics, Geosystems*.

Torsvik, T. H., Steinberger, B., Shephard, G. E., Doubrovine, P. V., Gaina, C., Domeier, M., Conrad, C. P., and Sager, W. W. (2019). "Pacific-Panthalassic reconstructions: Overview, errata and the way forward". In: *Geochemistry, Geophysics, Geosystems* vol. 20, no. 7, pp. 3659–3689.

Van Rossum, G. and Drake, F. L. (2011). *The python language reference manual*. Network Theory Ltd.

Vine, F. J. and Matthews, D. H. (1963). "Magnetic anomalies over oceanic ridges". In: *Nature* vol. 199, no. 4897, pp. 947–949.

Wessel, P., Smith, W. H., Scharroo, R., Luis, J., and Wobbe, F. (2013). "Generic mapping tools: improved version released". In: *Eos, Transactions American Geophysical Union* vol. 94, no. 45, pp. 409–410.

Worsley, T. R., Nance, R. D., and Moody, J. B. (1986). "Tectonic cycles and the history of the Earth's biogeochemical and paleoceanographic record". In: *Paleoceanography* vol. 1, no. 3, pp. 233–263.

Worsley, T., Moody, J., and Nance, R. (1985). "Proterozoic to Recent tectonic tuning of biogeochemical cycles". In: *The carbon cycle and atmospheric CO2: natural variations Archean to present* vol. 32, pp. 561–572.

Wu, L., Kravchinsky, V. A., and Potter, D. K. (2015). "PMTec: A new MATLAB toolbox for absolute plate motion reconstructions from paleomagnetism". In: *Computers & Geosciences* vol. 82, pp. 139–151.

Zahirovic, S., Seton, M., and Müller, R. (2014). "The Cretaceous and Cenozoic tectonic evolution of Southeast Asia". In: *Solid Earth* vol. 5, no. 1, p. 227.

Zahirovic, S., Matthews, K. J., Flament, N., Müller, R. D., Hill, K. C., Seton, M., and Gurnis, M. (2016). "Tectonic evolution and deep mantle structure of the eastern Tethys since the latest Jurassic". In: *Earth-Science Reviews* vol. 162, pp. 293–337.

Paper III

Spatiotemporal Variations in Surface Heat Loss Imply a Heterogeneous Mantle Cooling History

Krister S. Karlsen, Clinton P. Conrad, Mathew Domeier, Reidar G. Trønnes

Published in *Geophysical Research Letters.* , March 2021, DOI: 10.1029/2020GL092119.

Abstract

Earth's heat budget is strongly influenced by spatial and temporal variations in surface heat flow caused by plate tectonic cycles. Here we use a novel set of paleo-seafloor age grids extending back to the mid-Paleozoic to infer spatiotemporal variations in surface heat loss. The time-averaged oceanic heat flow is 36.6 TW, or ∼25 % greater than present-day. Our thermal budget for the mantle indicates that 149 K/Gyr of cooling occurred over this period, consistent with geochemical estimates of mantle cooling for the past 1 Gyr. Our analysis also suggests sustained rapid cooling of the Pacific mantle hemisphere, which may have cooled ∼50 K more than its African counterpart since 400 Ma. The extra heat released from the Pacific mantle may have been trapped there by the earlier long-lived supercontinent Rodinia (∼1.1-0.7 Ga), and the Pacific mantle may still be hotter than the African mantle today.

Plain Language Summary

Earth's interior is cooling because its rate of heat loss exceeds its rate of internal heat production. Heat loss happens at the Earth's surface and is highly variable, with thick continents providing strong insulation to Earth's interior and thin seafloor allowing more rapid heat transfer. Using models for how the continents and oceanic plates have moved for the past 400 million years, we reconstructed the history of heat loss from Earth's interior. We find that heat loss was on average 25 % higher in the past than it is today, which implies more rapid overall cooling than expected. We also find that the Pacific side of the world has lost heat at a much faster rate than the African side. This is partly due to positioning of continental landmasses, including the supercontinent Pangea, on the African side for most of the past 400 million years. By contrast, the oceans on the Pacific side offered "poor insulation" that led to ∼50°C more cooling of the Pacific mantle compared to its African counterpart. The extra heat lost from the Pacific side may have been trapped there by Rodinia, an older, long-lived supercontinent that covered the Pacific mantle about one billion years ago.

Contents

III.1 Introduction

Earth's thermal evolution is largely controlled by the rate of heat loss through the oceanic lithosphere. This cooling rate is time-dependent because changes in tectonic rates (e.g., rates of seafloor creation and consumption) affect the seafloor age distribution (e.g., Becker et al., 2009), and thus prescribe intervals of Earth history with greater or lesser oceanic heat loss. The rate of cooling is also highly variable spatially, with mantle beneath young seafloor cooling much more rapidly than its counterpart beneath large insulating continents (Fig. III.1a). These variations in mantle cooling rate change with time as the plate tectonic configuration evolves, potentially inducing large spatial and temporal variations in the heat content of the mantle (e.g., Lenardic et al., 2011). It is

important to understand such variations in order to better constrain Earth's thermal evolution back in time.

Over the past decades, the relationship between mantle heat flow and the age of the oceanic lithosphere has been continuously refined to fit geophysical data (e.g., Hasterok, 2013; Korenaga and Korenaga, 2008; Parsons and Sclater, 1977; Stein and Stein, 1992), allowing surface heat loss from the mantle to be reconstructed back in time through the use of paleo-seafloor age grids (Crameri et al., 2019; Loyd et al., 2007). However, existing reconstructions only provide estimates of global surface heat flow variations since 230 Ma, a period that adequately captures Pangea breakup, but not the earlier stages of supercontinent assembly. Early conceptual models for this "supercontinent cycle" (Nance et al., 1986; Worsley et al., 1986; Worsley et al., 1985) postulated that the age-area distribution of the oceanic lithosphere (Fig. III.1c) should vary through the different phases of this cycle, and this notion has since been reinforced by results from numerical geodynamic models (Coltice et al., 2012) and the construction and analysis of paleo-seafloor age grids (Karlsen et al., 2020; Müller et al., 2016). Thus, in order to derive a representative value of the long-term oceanic heat flow, it may be necessary to compute a time-averaged value across a wider swath of time, approximating a full supercontinent cycle. Using the first set of oceanic lithosphere age grids that extend backward to the mid-Paleozoic (400 Ma, Karlsen et al., 2020), we here reevaluate the time-dependence of oceanic heat flow and consider its implications for mantle cooling history.

We also reconstruct spatial variations in mantle heat loss across the interval spanning Pangea's assembly, duration and breakup. Such variations should cause some parts of the mantle to cool faster than others, producing spatial variability in mantle temperature. There is some geochemical and geophysical evidence for such variability. Major element geochemistry analyses of lavas from the Pacific and Atlantic ocean basins suggest that the central Atlantic upper mantle was hotter than the Pacific mantle during the 170-100 Ma interval and may have cooled by up to 150 K until the present (Brandl et al., 2013). This cooling released heat that was likely trapped by continental insulation of the central Atlantic by Pangea (∼320-180 Ma). Increases in mantle potential temperature (T_p) of similar magnitude, caused by supercontinent insulation, have also been reported in numerical and laboratory experiments (Lenardic et al., 2011). For the present-day, Brandl et al. (2013) present thermometric evidence (temperature of average zero-age MORB) that the Pacific mantle domain is 25-30 K hotter than the African domain (the Atlantic and Indian ridges). This finding agrees with the combined analysis of geophysical and geochemical data of Dalton et al. (2014), which indicates a higher mantle potential temperature in the Pacific. Such hemispheric variability in mantle temperature should be linked to spatial variations in the mantle's cooling rate. Here we use models for Earth's surface heat flow during the past 400 Myr to estimate individual cooling histories for the Pacific and African mantle domains, and briefly entertain some simple scenarios that could explain their potentially distinct thermal evolution.

III.2 Estimating Mantle Heat Loss Variations

For the present-day, Earth's total surface heat loss is estimated to be 46 TW. Of this, 29 TW is attributed to the cooling of oceanic crust (hereafter "oceanic heat loss"), 3 TW is delivered to the surface via plumes and 14 TW represents heat loss from the continents (Jaupart et al., 2015). The continental component of 14 TW includes 8 TW of radiogenic heat produced within the continental crust and lithosphere. Here we estimate changes to the heat flow conducted from the mantle through the oceanic and continental lithosphere (currently 35 TW; the 3 TW plume heat flux is treated separately according to the description in the extended methods section, supplementary Text S1). We focus particularly on the oceanic heat loss, both because it is largest component, it exhibits large variations in space and time, and it can be estimated directly from tectonic reconstructions of past seafloor.

We compute oceanic heat loss (Q_{ocean}) from the mantle by applying the age-heat flow relation (see Text S1) of Hasterok (2013) to paleo-seafloor age grids that extend back to 400 Ma, generated using the method of Karlsen et al. (2020). The plate reconstruction that was used to generate these age grids was the updated version of Matthews et al. (2016), which includes corrections for the Pacific after Torsvik et al. (2019). Mantle heat loss through the continental lithosphere (Q_{cont}) is taken to be 6 TW, evenly spread over the continental area. Note that this excludes the 8 TW of radiogenic heat production in the crust and lithospheric mantle (Jaupart et al., 2015). Although the mantle heat loss through the continents ($\sim$6 TW) might vary with time, the amplitudes of its variations are likely small compared to the more than four times larger oceanic heat flow ($\sim$29 TW at present-day). Snapshots of the resulting global heat loss grids covering the past 400 Myr are shown in Figure III.1a. Note the strong time-dependence, and that present-day heat loss from Earth's mantle represents an absolute minima for the 400-0 Ma time period, having been up to $\sim$15 TW higher in the past (Fig. III.1b). These variations are driven by changes to the age-area distribution of the seafloor (Fig. III.1c), which are caused by fluctuations in the rates of seafloor spreading and subduction during the supercontinent cycle (e.g., East et al., 2020; Karlsen et al., 2019). This emphasizes the need for a long time-series (ideally spanning one complete supercontinent cycle) of heat flow to robustly infer long-term average values. Based on the 400 Myr reconstruction of seafloor ages, we estimate the time-averaged value for oceanic heat loss to be 36.6 TW (Fig. III.1b), which is $\sim$25 % higher than the present-day value of $\sim$29 TW (Fig. III.1b). The present-day low in oceanic heat flow has also been noted before, although based on significantly shorter time-histories (Crameri et al., 2019; Loyd et al., 2007).

To investigate spatial variations in time-integrated surface heat loss, we computed the total heat loss accumulated over the past 400 Myr (Fig III.2a-b). Our results show that even over the time scale of several hundred million years, heat loss from the mantle is far from uniform. For instance, the region of the Pacific overlying

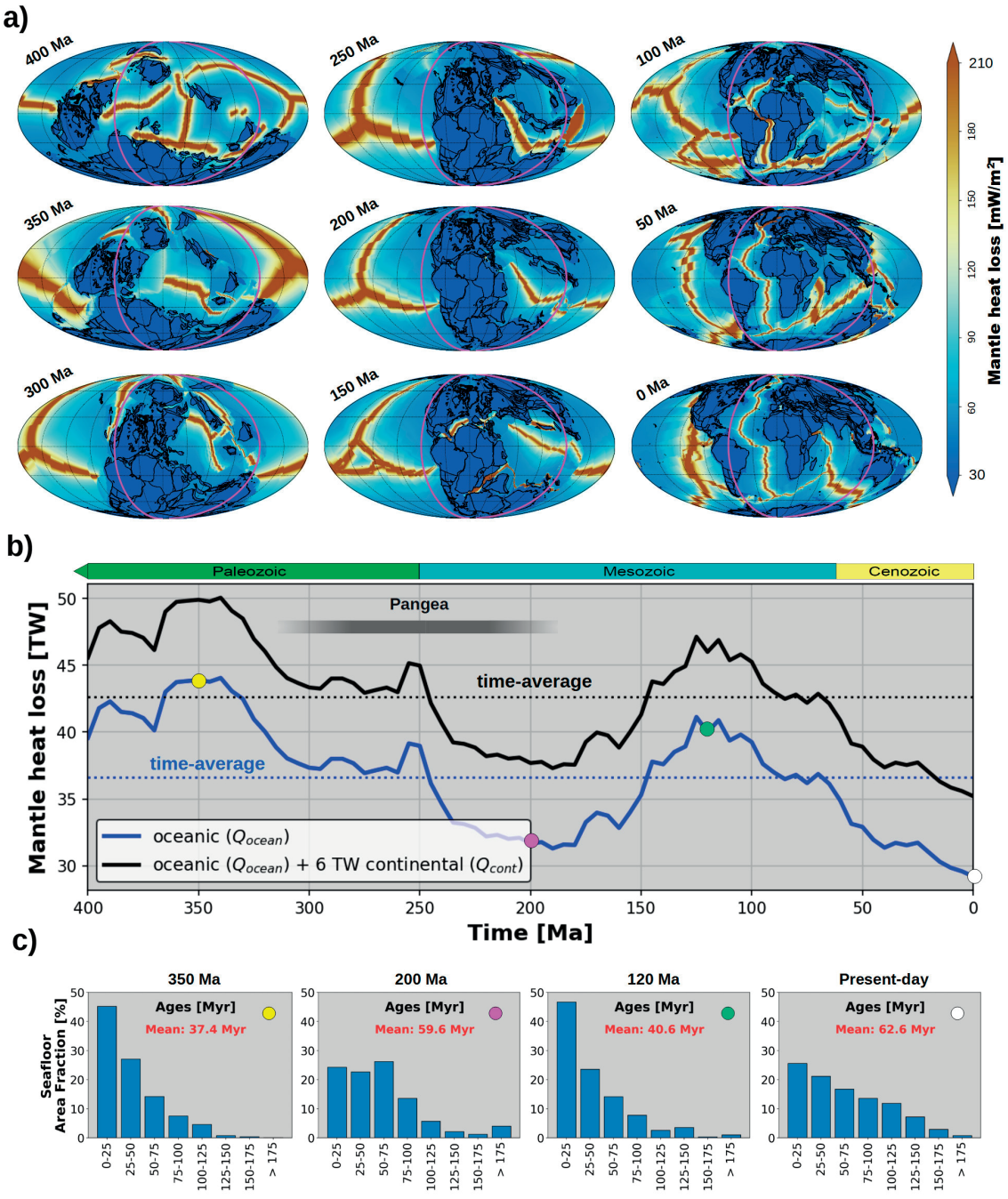

Figure III.1: **The time-dependent distribution of mid-ocean ridges and continents produces large variations in surface heat flow.** (a-b) Heat loss from Earth's mantle through time, computed according to the description in Section III.2. Meridians (60° W and 120° E) drawn in magenta indicate the separation of the Pacific and African hemispheres. (c) Seafloor age-area distributions based on the paleo-seafloor age girds generated after Karlsen et al. (2020).

the large low-shear-velocity province (LLSVP) "Jason" has lost 2-3 times as much heat as the region above "Tuzo", the African LLSVP (Fig. III.2b). This is partly due to the time-dependent distribution of continental masses and the assembly of Pangea over Tuzo, which insulated the mantle beneath Pangea but left the Pacific "exposed" to more rapid cooling via cycling of oceanic lithosphere, and partly due to the persistence of fast-spreading ridge systems (now the East Pacific Rise) positioned over Jason. Note, however, that the position of ridges in the Pacific-Panthalassic Ocean is entirely inferred before ∼150 Ma (Torsvik et al., 2019); we will return to this limitation later.

III.3 Implications for Mantle Cooling History

To estimate the impact of spatiotemporal variations in surface heat loss on the mantle's thermal evolution, we formulated a heat budget for the mantle, which we further break down into individual heat budgets for the Pacific and African mantle domains (here approximated as two hemispheres, Fig. III.1a and III.2, delineated as described in supplementary Text S1). These two mantle domains are considered separate and persistent degree-two convection cells (Conrad et al., 2013), each bounded, at least since Pangea formation, by the long-lived circum-polar belt of subduction and persistent downwelling (e.g., Torsvik et al., 2016). The fact that slabs tend to continually sink between the LLSVPs (Fig. III.4) indicates little mixing, and thus limited heat transport, between the Pacific and African mantle domains. Assuming negligible heat exchange between these domains (thermal conduction across such large spatial scales is small, Fig. III.5), we can treat the thermal history of each domain separately. Indeed, limited thermal mixing by convection, combined with an uneven distribution of continental landmasses, has been shown to cause large lateral temperature variations in numerical and laboratory experiments (Lenardic et al., 2011).

We construct a mantle heat budget following Jaupart et al. (2015), taking mantle heat sources to be 11 TW (Q_{radio}) from radiogenic heat production (which excludes the 8 TW from the continental crust and lithosphere), plus 11 TW (Q_{core}) from the core. For heat sinks we include our estimates of oceanic (Q_{ocean}) + continental (Q_{cont}) heat loss (Fig. III.1b, black line) and an additional 3 TW ($Q_{hotspots}$) heat output from hotspots (Arnould et al., 2020; Jaupart et al., 2015). This value might be relatively conservative, considering a recent estimate based on excess topography (including amagmatic swells) suggesting that the present-day plume heat flux may be as high as ∼6.3 TW (Hoggard et al., 2020). The heat sources and plume heat flux are assumed to be constant through time and evenly distributed between the Pacific and African mantle domains. This assumption allows us to isolate the effect of variations in oceanic heat loss on mantle cooling. A relatively stable plume heat flux with time, around 3 TW, is supported by state of the art mantle convection models with Earth-like tectonics on the surface (Arnould et al., 2020), while time-variations in the core heat flux were probably less than ∼3 TW during the Phanerozoic (Nakagawa and Tackley,

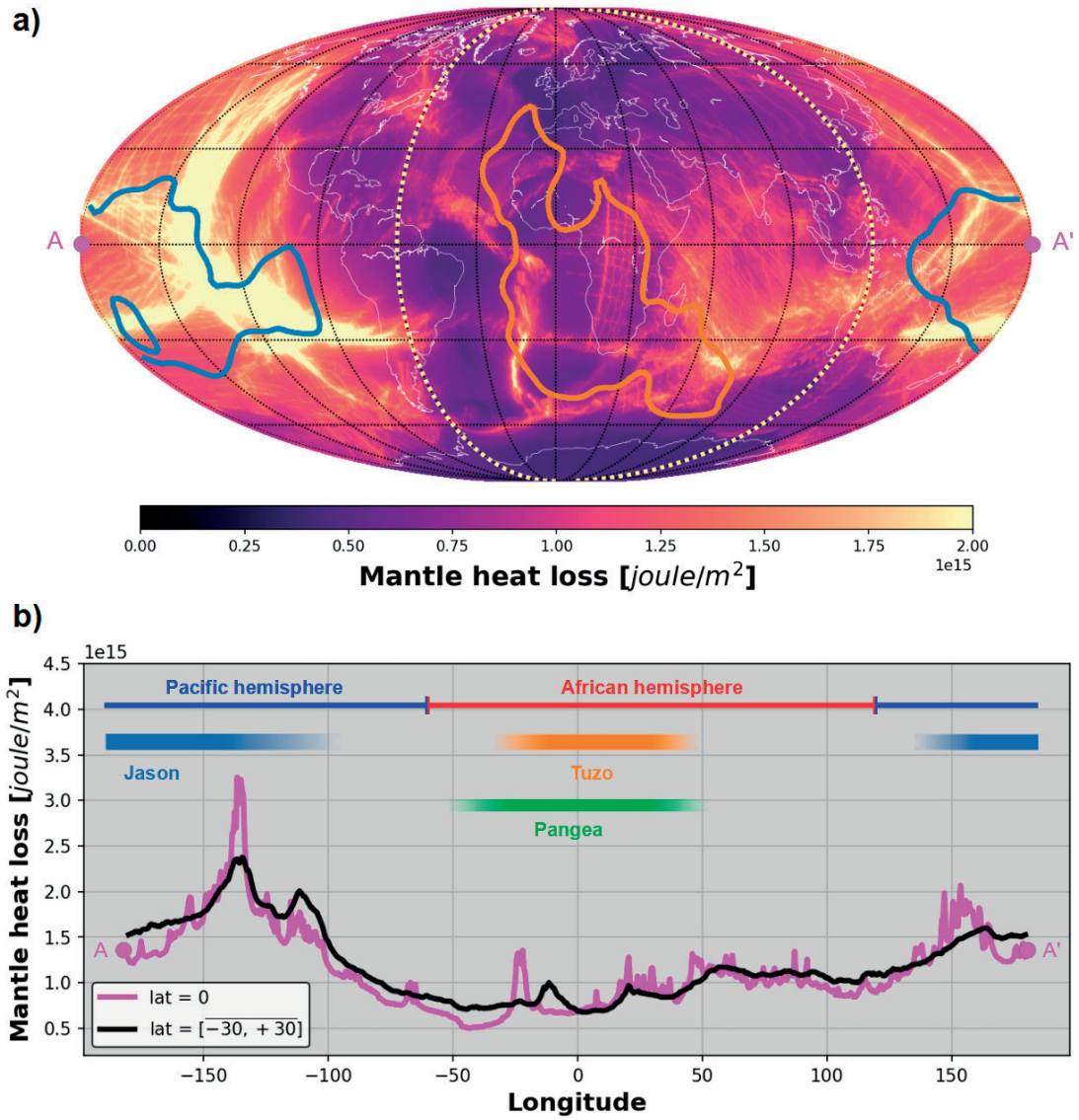

Figure III.2: **The Pacific mantle domain has lost significantly more heat than the African over the past 400 Myr.** (a) Accumulated mantle heat loss (oceanic + continental) over the past 400 Myrs. Regions above the Pacific and African LLSVPs (Jason and Tuzo), with edges defined after Torsvik et al. (2010), are shown using blue and orange lines. Dashed, light-colored meridians indicate the separation of the Pacific and African hemispheres. (b) Equatorial slice (magenta line) shows longitudinal variations in heat loss, and mean values (black line) from a region within 30° of the equator show smoother variations. Bars indicate the approximate present positions of the LLSVPs Jason and Tuzo, and the past position of Pangea.

2011; Olson, 2016; Zhang and Zhong, 2011). By comparison, the continuous surface heat loss estimated herein has varied by ∼15 TW since 400 Ma (Fig. III.1b, black line).

Based on the mantle heat budget adopted, we can calculate rates of mantle cooling for the entire mantle and for each of the two domains separately using:

$$dT/dt = \frac{Q_{sinks} - Q_{sources}}{m \cdot c} \tag{III.1}$$

where, $c = 1250$ J/(K kg) and $m = 4.01 \cdot 10^{24}$ kg (or $m/2$ for each hemisphere; see Text S1 for more details). The resulting estimates indicate that since 400 Ma the whole mantle has cooled ∼60 K (Fig. III.3c), or at a time-averaged rate of 149 K/Gyr, with a maximum of ∼200 K/Gyr at 350 Ma, and a minimum of ∼100 K/Gyr at the present-day (Fig. III.3b). However, that cooling was unevenly distributed with significantly more heat having left through the Pacific hemisphere. Our calculations suggest that the Pacific cooled at a time-averaged rate of 208 K/Gyr since 400 Ma, more than twice that of the 90 K/Gyr time-averaged rate for the African hemisphere (Fig. III.3b). In the context of cumulative heat loss, the Pacific and African domains cooled by 83 K and 36 K respectively since 400 Ma, implying a differential in mantle cooling of almost 50 K since at least the mid-Paleozoic (Fig. III.3c).

III.4 Discussion

III.4.1 Implications for the Whole-Mantle: Heat Budget and Cooling History

The mantle heat budget and its related cooling history are often inferred based on present-day values of surface heat loss (e.g., Jaupart et al., 2015). Here we have shown, using a novel set of seafloor age grids that extend back to the mid-Paleozoic (400 Ma), that the present-day likely represents a time of anomalously low surface heat flow caused by an "all time old" configuration of ocean basins (see e.g. Müller et al., 2016 for a review). Considering that the time-averaged value of mantle heat loss from cooling oceanic lithosphere might be closer to 36.6 TW, rather than ∼29 TW (Fig. III.1b), the long-term rate of planetary cooling may be significantly higher than previous estimates based on the present state of the Earth.

Using source temperatures from non-arc basaltic rocks covering the past 4 Gyr (Herzberg et al., 2010), and assuming a present-day mantle potential temperature of a little more than 1400 °C, Jaupart et al. (2015) estimated the mantle's long-term cooling rate to be 50-100 K/Gyr. However, if we instead consider the data from Herzberg et al. (2010) only for the past 1 Gyr and use a present-day potential temperature of 1350 °C, the least squares solution suggests a more recent mantle cooling rate of 155 K/Gyr (Fig. III.6). This rate is comparable to cooling rate estimates for the past 1 Gyr from Korenaga (2008a) and Korenaga (2008b), and is close to our time-averaged whole-mantle cooling rate of 149 K/Gyr for the past 400 Myr (Fig. III.3b). An alternative explanation, which would reconcile our high time-averaged oceanic heat flow (Fig. III.1b) with the slower cooling rates of Jaupart et al. (2015) (50-100 K/Gyr), is that the poorly

constrained internal heat sources are larger than the typical "preferred values" that we used in our mantle heat budget (Section III.3). Indeed, we assumed a core heat flux of 11 TW and a radiogenic mantle heat production of 11 TW, but Jaupart et al. (2015) suggest that these could be as high as 17 TW and 17 TW, respectively. We therefore explore the effect of higher (and lower) values for these heat sources on time-averaged mantle cooling rates and total mantle cooling over the past 400 Myr in Figure III.7. Note that the nearly 50 K of accumulated temperature difference between the Pacific and African mantle domains since 400 Ma is independent of the magnitude of these heat sources, as long as they are evenly distributed between the domains (Fig. III.7e,f).

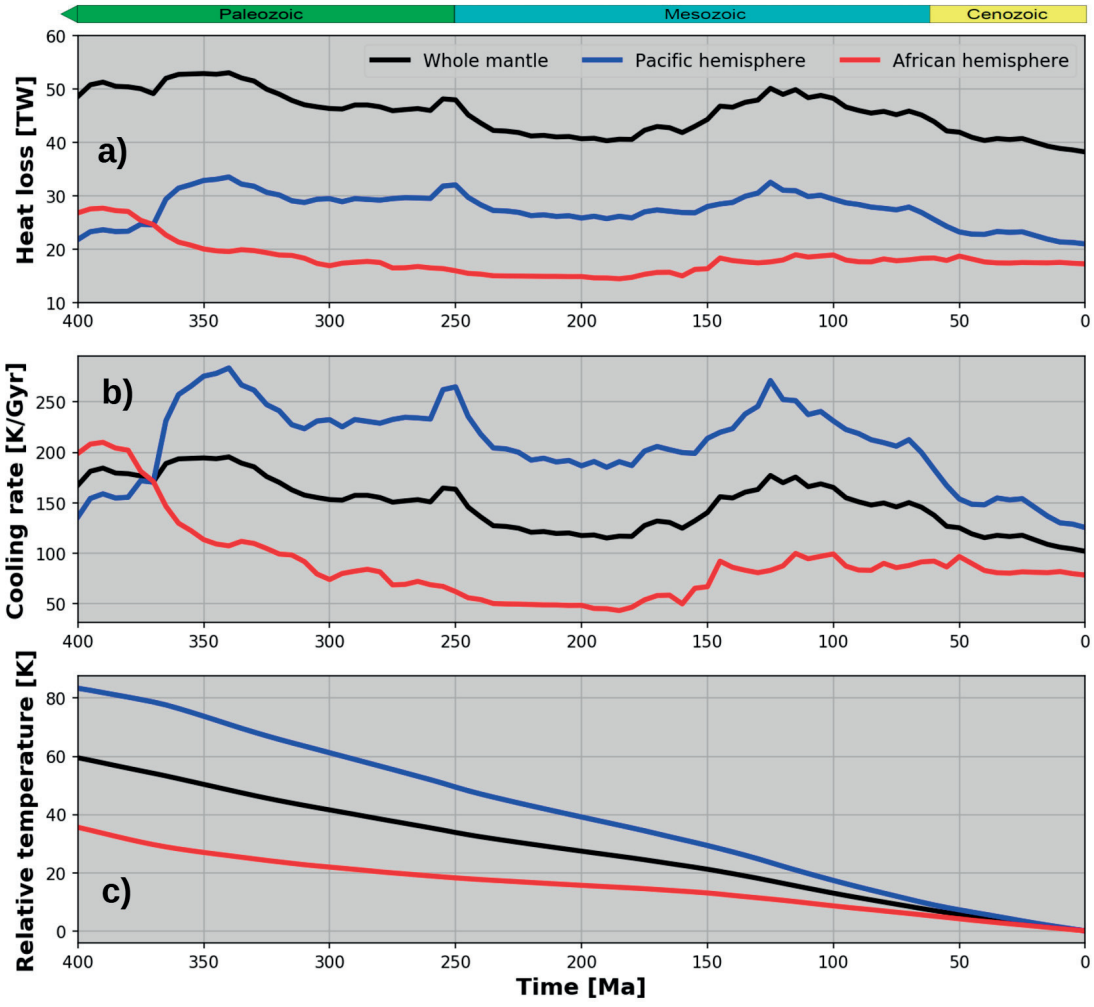

Figure III.3: **Estimated mantle cooling rates suggest significantly more cooling of the Pacific mantle domain over the past 400 Myr, compared to the African domain.** (a) Total mantle heat loss (oceanic + continental + hotspots) and its distribution between the hemispheres (defined in Fig. III.2). (b) Mantle cooling rates are computed from Eq. III.1, based on the balance between heat loss (a) and heat sources (see Section III.3). (c) Curves showing mantle temperatures relative to the present-day, obtained by integrating the cooling rates (b) backwards in time.

III.4.2 Is the Pacific Mantle Hotter than the African Mantle?

Although our calculations suggest that the Pacific hemisphere has been cooling at a higher rate, this does not necessarily mean that it is currently colder than the African hemisphere. The currently higher heat flow in the Pacific may be the manifestation of a hotter mantle beneath the Pacific (Brandl et al., 2013; Dalton et al., 2014). Given our rates of cooling (Fig. III.3b), this would imply that the Pacific has been hotter for more than 400 Myrs, and remains so, despite its faster cooling. The initial heating may have been caused by supercontinental thermal insulation (e.g., Lenardic et al., 2011) by the Precambrian supercontinent Rodinia, which may have covered the paleo-Pacific (Panthalassic) mantle domain (e.g., Tegner et al., 2019). In the case of an "ideal" supercontinent configuration (i.e. at ∼250 Ma, Fig. III.1a), one hemisphere is stripped of continents and cools about 150 K/Gyr faster than the one occupied by the supercontinent (Fig. III.3b). This suggests that if Rodinia lasted for about 400 Myr (∼1.1-0.7 Ga, e.g. Torsvik and Cocks, 2016), the Pacific mantle domain may have accumulated heat corresponding to an extra 60 K compared to the African. Given that the rate of mantle heat loss in the Pacific hemisphere may not have increased above its African counterpart until the Pacific lost most of its continents, the heat accumulation within the Pacific domain may have persisted up until about ∼370-350 Ma (Fig. III.1a and 3a). In this scenario, much of that 'residual' (Rodinian) heat has been lost in the past 400 Myr, but some still remains (as the Pacific mantle domain has cooled ∼50 K relative to the African over this period). Of course, this assumes that heat transfer between these hemispheres has been limited. A "long-lived hotter Pacific"-scenario could explain the consistently higher plate velocities of the Pacific hemisphere during the past 400 Myr (Fig. III.8), because a hotter mantle implies lower mantle viscosity and smaller resistance to plate motions.

III.4.3 Constraints on Mantle Temperature Variations

The notion of a persistently hotter Pacific mantle domain may seem partly contradictory to geochemical and crustal thickness constraints. The compositions of mid-ocean ridge basalts (MORB) from the Atlantic and Pacific basins suggest that the mantle potential temperature (T_p) beneath the early central Atlantic (∼170 Ma) was up to 150 K hotter than at present (Brandl et al., 2013). Finding no evidence of comparably elevated mantle temperatures for older Pacific MORB within the 170-5 Ma age range, Brandl et al. (2013) attributed the central Atlantic thermal anomaly to continental insulation. By contrast, the average T_p recorded by zero-age Pacific and central Atlantic basalts are about 1413 and 1385 °C, respectively (Brandl et al., 2013), suggesting a currently hotter Pacific domain. A slightly hotter present-day Pacific mantle is in agreement with our Rodinia scenario (Section III.4.2). A regression of oceanic crustal thickness for the Pacific and African hemispheres over the past 170 Myr presented by Van Avendonk et al. (2017), also supports a currently hotter Pacific but a faster-cooling African domain. Their results indicate that the present average crustal thickness, broadly

corresponding to T_p, of the East Pacific Rise exceeds that of the Atlantic and Indian Ocean ridges, but that the crustal thickness in the African hemisphere has thinned considerably more than in the Pacific hemisphere during the past 170 Myr. The strong decrease in oceanic crustal thickness in the African domain corresponds to an estimated cooling of 390 K/Gyr. Such rapid cooling is also reflected by the T_p decrease of 880 K/Gyr estimated for the central Atlantic by Brandl et al. (2013). Both estimates are for the last 170 Myr. The major caveat to these geothermometric and crustal thickness constraints, however, is that they may reflect more fertile source compositions combined with a hot asthenosphere shortly after continental rifting (Text S2).

The apparent faster cooling of the African hemisphere suggested by Van Avendonk et al. (2017) and Brandl et al. (2013) may be limited to just the upper mantle. In this case, the geochemically-constrained rapid cooling of the African domain could represent the release of heat trapped shallowly beneath Pangea. Slow thermal mixing within the African domain, as indicated by the slow plate speeds there (Fig. III.8), would allow rapid cooling of the uppermost mantle without rapid cooling of the entire African domain (upper and lower mantles). In comparison, the Pacific mantle domain, with its fast spreading ridges and plates (Fig. III.8), may be more vigorously convecting and well-mixed (King and Adam, 2014). Therefore, it is not straightforward to compare our hemispheric cooling rates (Fig. III.3b), which represent averages of the full mantle depth, with cooling rates inferred from analyses of oceanic crust. The thick oceanic crust and elevated T_p estimates of the early Atlantic and Indian ocean basin might also be related to more fertile upper mantle sources resulting from the Pangea assembly and breakup processes, as well as from plume head materials supplied by a number of large igneous provinces (e.g. Doucet et al., 2020; Torsvik, 2020; Text S2). Alternatively, additional heat sources in the Pacific mantle, such as elevated core heat flow or extra heat-producing elements, could explain the more rapid long-term heat flow there, but there is currently no evidence of such a source (Olson, 2016).

III.4.4 Limitations

The quality of our surface heat loss calculations depends on paleo-seafloor age grids generated based on the plate tectonic reconstructions of Matthews et al. (2016), using the algorithm of Karlsen et al. (2020). This algorithm has been shown to introduce only negligible errors beyond those already present in the underlying plate tectonic model. Thus, the quality of the age-grids depends on the restoration of mid-ocean ridges and subduction zones, and the reconstruction of global plate kinematics, for which formal errors are difficult to impossible to estimate. Despite being unquantified, it is reasonable to assume that these spatial uncertainties are very significant for time-periods lacking preserved oceanic lithosphere (i.e. older than ∼200 Ma). Nevertheless, our main conclusions, namely (1) that the present-day represents a time of anomalously low surface heat flow and (2) that the Pacific mantle domain has been cooling

more rapidly than its African counterpart, persist even if we consider only the last 200 Myr.

Notwithstanding that the spatial uncertainties may be very large for times lacking preserved oceanic crust, estimates of global surface heat flow for these times may still be reasonable. This is because global sea level variations on time-scales of $\sim 10^8$ yr are dominated by ocean basin volume changes driven by the time-dependent seafloor age-area distribution (Conrad, 2013; Karlsen et al., 2019; Müller et al., 2008). Thus, the sea level record serves as a first-order proxy for oceanic surface heat flow (Harrison, 1980; Fig. III.9). Karlsen et al. (2020) demonstrated that their seafloor age grids show good agreement with the history of sea level extending back to 400 Ma. With this in mind, we suggest that the temporal variations in global heat flow presented here are likely reasonable, but the spatial variations in oceanic heat flow for times older than ∼200 Ma should be cautiously interpreted.

III.5 Conclusions

Earth's thermal evolution is the result of an imbalance between surface heat loss and internal heat production. Here we have shown that the former is strongly time-dependent, and far from spatially uniform. The assembly and breakup of supercontinents alters the age-area distribution of the ocean basins, resulting in uneven thermal insulation and cooling of the mantle. These variations create large lateral temperature variations between mantle domains. We summarize our main findings as follows:

- Surface heat flow, just like the sea level (Conrad, 2013; Fig. III.9), shows peaks during the assembly and dispersal phases of the supercontinent cycle, and lows during the lifetime of the supercontinent (Pangea) and periods of maximally dispersed continents (such as present-day). Over the past 400 Myr, variations in oceanic heat flow ranged from a maximum of ∼44 TW during the assembly phase of Pangea (350 Ma), to an all time low of ∼29 TW at present-day, with a time-averaged value over the supercontinent cycle of 36.6 TW (Fig. III.1b). This loss of heat exceeds that gained from mantle heat sources, and we estimate overall cooling of 149 K/Gyr since 400 Ma, consistent with observations of mantle potential temperature during the past 1 Gyr (Herzberg et al., 2010; Fig. III.6).
- The proportion of fast-spreading ridges and area covered by cooling oceanic crust determines the relative heat loss between the Pacific and African hemispheres. We find that high spreading activity in the Pacific hemisphere (Fig. III.1a) led to greater heat flow there and drove ∼50 K more cooling in the Pacific mantle domain compared to the African domain during the past 400 Myr. This excess heat may have accumulated during an earlier

period of slow cooling in the Pacific domain, caused by presence of the long-lived supercontinent Rodinia (∼1.1-0.7 Ga). The two hemispheres may thus have experienced alternating periods of slower and faster cooling, according to the formation and dispersal of supercontinents.

Looking ahead, we consider improved plate tectonic reconstructions, combined with better geophysical and geochemical constraints on large-scale temperature variations within the mantle, both past and present, to be crucial for a greater understanding of hemispheric differences in mantle temperature. We contend that such temperature differences result from tectonic cycles at the surface, and we expect them to have significantly impacted Earth's thermal evolution.

Acknowledgements

We appreciate efficient editorial handling by Steve Jacobsen, constructive journal reviews by Alana Semple and an anonymous reviewer, as well as additional feedback from Adrian Lenardic.

All the data and software necessary to reproduce our results, obtained as described in Section III.2, are publicly available. The plate model used can be downloaded from https://www.earthbyte.org/global-plate-boundary-evolution-and-kinematics-since-the-late-paleozoic/ and the code used to calculate the seafloor age grids (Karlsen et al., 2019b) can be downloaded from http://doi.org/10.5281/zenodo.3687548. This research was funded by the Research Council of Norway's (RCN) Centres of Excellence Project 223272 and RCN project 250111.

Appendix III.A Supporting Information

Text SI III.1: Methods

Generating Seafloor Age Grids

Karlsen et al. (2020) developed a code (http://doi.org/10.5281/zenodo.3687548) that generates seafloor age grids from plate tectonic reconstructions. We used this software to produce age grids from the present-day back to 400 Ma using the updated plate model of Matthews et al. (2016), which includes corrections for the Pacific after Torsvik et al. (2019).

Calculating Heat Flow

We divide the surface of the Earth into grid cells (0.5 degree resolution). Because Matthews et al. (2016) provides the reconstructed locations of continents, and Karlsen et al. (2020) provides seafloor ages, each cell is at a given point in time (400 Ma to present) defined as either a continent cell or seafloor cell. A

seafloor cell has a crustal age τ associated with it, while a continent cell does not. The heat flow from a continent cell is calculated as 6 TW divided by the total continental area at the time. The heat flow $q(\tau)$ from a seafloor cell is calculated after Hasterok (2013) as:

$$q(\tau) = \begin{cases} 506.7\,\tau^{-1/2}, & \tau \leq 48.1\,\text{Myr} \\ 53 + 106\,e^{-0.034607\,\tau}, & \tau > 48.1\,\text{Myr} \end{cases}$$

The result is a global grid, where every cell has a heat flow value assigned to it (Fig. III.1a). The total continental heat flow (Q_{cont}) is 6 TW by our definition, but the total oceanic heat flow (Q_{ocean}) is calculated by integrating over the ocean basin area.

Separation into Hemispheres

We approximate the Pacific and African mantle domains as two hemispheres, separated by the 60°W and 120°E meridians (see Fig. III.1a and III.2). These meridians approximately follow the circumpolar belt of seismically-observed slab material in the mantle, which delineates a curtain of downwelling flow in the mantle that separates the two hemispheres and prevents heat transfer between them (Torsvik et al., 2016). To calculate the mantle heat loss associated with each of these two domains, we integrate the surface heat loss grid (Fig. III.1a) over each hemisphere separately. Since we do not know the time-dependent spatial distribution of the surface heat loss associated with plumes (3 TW), we add 1.5 TW to each hemisphere's surface heat loss. We denote the heat loss from each of the mantle domains Q_{Pac} and Q_{Af}. Thus, Q_{Pac} and Q_{Af} each contain contributions from both oceanic and the continental heat loss, as well as half the global plume heat flux. Time-variations in Q_{Pac} and Q_{Af} are plotted in Fig. III.3a.

Calculating Mantle Cooling

Based on the mantle heat budget described in Section III.3 we can calculate the cooling rates (K/Gyr, defined as positive when the mantle is cooling, Fig. III.3b) of the whole mantle following

$$dT/dt = \frac{Q_{ocean} + Q_{cont} + Q_{hotspots} - Q_{radio} - Q_{core}}{m\,c},$$

and for each of the two hemispheres

$$dT/dt = \frac{Q_{Pac} - \frac{1}{2}Q_{radio} - \frac{1}{2}Q_{core}}{\frac{1}{2}m\,c},$$

and

$$dT/dt = \frac{Q_{Af} - \frac{1}{2}Q_{radio} - \frac{1}{2}Q_{core}}{\frac{1}{2}m\,c}.$$

Here, $c = 1250$ J/(K kg) and $m = 4.01 \cdot 10^{24}$ kg. Note that heat contributions related to radiogenic heating and core-mantle heat flow are assumed evenly distributed between the two hemispheres. To obtain mantle cooling curves relative to the present-day (Fig. III.3c), the cooling rate curves dT/dt are integrated backwards in time from 0 Ma to 400 Ma.

Text SI III.2: Pangea Assembly and Breakup

While the Pacific domain was almost entirely covered by oceanic lithosphere generated by rapidly spreading mid-ocean ridges for the last 350 Ma (Fig. III.1a), the African hemisphere included abundant continental lithosphere and was characterized by the assembly and breakup of Pangea. The assembly of Pangea followed the subduction of large ocean basins and major orogenic events associated with continental collision. This contaminated the asthenosphere of the African mantle domain with metasomatised mantle wedge material and detached continental lithosphere and lower continental crust. The sinking slabs of oceanic lithosphere would have contaminated deeper parts of the sub-Pangean mantle. The chemical imprints of such material are seen in both ocean island basalts (Doucet et al., 2020) and mid-ocean ridge basalts (Meyzen et al., 2007) of the African hemisphere, most notably in the DUPAL region of the south Atlantic and Indian basins (Hart, 1984).

The elevated thickness of old oceanic crust close to the passive margins in the African hemisphere may result from a combination of more fertile sources and an elevated mantle potential temperature. Both factors were probably important during continental rifting and early spreading along the Central Atlantic ridge from 195 Ma, along the South Atlantic, Southwest Indian and Central Indian ridges from about 130 Ma, as well as along the Labrador Sea, Baffin Bay and NE Atlantic ridges after 62-54 Ma (Jones et al., 2017; Torsvik and Cocks, 2016). Continental break-up and incipient oceanic spreading caused upwelling and extensive melting of enriched and hot asthenosphere, stemming from the assembly of, and subsequent thermal insulation by, Pangea. The eruption of large igneous provinces (LIPs), which instigated rifting and oceanic spreading, partly preceded and partly accompanied the breakup. In this context, the important LIPs are: the Central Atlantic Magmatic Province (201 Ma), Karoo-Ferrar (183 Ma), Parana-Etendeka (134 Ma), Rajmahal (118 Ma), South (114 Ma) and Central (100 Ma) Kerguelen, the Agulhas Plateau (100 Ma), Marion-Madagascar (87 Ma) and the North Atlantic Igneous Province (62 Ma) (Torsvik, 2020). The plume heads associated with these LIP events distributed fertile and hot mantle material laterally over long distances, commonly exceeding 1000 km. Although the main LIP activity mostly preceded the early generation of oceanic crust, some of the fertile and hot plume head material was likely incorporated into the asthenosphere, and may have contributed to the thick oceanic crust.

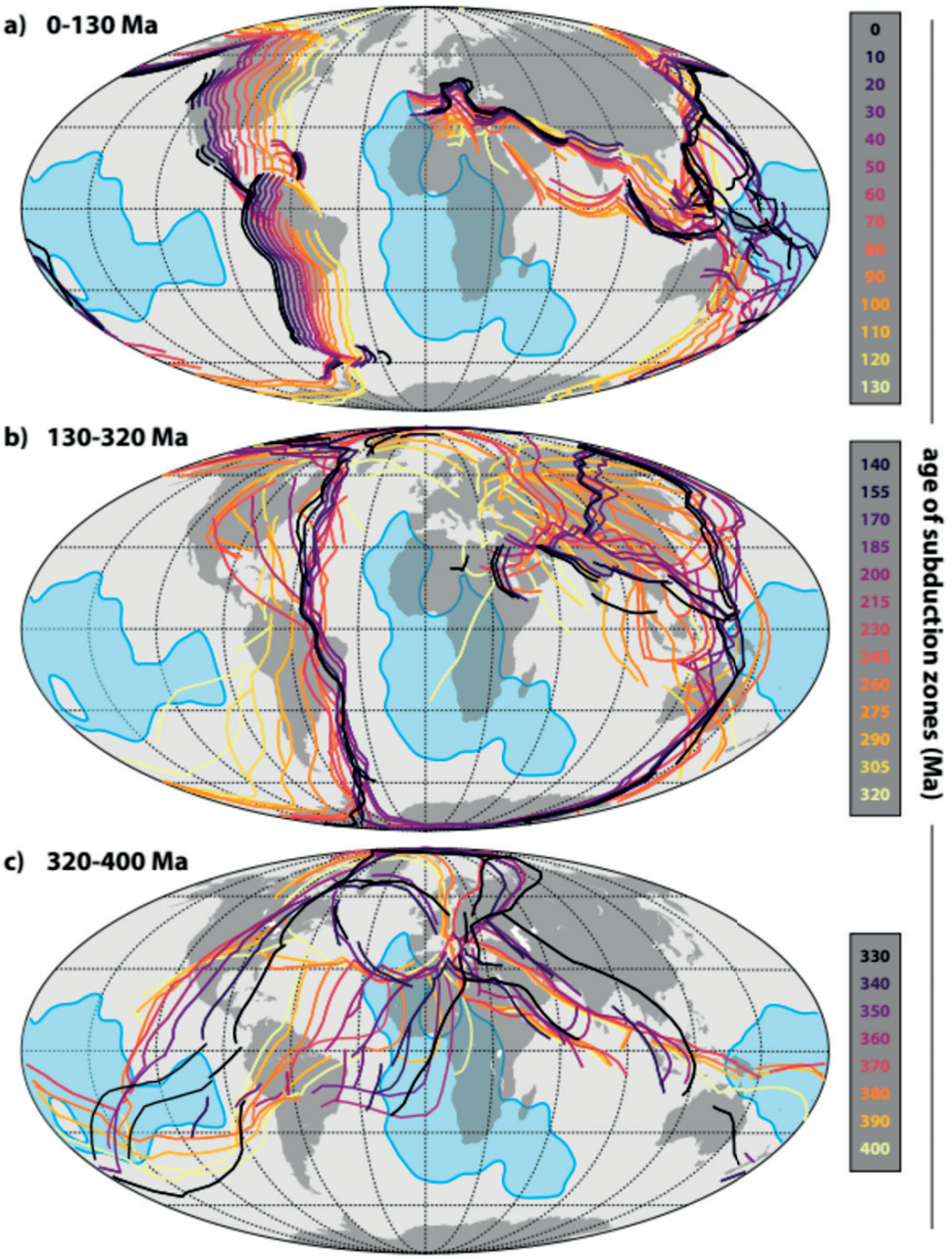

Figure III.4: Reconstructed subduction zones through time, draped on the present-day geography and position of the large low shear velocity provinces (LLSVPs) of the lowermost mantle (blue polygons). Reconstructed subduction zones are from the model of Matthews et al. (2016), in the mantle reference frame. a) 0-130 Ma: time for which longitude is determinable from hotspot tracks. b) 140-320 Ma: less well-constrained paleogeography back to Pangea assembly (~320 Ma); longitude is assumed by holding Africa fixed in longitude. c) 320-400 Ma: pre-Pangea assembly, even less well-constrained paleogeography; longitude estimations are based on the plume generation zone method that assumes the LLSVPs to be fixed.

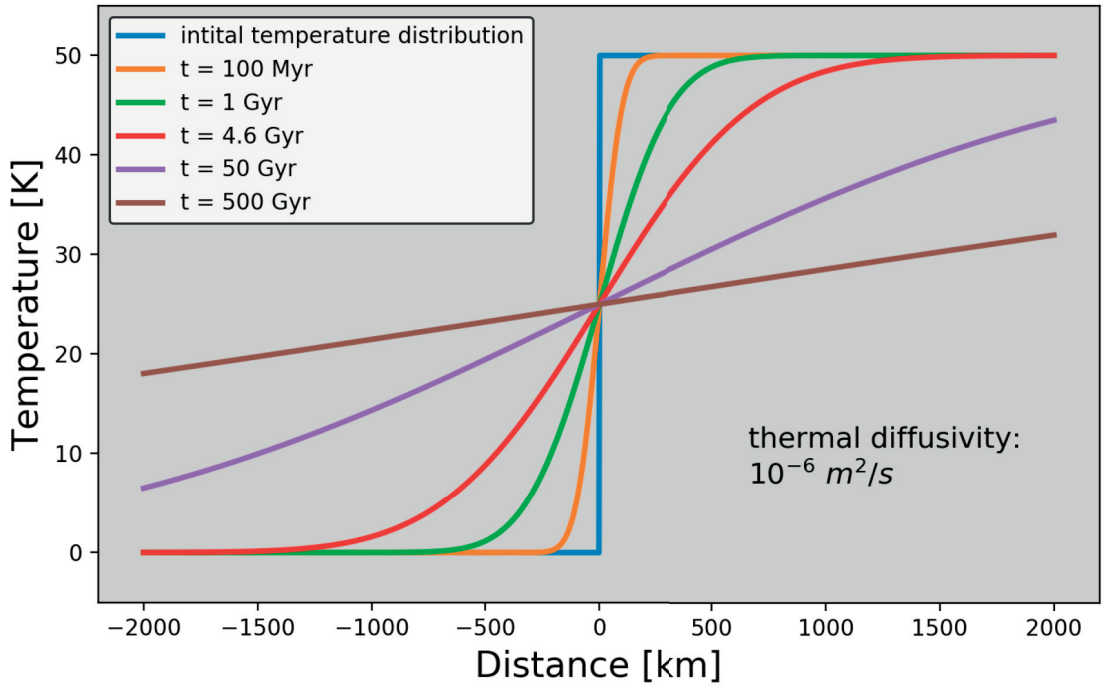

Figure III.5: The evolution of a 50 K temperature jump over geologic time based on an analytical solution to the heat equation with a step-function as an initial condition (blue line), see e.g. Stüwe (2007). We note that it takes several times the age of the Earth for a 50 degree temperature jump to smooth by pure conduction across $\sim 10^3$ km spatial scales.

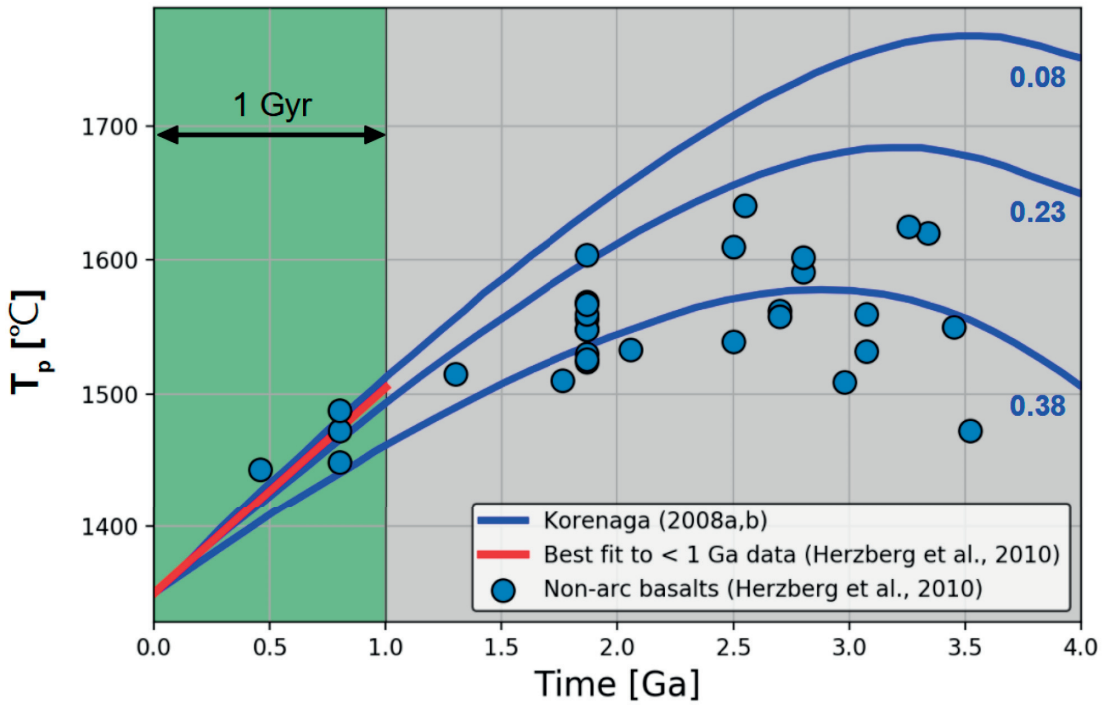

Figure III.6: Ambient mantle cooling models and data. Blue curves show mantle cooling models for different present-day Urey ratios, after Korenaga (2008a) and Korenaga (2008b). Dots indicate petrological estimates of mantle potential temperature from non-arc lavas (Herzberg et al., 2010). The red line indicates the best fitting straight line (least squares fit) to the petrological estimates of mantle potential temperature for the past 1 Gyr. The slope of the red line is 155 K/Gyr.

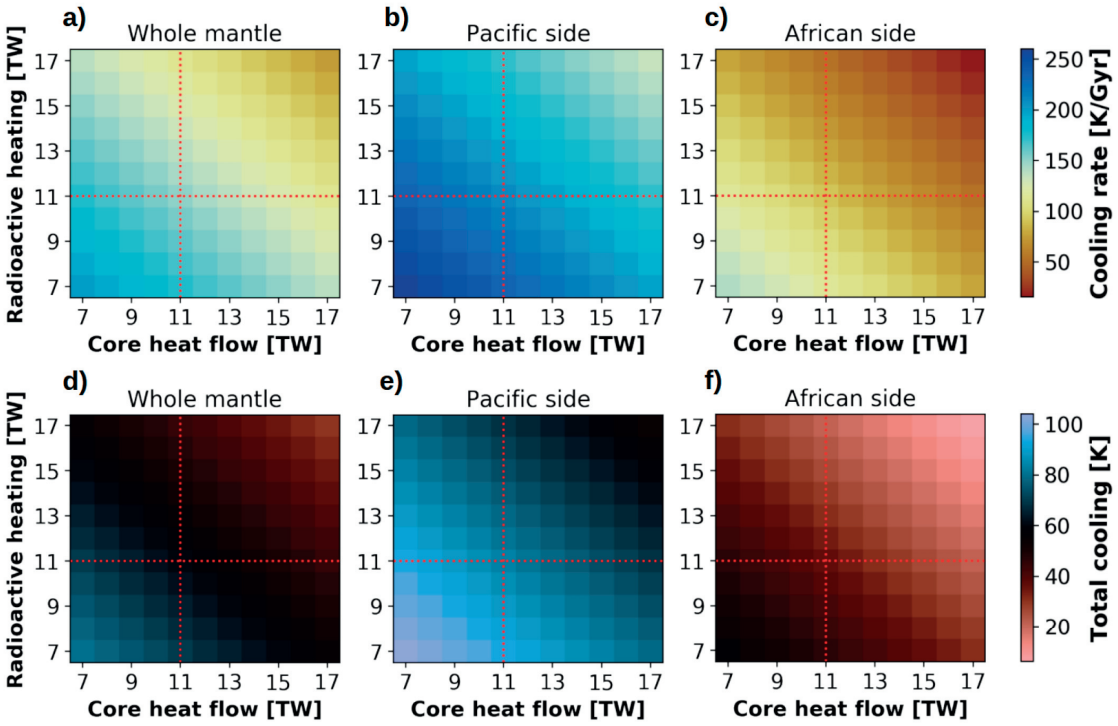

Figure III.7: Time-averaged mantle cooling rates (a-c) and total mantle cooling (d-f) over the past 400 Myr for a range of radioactive heat production and core heat flow values. Note that the difference between all corresponding points in e) and f) is ∼50 K, indicating that the resulting temperature difference between the Pacific and African mantle domains is independent of internal heat sources. Dashed red lines indicate the preferred values of mantle heat sources.

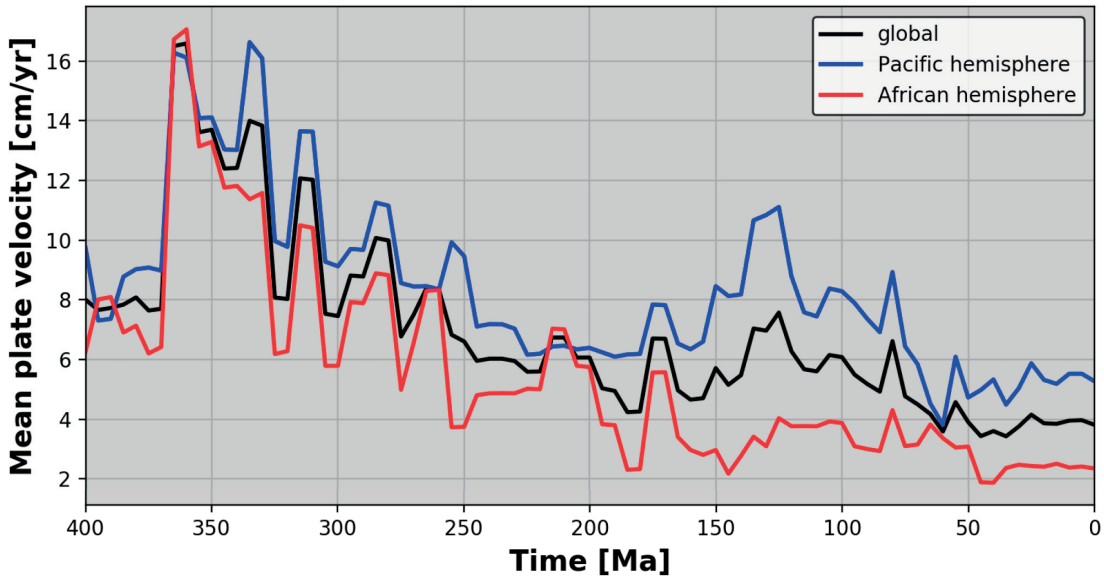

Figure III.8: Mean plate speeds from the Pacific (blue) and African (red) hemispheres, compared to the global average (black). These are computed based on the plate tectonic reconstruction of Matthews et al. (2016), corrected after Torsvik et al. (2019)).

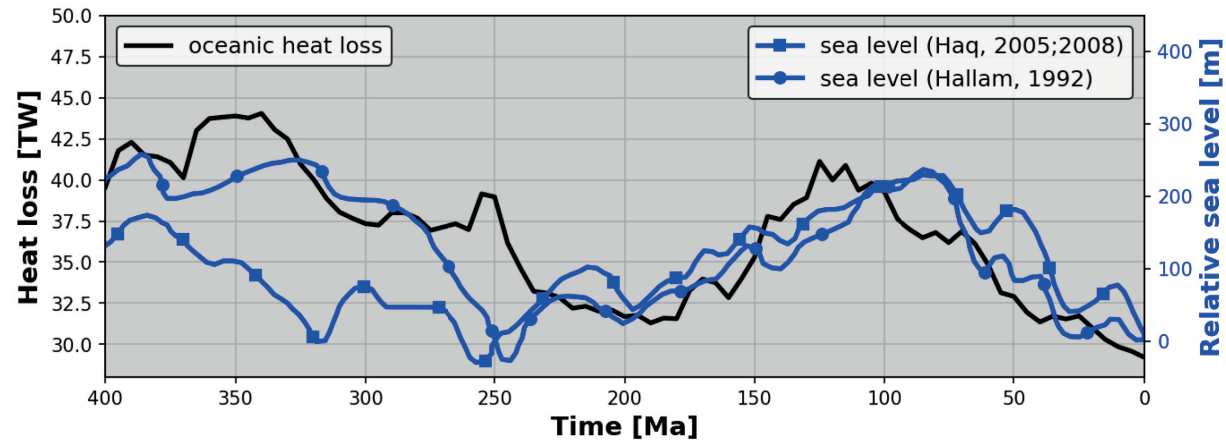

Figure III.9: Time-dependence of oceanic heat loss (black line), calculated according to the description in Section III.2 of the main text, and compared against the sea level record (blue lines, Hallam, 1992; Haq and Al-Qahtani, 2005; Haq and Schutter, 2008).

References

Arnould, M., Coltice, N., Flament, N., and Mallard, C. (2020). "Plate tectonics and mantle controls on plume dynamics". In: *Earth and Planetary Science Letters* vol. 547, p. 116439.

Becker, T. W., Conrad, C. P., Buffett, B., and Müller, R. D. (2009). "Past and present seafloor age distributions and the temporal evolution of plate tectonic heat transport". In: *Earth and Planetary Science Letters* vol. 278, no. 3-4, pp. 233–242.

Brandl, P. A., Regelous, M., Beier, C., and Haase, K. M. (2013). "High mantle temperatures following rifting caused by continental insulation". In: *Nature Geoscience* vol. 6, no. 5, pp. 391–394.

Coltice, N., Rolf, T., Tackley, P. J., and Labrosse, S. (2012). "Dynamic causes of the relation between area and age of the ocean floor". In: *Science* vol. 336, no. 6079, pp. 335–338.

Conrad, C. P. (2013). "The solid Earth's influence on sea level". In: *Geological Society of America Bulletin* vol. 125, no. 7-8, pp. 1027–1052.

Conrad, C. P., Steinberger, B., and Torsvik, T. H. (2013). "Stability of active mantle upwelling revealed by net characteristics of plate tectonics". In: *Nature* vol. 498, no. 7455, p. 479.

Crameri, F., Conrad, C. P., Montési, L., and Lithgow-Bertelloni, C. R. (2019). "The dynamic life of an oceanic plate". In: *Tectonophysics* vol. 760, pp. 107–135.

Dalton, C. A., Langmuir, C. H., and Gale, A. (2014). "Geophysical and geochemical evidence for deep temperature variations beneath mid-ocean ridges". In: *Science* vol. 344, no. 6179, pp. 80–83.

Doucet, L. S., Li, Z.-X., El Dien, H. G., Pourteau, A., Murphy, J. B., Collins, W. J., Mattielli, N., Olierook, H. K., Spencer, C. J., and Mitchell, R. N. (2020). "Distinct formation history for deep-mantle domains reflected in geochemical differences". In: *Nature Geoscience* vol. 13, no. 7, pp. 511–515.

East, M., Müller, R. D., Williams, S., Zahirovic, S., and Heine, C. (2020). "Subduction history reveals Cretaceous slab superflux as a possible cause for the mid-Cretaceous plume pulse and superswell events". In: *Gondwana Research* vol. 79, pp. 125–139.

Hallam, A. (1992). *Phanerozoic sea-level changes*. Columbia University Press.

Haq, B. U. and Al-Qahtani, A. M. (2005). "Phanerozoic cycles of sea-level change on the Arabian Platform". In: *GeoArabia* vol. 10, no. 2, pp. 127–160.

Haq, B. U. and Schutter, S. R. (2008). "A chronology of Paleozoic sea-level changes". In: *Science* vol. 322, no. 5898, pp. 64–68.

Harrison, C. (1980). "Spreading rates and heat flow". In: *Geophysical Research Letters* vol. 7, no. 12, pp. 1041–1044.

Hart, S. R. (1984). "A large-scale isotope anomaly in the Southern Hemisphere mantle". In: *Nature* vol. 309, no. 5971, pp. 753–757.

Hasterok, D. (2013). "A heat flow based cooling model for tectonic plates". In: *Earth and Planetary Science Letters* vol. 361, pp. 34–43.

Herzberg, C., Condie, K., and Korenaga, J. (2010). "Thermal history of the Earth and its petrological expression". In: *Earth and Planetary Science Letters* vol. 292, no. 1-2, pp. 79–88.

Hoggard, M. J., Parnell-Turner, R., and White, N. (2020). "Hotspots and mantle plumes revisited: Towards reconciling the mantle heat transfer discrepancy". In: *Earth and Planetary Science Letters* vol. 542, p. 116317.

Jaupart, C., Labrosse, S., Lucazeau, F., and Mareschal, J. (2015). "Temperatures, heat and energy in the mantle of the earth". In: *Treatise on geophysics* vol. 7, pp. 223–270.

Jones, M. T., Augland, L. E., Shephard, G. E., Burgess, S. D., Eliassen, G. T., Jochmann, M. M., Friis, B., Jerram, D. A., Planke, S., and Svensen, H. H. (2017). "Constraining shifts in North Atlantic plate motions during the Palaeocene by U-Pb dating of Svalbard tephra layers". In: *Scientific reports* vol. 7, no. 1, pp. 1–9.

Karlsen, K. S., Conrad, C. P., and Magni, V. (2019). "Deep Water Cycling and Sea Level Change Since the Breakup of Pangea". In: *Geochemistry, Geophysics, Geosystems* vol. 20, no. 6, pp. 2919–2935.

Karlsen, K. S., Domeier, M., Gaina, C., and Conrad, C. P. (2020). "A tracer-based algorithm for automatic generation of seafloor age grids from plate tectonic reconstructions". In: *Computers & Geosciences* vol. 140, p. 104508.

King, S. D. and Adam, C. (2014). "Hotspot swells revisited". In: *Physics of the Earth and Planetary Interiors* vol. 235, pp. 66–83.

Korenaga, J. (2008a). "Plate tectonics, flood basalts and the evolution of Earth's oceans". In: *Terra Nova* vol. 20, no. 6, pp. 419–439.

Korenaga, J. (2008b). "Urey ratio and the structure and evolution of Earth's mantle". In: *Reviews of Geophysics* vol. 46, no. 2.

Korenaga, T. and Korenaga, J. (2008). "Subsidence of normal oceanic lithosphere, apparent thermal expansivity, and seafloor flattening". In: *Earth and Planetary Science Letters* vol. 268, no. 1-2, pp. 41–51.

Lenardic, A., Moresi, L., Jellinek, A., O'neill, C., Cooper, C., and Lee, C. (2011). "Continents, supercontinents, mantle thermal mixing, and mantle thermal isolation: Theory, numerical simulations, and laboratory experiments". In: *Geochemistry, Geophysics, Geosystems* vol. 12, no. 10.

Loyd, S., Becker, T., Conrad, C., Lithgow-Bertelloni, C., and Corsetti, F. (2007). "Time variability in Cenozoic reconstructions of mantle heat flow: plate tectonic cycles and implications for Earth's thermal evolution". In: *Proceedings of the National Academy of Sciences* vol. 104, no. 36, pp. 14266–14271.

Matthews, K. J., Maloney, K. T., Zahirovic, S., Williams, S. E., Seton, M., and Mueller, R. D. (2016). "Global plate boundary evolution and kinematics since the late Paleozoic". In: *Global and Planetary Change* vol. 146, pp. 226–250.

Müller, R. D., Sdrolias, M., Gaina, C., Steinberger, B., and Heine, C. (2008). "Long-term sea-level fluctuations driven by ocean basin dynamics". In: *science* vol. 319, no. 5868, pp. 1357–1362.

Müller, R. D., Seton, M., Zahirovic, S., Williams, S. E., Matthews, K. J., Wright, N. M., Shephard, G. E., Maloney, K. T., Barnett-Moore, N., Hosseinpour, M., et al. (2016). "Ocean basin evolution and global-scale plate reorganization

events since Pangea breakup". In: *Annual Review of Earth and Planetary Sciences* vol. 44, pp. 107–138.

Meyzen, C. M., Blichert-Toft, J., Ludden, J. N., Humler, E., Mével, C., and Albarède, F. (2007). "Isotopic portrayal of the Earth's upper mantle flow field". In: *Nature* vol. 447, no. 7148, pp. 1069–1074.

Nakagawa, T. and Tackley, P. J. (2011). "Effects of low-viscosity post-perovskite on thermo-chemical mantle convection in a 3-D spherical shell". In: *Geophysical research letters* vol. 38, no. 4.

Nance, R. D., Worsley, T. R., and Moody, J. B. (1986). "Post-Archean biogeochemical cycles and long-term episodicity in tectonic processes". In: *Geology* vol. 14, no. 6, pp. 514–518.

Olson, P. (2016). "Mantle control of the geodynamo: Consequences of top-down regulation". In: *Geochemistry, Geophysics, Geosystems* vol. 17, no. 5, pp. 1935–1956.

Parsons, B. and Sclater, J. G. (1977). "An analysis of the variation of ocean floor bathymetry and heat flow with age". In: *Journal of geophysical research* vol. 82, no. 5, pp. 803–827.

Stüwe, K. (2007). *Geodynamics of the lithosphere: an introduction*. Springer Science & Business Media.

Stein, C. A. and Stein, S. (1992). "A model for the global variation in oceanic depth and heat flow with lithospheric age". In: *Nature* vol. 359, no. 6391, pp. 123–129.

Tegner, C., Andersen, T. B., Kjøll, H. J., Brown, E. L., Hagen-Peter, G., Corfu, F., Planke, S., and Torsvik, T. H. (2019). "A mantle plume origin for the Scandinavian dyke complex: A "piercing point" for 615 Ma plate reconstruction of Baltica?" In: *Geochemistry, Geophysics, Geosystems* vol. 20, no. 2, pp. 1075–1094.

Torsvik, T. H., Burke, K., Steinberger, B., Webb, S. J., and Ashwal, L. D. (2010). "Diamonds sampled by plumes from the core–mantle boundary". In: *Nature* vol. 466, no. 7304, pp. 352–355.

Torsvik, T. H. and Cocks, L. R. M. (2016). *Earth History and Palaeogeography*. Cambridge University Press.

Torsvik, T. H., Steinberger, B., Ashwal, L. D., Doubrovine, P. V., and Trønnes, R. G. (2016). "Earth evolution and dynamics—a tribute to Kevin Burke". In: *Canadian Journal of Earth Sciences* vol. 53, no. 11, pp. 1073–1087.

Torsvik, T. H., Steinberger, B., Shephard, G. E., Doubrovine, P. V., Gaina, C., Domeier, M., Conrad, C. P., and Sager, W. W. (2019). "Pacific-Panthalassic reconstructions: Overview, errata and the way forward". In: *Geochemistry, Geophysics, Geosystems* vol. 20, no. 7, pp. 3659–3689.

Torsvik, T. H. (2020). "Connecting the deep Earth and the atmosphere". In:

Van Avendonk, H. J., Davis, J. K., Harding, J. L., and Lawver, L. A. (2017). "Decrease in oceanic crustal thickness since the breakup of Pangaea". In: *Nature Geoscience* vol. 10, no. 1, pp. 58–61.

Worsley, T. R., Nance, R. D., and Moody, J. B. (1986). "Tectonic cycles and the history of the Earth's biogeochemical and paleoceanographic record". In: *Paleoceanography* vol. 1, no. 3, pp. 233–263.

Worsley, T., Moody, J., and Nance, R. (1985). "Proterozoic to Recent tectonic tuning of biogeochemical cycles". In: *The carbon cycle and atmospheric CO2: natural variations Archean to present* vol. 32, pp. 561–572.

Zhang, N. and Zhong, S. (2011). "Heat fluxes at the Earth's surface and core–mantle boundary since Pangea formation and their implications for the geomagnetic superchrons". In: *Earth and Planetary Science Letters* vol. 306, no. 3-4, pp. 205–216.